Identifying and Overcoming Some Operational Limitations of Reconfigurable Intelligent Surfaces in 5G and Beyond Wireless Networks

By

Souvik Deb

A thesis submitted in partial fulfillment of the requirements for the degree

of

Doctor of Philosophy in Computer Science

at

INDIAN STATISTICAL INSTITUTE, KOLKATA

Under the supervision of

Prof. Sasthi Charan Ghosh

ADVANCED COMPUTING AND MICROELECTRONICS UNIT

Indian Statistical Institute

203 B. T. Road, Kolkata-700108

5 January 2026

Abstract

Reconfigurable intelligent surfaces (RIS) can dynamically reshape the propagation environment to enhance signal strength, spectral efficiency and reliability in 5th generation (5G) cellular as well as device to device (D2D) communications. However, to reap such benefits, a range of practical and operational challenges need to be addressed for effectively utilizing RIS in realistic urban environments. This includes maintaining line of sight (LoS) between the RIS and the communicating devices for reliable signal reflection in millimeter wave (mmWave) communication, reducing high channel estimation overhead for communication using multipath rich channels and preventing violation of strict latency constraints due to high complexity of optimal RIS configuration, among others.

We begin by examining the limitations of RIS in mmWave D2D networks, where stationary RISs require a fixed LoS and strategic placement to accommodate user mobility. To overcome this, we first formulate the RIS placement task as a set-cover problem and place the fewest possible number of RIS by using a greedy approximation algorithm in a preprocessing stage. Then, once devices are deployed, we select an optimal RIS subset to provide indirect LoS to D2D pairs that have their direct LoS link blocked. Here we have considered that the RIS will be allowed to be placed in any of the desired locations.

Next, the mmWave D2D network scenario where optimal RIS locations may be inaccessible is considered. This is due to third-party building ownership, and prohibition from deploying dedicated support structures by regulatory authorities. In these situations, one must leverage the existing RIS deployment which may not be optimal. Moreover, user mobility results in continuous change in RIS-user LoS status. To overcome this challenge, a novel visibility polygon based deterministic RIS selection algorithm is proposed.

Next, the focus of the study moves to 5G cellular networks. In obstacle rich dense urban environments, multipath propagation results in high channel estimation overhead for both sub-6 GHz and mmWave channels, leading to outdated channel state information (CSI). Therefore, performing channel estimation at the beginning of every coherence time interval incurs massive pilot overhead. To reduce the pilot overhead, an algorithm is proposed that dynamically schedules the next channel estimation time based on outdated CSI. First, RIS phase shifts are computed based on current CSI. Next, user transmit powers and bandwidth are allocated based on outdated CSI to maximise the aggregate throughput. Using this, the proposed algorithm dynamically adjusts the duration between consecutive channel estimation instants such that pilot overhead is reduced without harming the throughput performance. The primary focus of this study is the enhanced mobile broadband (eMBB) users whose objective is to maximize the throughput.

Pilot overhead and high complexity of RIS configuration increase latency, which is detrimental to the performance of ultra reliable low latency (URLLC) users requiring strict delay constraints. Moreover, mobility of such users results in a frequent change of channel conditions and handovers between networks. To maintain seamless connectivity and strict latency constraints during handovers, a joint base station (BS) and RIS selection algorithm based on contextual multi-armed bandits (C-MAB) has been proposed. The algorithm learns when to take the assistance of RIS while communicating with the BS to maintain latency without losing reliability.

Both resource block (RB) allocation and RIS selection in RIS assisted cellular networks are dependent on the CSI of direct BS-user as well as RIS assisted channels, thereby being affected by channel estimation overhead. This is established by proposing a MAB based RB allocation algorithm to allocate RBs in an RIS assisted network which utilizes both direct and RIS assisted channel information as opposed to using only the direct channel information. After establishing this, an efficient RIS-RB pair allocation algorithm based on adversarial bandit and bipartite graph matching has been proposed for mmWave non orthogonal multiple access networks. This algorithm addresses the challenge of high CSI overhead to find the optimal RIS in the presence of dynamic obstacles and allocate RBs optimally to user groups to maximize throughput while ensuring that users with worse channel conditions are not ignored.

Dedicated

to

my beloved mother Mrs. Rinku Deb and father Mr. Goutam Deb

ACKNOWLEDGEMENTS

It is with immense gratitude that I acknowledge the support of my supervisor Prof. Sasthi C. Ghosh. He gave me the freedom to explore on my own, and at the same time the guidance to recover when my steps faltered. I deeply appreciate his valuable insight, his timely response to every query and correspondence for every submission. He has always been a source of inspiration for me. The lectures he used to deliver during course works have always helped me in understanding the research area rigorously. I am also grateful to him for giving me chances to assist in some of the courses he taught, which were a very enjoyable and rewarding experience.

I want to express my sincere gratitude to Dr. Shankar K. Ghosh, whose visionary guidance has been transformative. I have had the honour of participating in enlightening discoveries and internalising the fundamental ideas that characterise our field during our collaborations. His contributions in problem formulation and modelling during our collaborative work have yielded significant insights and impactful outcomes, for which I remain deeply appreciative.

I would also like to register my heartfelt gratitude to all of my teachers who taught me during PhD course work and always inspired me to go beyond the limit.

I am also thankful to my lab mates for stimulating discussions, their everlasting enthusiasm, rational and free-thinking inputs.

Finally, I dedicate this work to my beloved parents whose dream it was that I wear this feather in my cap. Above all, I am thankful to God for giving me the ability, intellect and good health to carry on.

Publications from the content of the Thesis

In journals

- **Souvik Deb**, Sasthi C. Ghosh, "Time varying channel estimation for RIS assisted network with outdated CSI: Looking beyond coherence time", **Computer Communications (Elsevier)**, Volume 240, August 2025, 108202, ISSN 0140-3664, https://doi.org/10.1016/j.comcom.2025.108202.

In conferences

- **Souvik Deb** and Sasthi C. Ghosh, "An RIS deployment strategy to overcome static obstacles in millimeter wave D2D communication," **The 20th IEEE International Symposium on Network Computing and Applications (IEEE NCA 2021)**, Boston, MA, USA, pp. 1-8, 23-26 November 2021.
- **Souvik Deb**, Shankar K. Ghosh and Sasthi C. Ghosh, "A Multi-arm-bandit based resource block allocation in RIS assisted wireless network," **The 20th IEEE International Symposium on Network Computing and Applications (IEEE NCA 2021)**, Boston, MA, USA, pp. 1-6, 23-26 November 2021.
- **Souvik Deb**, Shankar K. Ghosh and Sasthi C. Ghosh, "MAB based network selection mechanism for URLLC users in RIS assisted network," **The 21st IEEE International Symposium on Network Computing and Applications (IEEE NCA 2022)**, Boston, MA, USA, pp. 173-179, 14-16 December 2022.
- **Souvik Deb** and Sasthi C. Ghosh, "Visibility polygon-based obstacle aware RIS selection for millimeter wave D2D communication", **The 5th IEEE International Mediterranean Conference on Communications and Networking (IEEE MEDITCOM 2025)**, Nice, France, 7-10 July 2025 (Accepted for publication).
- **Souvik Deb**, Sasthi C. Ghosh and Shankar K. Ghosh, "An efficient RIS selection and resource block allocation algorithm for mmWave NOMA systems",communicated to the **13th Wireless Days Conference (WD 2025)**, Niterói, Rio de Janeiro, Brazil, December 01-03, 2025 (Accepted for publication).

Contents

List of Figures

List of Tables

List of Abbreviations

Table 1: List of Abbreviations

Acronym	Full Form
3GPP	Third Generation Partnership Project
BS	Base Station
UE	User Equipment
CE	Channel Estimation
D2D	Device-to-Device
eMBB	Enhanced Mobile Broadband
URLLC	Ultra-Reliable Low-Latency Communications
mMTC	Massive Machine-Type Communications
RB	Resource Block
RIS	Reconfigurable Intelligent Surface
PIN	P-type/Intrinsic/N-type
UPA	Uniform Planar Array
QoS	Quality of Service
FPGA	Field-Programmable Gate Array
FR1	Frequency Range 1
FR2	Frequency Range 2
IoT	Internet of Things
LoS	Line of Sight
MAB	Multi-Armed Bandit
mmWave	millimeter-wave
MIMO	Multiple-Input Multiple-Output
NOMA	Non-Orthogonal Multiple Access
PD-NOMA	Power-Domain NOMA
SIC	Successive Interference Cancellation
SINR	Signal-to-Interference-plus-Noise Ratio
DAPS	Dual active protocol stack
RSRP	Reference signal received power

Chapter 1

Introduction

The twenty first century has witnessed a rapid growth in wireless communications with more than 5 billion unique mobile subscribers in 2024 comprising 71% of the global population. Furthermore, it is estimated that the number of unique mobile subscribers will increase up to 6.5 billion by 2030 with more than 5 billion users subscribed to mobile internet [2]. Along with the surge in number of subscribers, there is a rising demand for advanced services such as enhanced mobile broadband (eMBB) which targets peak data rates of 20 Gbps; ultra reliable low latency communication (URLLC) which guarantee data transfer with a reliability of 99.999 % and maximum latency of 1 ms, and massive machine type communication (mMTC) supporting connectivity for millions of internet of things (IoT) devices [3, 4]. These capabilities form the foundation of fifth-generation (5G) and beyond wireless networks as standardized by the third generation partnership project (3GPP) [5]. The scope of this thesis encompasses eMBB and URLLC based services. High-frequency signals such as millimeter waves (mmWave) have been widely used in recent years to achieve these objectives for both cellular and D2D communications [6]. Although mmWaves is well suited for short-distance communication in D2D and 5G small cell networks, it comes with its own set of challenges like high propagation and penetration losses. This forces devices communicating in mmWave bands to have a direct line of sight (LoS) between them for successful communication. Moreover, it comes with high costs of hardware and high power consumption and requires additional active antennas and expensive radio frequency (RF) chains to operate at such high frequency bands [7]. Furthermore, such antennas are incapable of making any adjustments to the propagation environment. However, the challenges commonly faced by mmWave communications, such as high propagation loss, severe penetration loss through obstacles, and signal blockage due to environmental

dynamics, can be significantly alleviated by deploying a promising new technology in the network called reconfigurable intelligent surfaces (RIS) [8]. The RIS can enhance the spectral efficiency, coverage, reliability and energy efficiency for both mmWave and sub-6 GHz cellular communication in 5G and beyond wireless networks. An RIS is a passive reflector board that can be set on the side of building walls. An RIS can reflect a signal incident on it in any desired direction, thereby enhancing coverage. The passive reflective elements of an RIS can be configured to generate reflective beams that can increase spectral efficiency and mitigate inter-user interference in both sub-6 GHz cellular and mmWave D2D networks. The RIS provides an additional channel that can be used when the LoS between the transmitter and receiver of a mmWave D2D pair is blocked. Furthermore, RISs are cost effective, easy to set up in the wireless environment and consume only a fraction of the power compared to active antennas [8, 9]. However, implementation of RISs to reap the aforementioned benefits comes with its share of operational challenges.

In mmWave communication, an LoS between the devices and the RIS is crucial for reliable signal reflection and propagation. Moreover, RISs once placed, remain stationary and cannot dynamically change positions along with the mobile users. Therefore, optimal placement and selection of RISs in mmWave D2D networks to avoid link blockages is a critical operational challenge to overcome.

Effective RIS configuration requires accurate information about the wireless channel conditions. However, in urban 5G cellular environments characterised by rich, unstructured multipath channels and frequent blockages, obtaining precise estimates of channel conditions incurs substantial pilot signalling overhead. Coupled with user mobility, the estimated channel information may rapidly become outdated. Therefore, deciding when to estimate the RIS assisted channel, taking into account the effect of outdated channel information is a crucial challenge to overcome.

Another limitation caused by the pilot overhead is the possible violation of strict latency requirements for highly mobile URLLC-based users. Apart from violating latency the pilot overhead also reduces the time left for actual data communication, thereby degrading the system throughput. Furthermore, in environments with urban canyons and dynamic obstacles, mmWave channels also exhibit multipath fading. Therefore, designing a strategy to select an optimal RIS and resource blocks for mobile users that minimizes the pilot overhead requirement while maximizing the system throughput is of paramount importance.

In this thesis, our objective is to propose efficient algorithms for optimal placement and selection of RISs, reducing pilot overhead and ensuring strict latency constraints under user

mobility and changing channel conditions.

1.1 Background: RIS and its uses

The RIS is a two dimensional board that is composed of a large number of tunable passive reflecting elements made of meta materials such as positive-intrinsic-negative (PIN) diodes, arranged in a uniform planar array (UPA) [10, 9]. By passive RIS, we mean that the RIS operates by reflecting incident signals through adjustable phase shifts without any amplification, relying solely on passive meta-materials that consume minimal power. The meta materials can manipulate the phase of the incident electromagnetic wave and reflect it in any desired direction without additional signal processing. The tunable meta materials are controlled by electrical operations that can be programmed in software via field programmable gate array (FPGA) [11]. Tuning the elements induces phase shift to the incident electromagnetic wave. This depends on the channel conditions and must be adjusted when the channel condition changes. The duration over which the channel condition of a UE is highly correlated and thus is assumed to be unvarying, i.e., the duration over which the RIS configuration is not changed, is called the *channel coherence time*. Let $f_{ud} = f_c V_u / c$ be the maximum Doppler spread, f_c be the carrier frequency, c be the velocity of light, and V_u be the velocity of the UE u. Formally, the coherence time for UE u denoted by T_{uc} is defined as the maximum time interval over which the time correlation of the channel is above a predefined threshold ρ^{th} [12, 13] and is approximately computed as follows [13]:

$$T_{uc} = \frac{c \cos^{-1}(\rho^{th})}{2\pi V_u f_c}. \tag{1.1}$$

There exist RISs that employ reflective elements based on RF switches, varactor diodes, liquid crystal (LC) meta materials and other technologies. However, in our study we focus exclusively on the variant most commonly adopted in the literature—namely, RIS elements implemented with P-type / Intrinsic / N-type (PIN) diodes. RISs can be easily incorporated with the already widely deployed 5G network to greatly improve the network performance [8].

1.1.1 Throughput enhancement

In RIS assisted 5G networks, data can be communicated to a receiver in two ways, as shown in Figure 1.1: firstly, through the direct signal stream from the transmitter to the receiver (namely stream A). Secondly, through the additional indirect signal stream via the RIS (namely stream B). The reflective elements of the RIS are configured such that the reflected signal adds constructively with the direct signal, thereby improving the signal strength. This allows sub-6 GHz macro cells to enhance spectral efficiency and meet the data rate requirements of eMBB services, complementing mmWave small cells that offer high capacity but limited coverage. The process of reconfiguring the RIS elements is called *phase shift optimization*. By providing an additional signal stream, the RIS improves the multiplexing gain of signal transmission and significantly enhances the throughput at the receiver, thereby greatly benefiting eMBB services.

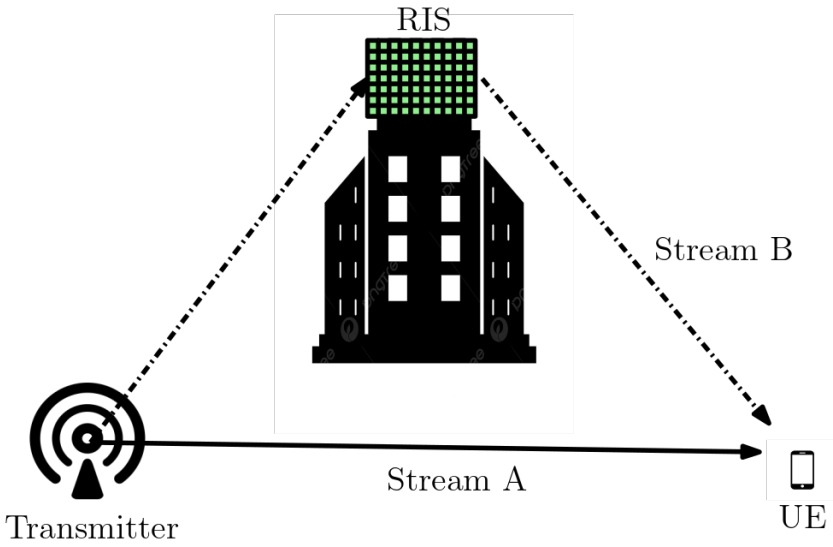

Figure 1.1: Typical RIS assisted communication

Since the RIS itself does not comprise of any active RF chains, the reflective elements of the RIS are configured to yield passive beamforming. Jointly optimizing the active beamforming at the transmitter and the passive beamforming at the RIS, the signal to interference plus noise ratio (SINR) at the user equipments (UEs) can greatly be enhanced to improve the system throughput [14, 15]. Similarly, the transmit power can also be jointly optimized with the RIS phase shifts to maximize the sum throughput of all UEs. Furthermore, to ensure fairness among all UEs an RIS can be optimally configured to maximize the sum rate under strict constraints of the tolerable outage probability of each UE and the power

budget of each transmitter [16]. Analytical studies in [17] demonstrate that the blackout probability of a UE can be reduced when it utilizes an RIS located in close proximity.

1.1.2 Coverage enhancement

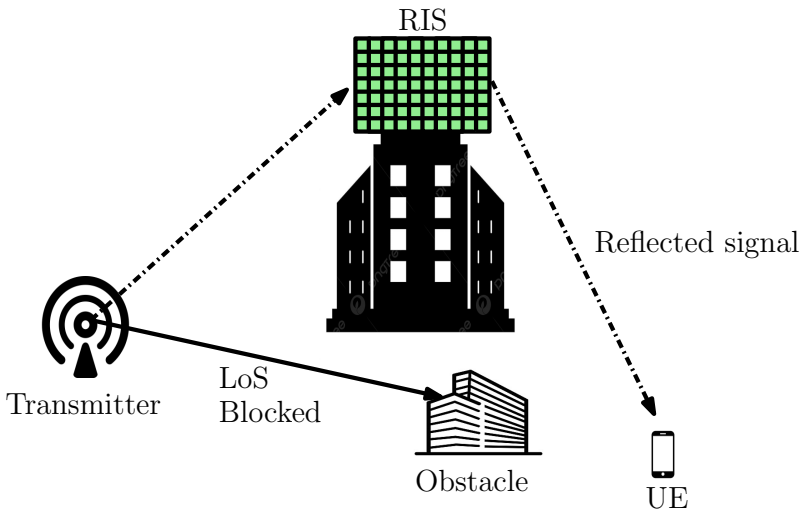

Figure 1.2: Coverage enhancement by RIS

According to 3GPP [18, 19], the frequency bands utilised by 5G technologies are categorised into two ranges: FR 1 (4.1 GHz to 7.125 GHz) and FR 2 (24.25 GHz to 52.6 GHz). The FR 2 bands provide high bandwidth and data rates for short range communication to achieve the high throughput requirement for eMBB services. Furthermore, unlicensed mmWave bands ($\geq$ 60 GHz) are used to achieve even higher bandwidth for D2D communication. However, mmWave frequencies are highly susceptible to propagation losses and suffer huge penetration loss. For example, the penetration loss due concrete is over 120 dB, while moving obstacles such as cars cause a loss of over 17 dB [8]. To overcome this, the transmitter and receiver are equipped with large antenna arrays to generate high gain directional beams. However, such high directional beams are effective only when there is direct LoS between the transmitter and the receiver. Moreover, when LoS is blocked as shown in Figure 1.2, even with multipath propagation, the received signal may fall below the threshold data rate required for eMBB services. In such a case, an RIS placed on the walls of the buildings enables communication between the transmitter and the UE. The RIS elements can be configured to reflect the signal incident on it from the transmitter in the desired direction as shown in Figure 1.2. Furthermore, in 5G cellular network using

FR 1 range, a UE may receive poor signal from the new radio (NR) BS also known as next generation node B (gNB) if it is in the shadow area of building, the street corner in dense urban area or the edge between indoor and outdoor. This reduces signal strength and increases bit error rate (BER) which in turn increases the number of retransmissions for successfully delivering the packet. Eventually reliability decreases and delay increases. The RIS can improve reliability in such a scenario by enhancing the coverage of the NR BS by means of reflecting the signal towards the UEs in blind spots of the BS.

1.1.3 Interference mitigation

Loss in spectral efficiency due to the limited number of RBs in dense multi-user networks with exploding UE populations is a major barrier for achieving the data rate required by eMBB services. One of the promising new technologies to enhance spectral efficiency by overcoming the challenge posed by limited resources is non-orthogonal multiple access (NOMA). NOMA has recently garnered considerable research interest due to its flexible combination with other emerging 5G technologies such as massive multiple input multiple output (MIMO), D2D communication, cognitive radio (CR), mmWave communication, and most importantly, RIS [20]. By allowing multiple users to share the same time–frequency resources via power-domain or code-domain superposition, NOMA can significantly increase system throughput without requiring additional bandwidth [21]. In our study we focus on RIS-assisted power domain NOMA (PD-NOMA). In PD-NOMA, the signals of multiple UEs are superimposed into a single waveform and are decoded at the receiver using successive interference cancellation (SIC), where each interfering signal is successively removed until the desired signal is obtained. The strongest signal is decoded by SIC first, with the others being considered as interference. Removing the first decoded signal from the received signal yields the remaining signals precisely if the signal decoding process is successful. SIC keeps on doing this until it finds the signal it wants. The success of the SIC relies primarily on the difference in channel conditions of different UEs sharing the same RB. The efficiency of SIC declines and error rates increases as UEs encounter comparable channel conditions. The receiver finds it challenging to consistently decode and cancel the stronger UE's signal before decoding the lesser one, mainly because of the decreased power differential between UEs. However, with the assistance of RIS, the propagation environment can be intelligently redesigned by reconfiguring the RIS, allowing control over the channel conditions of the UEs. Furthermore, the phase shifts of the RIS elements can

be appropriately designed to minimize interference among UEs sharing the same RIS. In [22], an appropriate design of phase shifts of each RIS element has been proposed such that the signal power received from the BS at the desired UE is maximised, while nullifying the interference power at the undesired UE. This not only allows for higher throughput for eMBB services, but also improves the SINR and thereby improving the reliability of any neighboring URLLC service-based UE. Therefore, integrating NOMA with RIS greatly benefits the spectral efficiency for eMBB services and increases reliability for URLLC services.

1.1.4 Improvement of reliability

The 5G and beyond wireless networks promise several URLLC services, such as autonomous and connected vehicles, industrial automation, remote surgery, virtual reality and tactile internet, and much more [23]. The 3GPP standard for the 5G NR states that, for a URLLC packet of 32 bytes, the URLLC latency must be less than 1 ms and the URLLC reliability must be greater than 0.99999 in less than 1 ms. Integrating RIS into 5G and beyond networks increases the transmission rate, thereby reducing the transmission latency significantly. Moreover, studies [24, 25] have shown a significant reduction in the BER, thereby increasing the transmission reliability, especially in scenarios where the direct link between the transmitter and the UE is blocked.

In a shared network environment, URLLC and eMBB UEs must coexist, competing for the same limited pool of resources—namely, time-frequency blocks and transmission power [26, 27]. A shortage of resources for URLLC-based UEs may lead to decreased transmission rates, thereby increasing BER and latency. At the same time, it must be ensured that the data rate of eMBB-based UEs does not fall below a required Quality of service (QoS) threshold. RIS plays a crucial role in facilitating the coexistence of such heterogeneous network services. The power allocation and RIS reflection matrix can be jointly optimized to minimise the interference between eMBB and URLLC-based UEs [28]. Again transmit power at the BS and phase shift configuration at the RIS can be jointly optimised to maximise spectral efficiency of eMBB services while ensuring the reliability and latency requirements of the URLLC service [29]. Thus it is evident that RISs are instrumental in enabling the harmonious coexistence of diverse network services.

1.2 Operational challenges and limitations of RISs

Recent studies such as [8, 14, 16, 22, 25, 28, 29] justify the integration of RIS with various 5G and beyond technologies. However, the benefits of RIS come with its share of operational challenges. Various hardware challenges like restricted phase shift resolution [23] and power consumption of multiple RISs [30] are some of the major hardware and physical layer issues. Although such physical layer challenges have been studied in many recent works, the studies regarding several operational challenges faced when actually implementing RISs are limited. In this thesis, we have focused on identifying and addressing some of the major operational issues for both mmWave D2D communication and 5G cellular networks.

1.2.1 Link blockages in mmWave D2D communication

Even though mmWave links provide high data rates, they suffer high penetration losses. Device pairs communicating using mmWave links must have unblocked LoS between them. An RIS can provide an indirect LoS path to D2D pairs that have their direct link blocked by an obstacle. Again, due to the high propagation loss of mmWaves the distance between two communicating devices must be within a threshold distance for successful communication. However, the RIS itself can be used only if the LoS between the devices and the RIS is not blocked and lies within the threshold distance of the devices. Moreover, the movement of the devices changes the relative position of the RIS over time. Therefore, proper placement and selection of RISs pose a significant challenge that needs to be conquered.

1.2.1.1 Placement of RIS

One of the key challenges when using RIS in mmWave D2D communication networks is the optimal placement of RISs. The presence of obstacles in the environment is a big challenge for establishing an LoS path between a pair of communicating devices. Static obstacles in the environment like buildings, houses, and trees often block the LoS needed between a device pair. The RISs need to be placed in such a way that whenever a device pair has its LoS obstructed, an RIS is always found in the vicinity such that an indirect LoS can be established. Moreover, it is to be noted that the RIS itself must have LoS with both the transmitter and receiver of the concerned device pair. Furthermore, it must be noted that even though the RIS consumed less power compared to active antenna arrays, it requires power to operate nonetheless. Therefore, it is also essential to minimise the number of

RISs placed in the network environment to improve energy efficiency. In the case of D2D communication, both the transmitter and the receiver are in motion, whereas the RIS stays fixed in location after placement. In such a scenario, RISs placed optimally for a given position of D2D pairs at an instant of time no longer remain optimal when the position of the D2D pairs change over time. Therefore, it is vital to address this challenge to fully utilise the benefit offered by RISs in the environment.

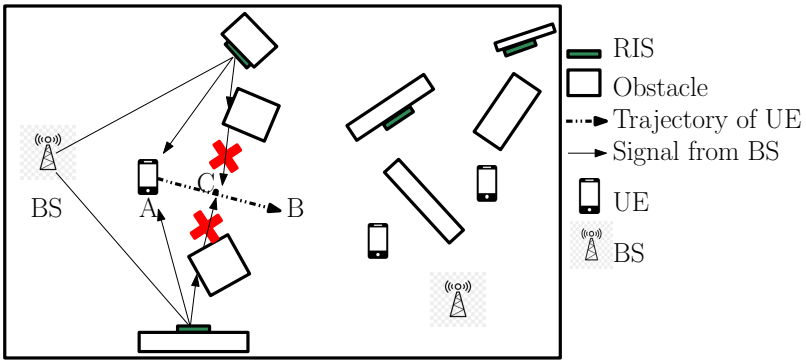

Figure 1.3: Changing LoS status of RIS as UEs move

1.2.1.2 Selection of RIS

Deploying RISs in dense urban environments poses significant challenges. However, the optimally computed locations for RIS placement may not be available for several reasons. Operators often cannot choose optimal wall locations [31], [8, 10, 11] because the buildings they need to use are owned by third parties who may withhold permission. Erecting dedicated support structures—such as towers or poles—to host RISs can be prohibitively expensive and may face strict regulations or outright refusal from municipal authorities. Consequently, finding cost-effective, permitted mounting sites often becomes a major barrier to widespread RIS deployment in cities. In such a scenario, where RIS placement options are limited and highly constrained, a new challenge arises for mmWave D2D communication. Thus, for an UE, the best RIS has to be selected among the RISs which may not be positioned optimally. As UEs move, the LoS status between the UE and the RIS continuously changes which needs to be taken into account as shown in Figure 1.3. Specifically, an RIS has LoS with a UE if the reflective side of the RIS is visible from the UE. In Fig. 1.4, we observe two cases where a D2D pair may not have LoS with an RIS in its vicinity. In case (a) the RIS is mounted at an angle such that its reflective side faces away from a UE of the concerned

D2D pair. On the other hand, in case (b) even if the RIS has its reflective side facing towards the D2D pair, the LoS between a UE of that pair is blocked by an obstacle. Therefore, selecting an optimum RIS in a multi-RIS network which can successfully assist a D2D pair and maximize their data rate is a critical network problem that needs to be addressed. The CSI can be utilized for selecting the optimal RIS. Although sparse mmWave channels can be estimated parametrically with very few pilot symbols, CSI acquisition still presents serious challenges in muli-RIS assisted D2D networks. First, since the UEs dont have the location of the RISs, identifying a common RIS that is simultaneously visible to both the transmitter and receiver requires the BS to query and process the location and visibility of every RIS sequentially, which introduces non-trivial delay. Second, limited pilot resources prevent all devices from estimating their channels simultaneously, so overhead grows as device density increases. Finally, at mmWave frequencies the channel coherence time decreases inversely with both carrier frequency and user speed, so the fraction of each coherence interval devoted to pilot transmission and RIS selection can easily dominate, leaving only a small window for actual data transfer.

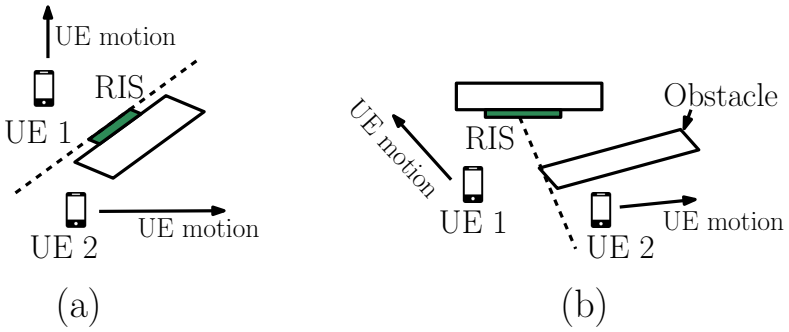

Figure 1.4: Cases where RIS is not visible

1.2.2 Channel estimation overhead in 5G cellular network

The channel estimation (CE) overhead for unstructured multipath-rich channels increases linearly with the number of reflective elements of RIS [32]. Moreover, multipath rich channels for mmWave frequencies are also observed in dense urban canyons filled with multiple dynamic obstacles [33, 34, 11]. It should be noted that, due to the mobility of the UE, the channel conditions change over time. As a consequence, the RIS needs to be reconfigured when the channel condition changes to suitably optimise the phase shifts of the RIS elements. In other words, the channel needs to be estimated at the beginning of

each channel coherence time interval. This results in a significant portion of the channel coherence time being spent on CE, reducing data communication time. Furthermore, due to the mobility of the UE and the time consumed during CE, the estimated channel state information (CSI) may become outdated during actual data communication. A detailed block diagram showing the CE process and actual data communication in channel coherence time is shown in Figure 1.5. Fully exploiting the benefits of an RIS hinges on acquiring highly accurate CSI within each coherence interval. However, this introduces a critical trade-off. The process of CSI acquisition—including pilot transmission, signal processing, and feedback—consumes a non-negligible portion of the coherence interval. Since the amount of overhead scales with the number of RIS elements, longer or more frequent estimation phases leave less time for data transmission, thereby reducing the network throughput. The massive CE overhead leads to the following operational challenges in 5G cellular networks. Due to user mobility coupled with CE overhead, the CSI used during actual data communication may become outdated. Again, during handovers of URLLC based UE with strict latency requirements, using an RIS to improve reliability may lead to violation of the delay constraints. Moreover, urban environments with towering urban canyons lead to multipath rich channels even for mmWave frequencies. In such cases, detecting obstacles and choosing the optimal RIS and RB pair for communication requires high CE overhead. These challenges are discussed in further detail in the subsequent subsections.

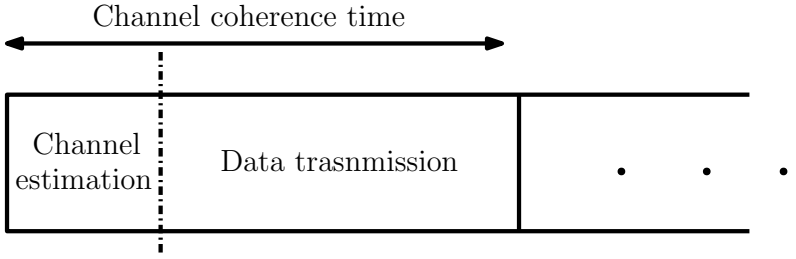

Figure 1.5: Time division for CSI and data communication in RIS assisted network

1.2.2.1 Outdated CSI due to user mobility

Outdoor cellular networks must serve multiple UEs simultaneously. Moreover, in dense urban areas the radio propagation channel becomes complex and rich in multipath due to reflection, diffraction, and scattering from high-rise buildings, vehicles, road signs and other city structures. This gives rise to unstructured stochastic channels. Such unstructured channels are primarily observed for sub-6 GHz frequencies. It is to be noted that CSI is

essential to optimise the phase shift of the RIS elements in networks with such unstructured channels. However, in outdoor cellular networks there are several UEs which are highly mobile. For high mobility UE, the rapid changes in channel conditions cause the estimated CSI to become outdated due to feedback delays [35]. This makes it essential to consider the performance of an RIS-assisted 5G network with outdated CSI as opposed to assuming that perfect instantaneous CSI is always available. Keeping outdated CSI in mind, one of the most essential questions is when to perform CE? The CE timing in recent studies is based only on the channel coherence time. The estimated channel conditions are assumed to be constant throughout the coherence time and the channel is estimated again once the coherence time runs out. However, there is still a non-zero delay between the estimated channel and the actual channel during data communication even within the coherence time interval. Moreover, the computation of channel coherence time is dependent on the velocity of the UE. A mobile UE changes its position with respect to the serving BS and the neighbouring cells over time. The velocity of the UE can also change over time. Consequently, the pathloss, fading and background interference experienced by a UE varies over time. Furthermore, different UEs in a multi-user system move at different velocities thereby leading to different coherence time intervals experienced by each UE. Therefore, the rate of degradation in datarate due to delay between outdated CSI and actual CSI varies differently for each UE over time. Moreover, the power allocated for each UE also determines the amount of degradation of SINR suffered by them. Therefore, intelligent transmit power sharing among the UEs can improve the aggregate throughput [36]. Furthermore, hardware limitations at the RIS such as phase adjustment speed pose a serious challenge for high speed UEs where the optimal RIS configuration is changed frequently. For high mobile UEs the channel becomes further outdated before the optimal phase shifts are fully set at the RIS. Energy consumption due to massive pilot overhead and power consumption of the RIS elements makes a network inefficient.

1.2.2.2 Violation of the latency constraint in URLLC handover

A critical challenge faced by high mobile UEs in outdoor cellular networks is the execution of seamless handover. A handover triggers during an ongoing call session when a UE moves out of the coverage of the current serving BS and must transfer the connection to a neighbouring BS without interrupting the ongoing session. It is to be noted that even though eMBB or conventional voice services can tolerate brief interruptions, URLLC services cannot afford any violation of the strict latency and reliability constraints. While roaming

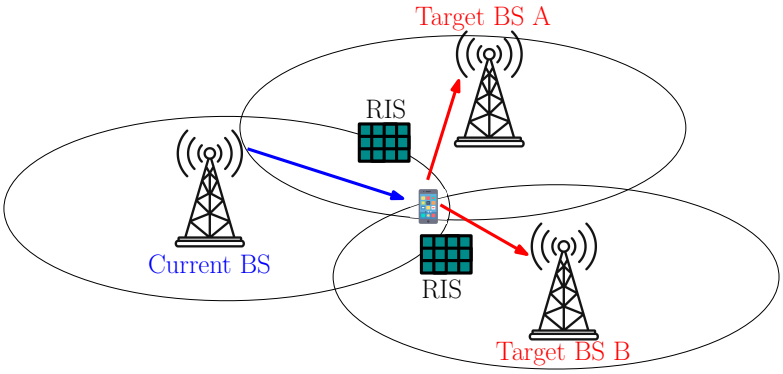

Figure 1.6: BS-RIS pair selection in RIS assisted network

across the network, a UE has to select either a BS or a BS-RIS pair in order to sustain connectivity with the network, as shown in Figure 1.6. It may be noted that in direct channel communication where a BS is selected, due to bad channel conditions at the cell edges, BER will be high, resulting in a higher number of retransmissions and low reliability. On the other hand, in an RIS assisted communication when a BS-RIS pair is chosen, the received signal strength at the UEs is high, resulting in high reliability. However, the time consumed for CE and RIS configuration may often lead to violations of the latency constraints. The RIS is not always helpful for supporting a URLLC based service. Moreover, in direct channel communication, only one wireless hop is involved. Hence, the one-way transportation delay for a packet will be less compared to RIS assisted communication where two wireless hops are involved. However, due to packet loss caused by reduced signal strength at the cell edges, transmission control protocol (TCP) may invoke a congestion avoidance mechanism resulting in higher end-to-end delay. Given such a prevailing situation and the fact that the traditional user association problem is NP-hard [37], it is very difficult to choose an appropriate BS or a BS-RIS pair in order to ensure both the latency and the reliability constraints. Therefore, simply always choosing an RIS for establishing a downlink URLLC connection may prove to be detrimental. It is essential to decide when the right situation is to choose an RIS and when it may be ignored.

1.2.2.3 CSI overhead for optimal RIS selection and RB allocation

The ever-growing number of cellular users puts pressure on the limited number of RB available for communication. The RB allocation mechanism considering only the direct channel conditions may not suitable for RIS assisted networks. This is because a distant

UE can achieve a high throughput through the indirect channel even if the direct channel condition is not good. Hence, an investigation on RB allocation mechanisms in RIS assited cellular networks is essential to understand the additional complexity added to the measurement of the channel conditions due to the assistance of an RIS. Furthermore, integration of NOMA in RIS assisted mmWave cellular networks adds additional challenges.

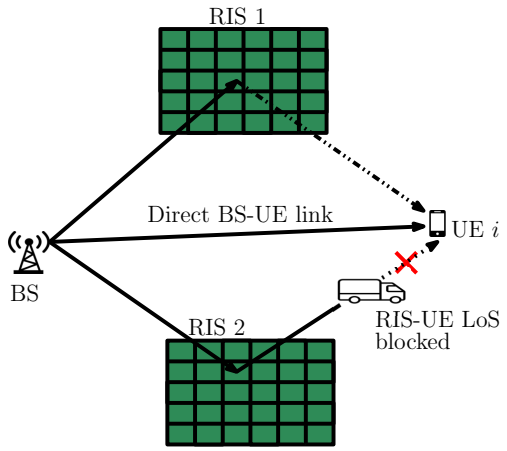

LoS between RIS 2 and UE blocked by dynamic obstacle

Figure 1.7: Dynamic obstacle blocking RIS-UE LoS

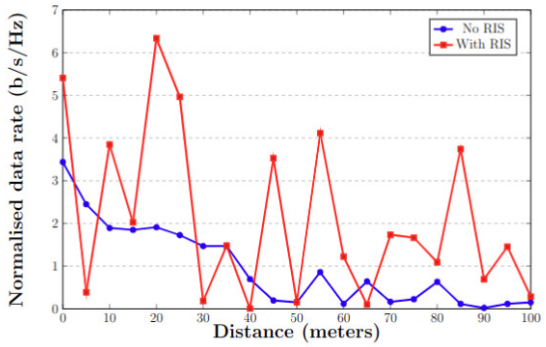

Figure 1.8: Pattern of received data rate (normalized) in the presence of dynamic obstacle as obtained from standard simulation set-up [1]

Dense urban environments characterised by towering urban canyons and a proliferation of dynamic obstacles such as cars and buses can produce richly scattered multipath propagation even at mmWave channels [33, 34, 11]. In these settings, parametric channel estimation

techniques, which aim to recover sparse channel parameters using few pilots, often fail to capture accurate CSI. As a result, traditional channel estimation schemes requiring heavy pilot overhead are used in such network environments[34]. Moreover, the double fading of the reflected mmWave channel and the presence of dynamic obstacles blocking LoS between RIS and UE may render many RISs unusable to certain UEs. In a scenario where multiple RISs are available to the UE [38], utilizing all of them simultaneously incurs extremely high CSI acquisition overhead [39], which consumes a significant amount of channel coherence time, thus leaving little time for actual data communication. In [40], multiple RISs placed on buildings have been used to extend the coverage of the BS to UEs that have no direct LoS with the BS. However, the RIS to UE channel itself is highly susceptible to the losses incurred due to blockage of LoS incurred by obstacles. For example, in Fig. 1.7, the reflected signal from RIS 2 to UE i is blocked by a dynamic obstacle, while had the UE chosen only RIS 1, it would be able to find an optimal path to the configured RIS without the additional CSI acquisition overhead wasted for RIS 2. Uncertainty caused by dynamic obstacles in accessing the RIS causes fluctuations in data rate received at the UE as shown in Fig. 1.8. Moreover, the UEs are unaware of the RIS locations. The UEs are divided into groups and each group share a set of non-interfering RBs, also known as orthogonal RBs. Different UE groups are allocated to orthogonal RBs to mitigate the inter-group interference. In case an RB is shared among a group of UEs each using separate RISs, a UE from that group has to estimate CSI for all the different RISs used by other UEs in the group, which increases the CSI overhead significantly [39]. Therefore, it is important to ensure that UEs using separate RISs are *not* allocated the same RB. Existing CSI based RB allocation mechanisms [29, 41, 42, 43, 44] cluster UEs based on the channel conditions without accounting the RIS chosen, and thereby cannot arrest the downfall of sum data date due to CSI overhead. Therefore, an efficient RIS selection and RB allocation mechanism needs to be developed for integrating NOMA with RIS in dense urban networks.

1.3 Literature review and research gap

1.3.1 RIS placement for mmWave D2D

In [45] authors gave a smart optimization formulation for placing RISs to minimize link outage probability for overcoming obstacles between a mmWave access point and a mobile device in an indoor environment. In [46] the authors have given simulation results on

how placing RISs close to users improves performance. But, they have not given any specific strategy of placement. In [47] the authors have formulated an RIS placement optimization problem to maximize the cell coverage by optimizing the RIS orientation and horizontal distance in a single BS, single-user downlink network. In the context of D2D communication, the idea of exploiting RISs to get energy efficiency has been studied in [48] by investigating the joint power control of the devices and passive beam-forming of the RISs. In [49], the authors have jointly optimized RIS placement and power allocation in D2D network. However, the D2D UEs are considered to be stationary throughout the communication period. This makes the approach proposed by the authors inapplicable for a scenario where the D2D UEs are mobile. In [50] the authors study an RIS assisted D2D network underlying a cellular network. Here, they propose a two-timescale optimization scheme to maximize the D2D ergodic weighted sum-rate (WSR) subject to a given outage probability constrained SINR target for each cellular user. In [34] authors used the ability of the RIS to reconfigure the phase shifts of the elements to create favourable beam steering to mitigate the aggravated interference caused by D2D links that share the same resources with the cellular links. Authors in their work in [51] have studied joint power control, receive beamforming, and passive beamforming for RIS assisted D2D underlying cellular communication systems to maximise the sum rate of the whole system. Authors in [52] developed a genetic algorithm to solve the rate maximisation problem for multiuser wireless networks. It is evident from the above discussion that RISs have been used in many creative ways to enhance the quality of service of wireless networks. More specifically, RISs have been used to cancel interference, avoid obstacles and increase the system sum rate for D2D networks. However, in most of the existing studies, either RISs were already deployed or random deployment of RISs is assumed. Strategically placing RISs can have a great impact on the performance of D2D networks. Properly placing a minimum number of RISs to overcome the hurdle of avoiding obstacles in an environment reduces the expenditure on resources. Proper positioning of RISs can enable better access of these reflectors to devices, thus utilising their full potential.

1.3.2 RIS selection in mmWave D2D

Several RIS selection strategies have been studied in recent works. In [53], authors propose an RIS selection policy where the RIS providing the maximum UE-RIS channel gain resulting in highest signal to noise ratio (SNR) is chosen for each hop in a multi-hop D2D

communication. Authors in [38] propose an algorithm to optimally select a sub set of RISs which aims to minimize the energy consumed by the RISs. In [54, 1], the authors select the RIS that gives the best end-to-end SNR. In all such studies, knowledge of perfect CSI is assumed. However, for multi-RIS networks, obtaining perfect CSI for all RISs consumes a large portion of the communication time interval leaving little time for actual data communication. Hence, an RIS selection strategy that can minimize the CSI overhead as much as possible is needed. In [55], RIS selection based on the knowledge of the UE's and RIS's location information mitigates the need for CSI. RIS providing the minimum pathloss for the cascaded transmitter-RIS-receiver channel is selected. However, the presence of static obstacles that may block the LoS between the RIS and the UE is not considered. Moreover, the status of the LoS between the RIS and the UE changes continuously as the UE moves. Since the RIS is passive and the phase shift design is computed by the BS, continuously updating the location of the UE throughout its trajectory increases the signaling overhead. Furthermore, checking the LoS status of all RISs at each time slot increases the complexity of the selection algorithm. Therefore, an algorithm is needed that considers the obstacles in the environment and can predict the LoS status of the RISs for future time slots. A deep reinforcement learning (DRL) based RIS selection scheme is used in [56] that aims to maximize the total secrecy data volume of D2D users. However, the set of available RISs and the optimal RIS among them keeps changing over time as the UE moves from one location to the other making the environment non-stationary. Convergence of proposed DRL schemes is no longer guaranteed in such scenarios. A deterministic selection algorithm is preferred in such cases. Finally, equipments such as *lidars* and *cameras* may be used to detect obstacles [57] however, these are expensive and energy consuming.

1.3.3 Outdated CSI and mitigating CE overhead

There have been several recent studies on minimizing the CE overhead. In [58] and [59], the authors have proposed an optimal RIS elements grouping to enhance throughput by reducing pilot overhead. In [60], the authors have analyzed the effect of grouping RIS elements on CE overhead. An analytical expression has been derived in [61] to find the optimal number of RIS elements to switch on in a large intelligent surface (LIS) for reducing pilot overhead. Estimating individual RIS assisted channels requires massive pilot overhead and computational complexity for the case where the RIS lacks sensing and signal processing capabilities. To address this, authors in [32] have proposed a novel pilot

transmission protocol and designed two different channel estimation algorithms that provide high accuracy and low pilot overhead. They have considered unstructured channels and used monostatic and bistatic full-duplex BSs for their study. In [62], a hierarchical training reflection design has been proposed to estimate the RIS channel utilizing RIS-element grouping and partition. However, even with reduced pilot overhead the estimated channel still becomes outdated as the UE continuously moves. The studies cited above do not consider the fact that due to the mobility of the UE the estimated channel may become outdated. To design an efficient CE schedule that minimizes CSI overhead, it is essential to quantify how CSI aging degrades throughput in RIS-assisted networks and then optimize the interval between successive estimations accordingly.

Recently many studies have also been done to understand the impact of outdated CSI on RIS-assisted network performance in terms of throughput, secrecy capacity and outage probability. The impact of outdated CSI in the performance of a secure RIS assisted mmWave communication has been studied in [63]. The authors have investigated the effect of outdated CSI on the joint optimization of transmit beamforming and RIS configuration. Their investigation reveals that adequate secrecy capacity can be achieved even with outdated CSI. In [64], the authors have studies a scenario where a passive ground user harvests energy from an unmanned aerial vehicle (UAV) through downlink (DL) channel and transfers information via the uplink (UL) channel. Here, the unavailable DL CSI is estimated by an outdated version of the UL CSI. The authors have proposed a two time scale active and passive beamforming optimization to maximize the ergodic throughput by capturing the effect of outdated CSI. In [65] the authors have derived secrecy outage probability (SOP) to study the resilience of an RIS assisted wireless network to aging CSI. They show that target SOP is achieved even for 10% outdated CSI indicating that channel estimation frequency can be reduced to decrease the system overhead. In [35], the authors propose an RIS deployment mechanism in centralized and distributed cases for outdated CSI. In [66], authors derive a closed form expression for the effective capacity for RIS-enabled mmWave downlink. In [67], an RIS selection strategy has been proposed for UAV based multi-user downlink network with imperfect and outdated CSI. In [68], authors enhance the secrecy rate by jointly optimizing the transmit power and RIS's reflective beamforming considering outdated CSI. The above-cited studies do not provide any insight on the CE timing for the scenario of outdated CSI. Furthermore, all the above cited studies either consider a single UE system or assume that all UEs move with same velocity and only consider a fixed channel coherence depending only on the velocity of a UE [13] as the interval between two consecutive CE.

However, in a multi user network UE speeds vary both across users and over time. Given that channel coherence time depends on the UE velocity, a fixed CE interval across all UEs and for all time may be suitable only for a subset of UEs in the system depending on their velocity. For faster UEs the CSI aging degrades the throughput faster while for slower UEs pilots are sent more often than necessary, wasting precious resources. Therefore, a dynamic CE scheduling strategy that adapts the CE interval based in the changing UE speeds and channel conditions is extremely necessary.

In [69], authors consider time-varying cascaded CE over RIS-assisted communication using structured channel model. They use deep learning for channel extrapolation in both time and antenna domains. However, they do not provide any particular strategy for computing the exact timing for CE. Moreover, the effect of channel conditions, interference and power allocation have not been captured for determining CE timing. In [70], the authors have proposed an algorithm that jointly optimizes the adaptive CE interval and passive beamforming of the RIS by modeling the problem as a bi-level partially observable Markov decision process. At each time step, past observations are leveraged to first decided weather or not to skip CE in that time slot. Next the action corresponding to the passive beamforming at the RIS is chosen. However, their proposed algorithm is designed only for a single UE making the adaptive beamforming inapplicable for multi-UE scenarios. Furthermore, the normalized mean square error of the proposed algorithm increases significantly with increase in channel correlation coefficient. Therefore, to mitigate the massive CSI overhead it is essential to design a dynamic CE scheduling mechanism for a multi user network that captures the impact of outdated CSI on each UE and adjusts the CE interval according to the changing channel conditions for all UEs.

1.3.4 RIS assisted URLLC handover

In the preceding literature, several handover mechanisms have been proposed for 5G cellular networks [71], [72]. However, studies involving both RIS and network selection for URLLC UEs during handover are quite limited. In [73], the authors have given a Q-learning based approach to select among various services in a heterogeneous network. In [74], the authors have studied various handover mechanisms suitable for URLLC users. These existing network selection algorithms consider only the presence of BSs and not BS-RIS pairs. In [75], authors have studied dynamic network selection in multiple RIS assisted environments. However, they have not considered the delay and reliability constraints for URLLC users. In

[76], the authors propose to optimise the handover using frequency offset along with power level. In [77], authors have used machine learning to learn the optimal handover time and destination. But in these works the authors do not consider the impact of RISs. The RIS can improve the reliability of the data transmission but at the same time introduce delay due to CSI overhead and high complexity of the phase shift optimization process. Therefore, an algorithm to decide when to use an RIS during a handover needs to be developed such that the URLLC constraints on reliability and delay are maintained.

1.3.5 RIS selection and RB allocation in urban 5G cellular networks

In RIS-assisted cellular mmWave NOMA systems, resource allocation consists of two essential parts: (a) assigning the UEs to the best RISs and (b) allocating RBs to the UEs after RIS allocation. State of the art RIS selection strategies such as [38, 54, 1, 78] propose RIS selection algorithms to either maximize the network sum rate or the energy efficiency. In [55], RIS selection is based on the knowledge of the UE's and RIS's location information. However, the instantaneous location information of cellular users may not always be available to the BS. Moreover, the above cited algorithms do not consider any RB allocation mechanism. Furthermore, the above cited studies assume that the BS knows the CSI for every RIS-UE cascaded channe. It is to be noted that dense urban "canyons" with moving obstacles (cars, buses) create rich multipath even at 28 GHz, breaking the sparsity assumptions of parametric estimators. Consequently, conventional high–pilot-overhead channel-estimation methods are still required in these environments. Furthermore, due to the double fading, the RIS assisted reflected mmWave link suffers propagation loss. As a result, blockage of RIS-UE LoS due to dynamic obstacles causes severe degradation of the reflected channel gain. The effect of such RIS-UE LoS blockage due to dynamic obstacles has not been considered in the existing RIS selection algorithms. Therefore, it is necessary to develop an RIS selection algorithm that not only reduces CE overhead but also is able to capture the impact of dynamic obstacles.

The RB allocation for RIS assisted NOMA systems have also been studied extensively [79, 80, 29, 44, 41]. In [29, 44], the authors jointly optimize power allocation, beamforming and RB allocation to maximize the sum rate. In [29] a deep and ensemble learning approach is adopted for RB allocation to facilitate the coexistence of eMBB and URLLC users in terahetz NOMA communication system. In [44], the authors consider both uplink and downlink full duplex NOMA system for RB allocation. These existing studies [79, 80, 29,

44], consider the RIS to be always accessible thus not accounting for the fluctuations in channel quality caused by random blockage of the RIS-UE link. Therefore, the choice of RIS should be considered when allocating RBs. The authors proposed a RB allocation and RIS assignment algorithm in [41] for a grant-free NOMA system. Therein, it was essential to estimate the CSI for all UE-RIS channels to optimize RB and RIS assignment, resulting in significant CSI acquisition overhead. Therefore, to enhance mmWave cellular NOMA performance, we need an RIS-RB pairing algorithm that minimizes CSI overhead while explicitly accounting for and mitigating RIS–UE LoS blockages.

1.4 Scope of the thesis

Effectively utilising RIS in real world 5G wireless systems with either mmWave or unstructured channels pose significant operational challenges that need to be overcome to meet required QoS thresholds for various 5G and beyond services. In this thesis, we have identified some of the major challenges and developed algorithms to overcome them. In chapter 2, we address the challenge of strategically deploying RISs in a mmWave D2D network. It is to be noted that in the D2D scenario both the transmitter and the receiver are mobile, whereas the RIS once deployed, remains static in both position and orientation. Furthermore, since RISs consume a non-zero amount of energy, the number of RISs to be used must also be limited. To address this issue, we develop a strategy for placing minimum number of RISs in an environment filled with obstacles such that any pair of devices in the environment who does not have direct LoS can communicate via these RISs by establishing an indirect LoS. Contributions in this chapter can be summarised as follows: First, we model the environment by partitioning the service area into *regions* and then identifying locations or regions in the environment that are *blocked* from each other's view due to the presence of obstacles. We call two such regions as *blind* to each other. So if a transmitter falls in one of these regions and the receiver in the other, they will not have direct LoS. In such case, an RIS is used to bypass obstacles and provide an indirect LoS. Secondly, we develop a *near optimal* strategy for placing a minimum number of poles/towers to mount RISs upon them with proper orientations using *set cover* formulation such that in an environment filled with obstacles, the device pairs that do not have direct LoS can communicate via these RISs by establishing an indirect LoS. This is done as *preprocessing* before the actual devices are deployed in the region. Finally, given a number of devices deployed in the environment, we give an algorithm to select the collection of RISs among all the RISs

placed in the region which can be used to serve the communicating device pairs. All other RISs that are not selected are kept OFF and not used. After selecting the RISs to be in operation, we determine the values of the phase shift of the elements of these RISs and the channel coefficients between the devices and the reflectors such that system sum throughput is maximised. Simulation results show that our strategic deployment of RISs can improve system throughput significantly in comparison to the deployment strategies that deploys RISs only on the walls of the obstacles [52, 81, 82] and a random placement strategy [48].

In chapter 3, we identify that in a mmWave D2D underlay network, complex phase shift design, CE overhead, and potential LoS blockage between RISs and UEs make optimal RIS selection in multi-RIS networks critical. Moreover, as UEs move, the LoS status between the UE and the RIS continuously changes which needs to be taken into account. Challenges such as massive CE overhead and changing RIS-UE LoS status have not been adequately addressed in existing studies on RIS selection. We propose a novel *visibility polygon*-based deterministic RIS selection algorithm to address the above-cited challenges and accordingly select the optimal RIS to maximise the sum rate. The contributions of this chapter are as follows: In a preprocessing step, a visibility polygon is constructed for each RIS and its segments are stored in a segment tree. Utilizing the segment tree, we develop an algorithm to predict the RIS-UE LoS status for a fixed number of future time slots. This allows us to avoid updating location of the UE in every time slot thereby reducing signaling overhead and time complexity for checking the LoS status significantly. Then using the processed data structure, we develop an algorithm that utilizes the predicted LoS status to determine if there exist a common RIS visible to both the UEs in a given D2D pair. If such RISs exist, we select the RIS providing minimum pathloss for the cascaded transmitter-RIS-receiver channel. Our suggested technique only requires the CSI for each RIS to be acquired once, at the start of the communication session. For the remaining part, a UE acquires CSI for the selected RIS only, thereby reducing the CE overhead significantly. In case no such common RIS is found, the D2D pair communicates via the BS with or without the assistance of an RIS depending on its visibility status. Extensive system level simulation shows the superiority of our proposed algorithm over existing CSI based [53, 54, 1] and location based [55] approaches in terms of the achieved sum data rate by all the D2D pairs.

In chapter 4, we address the challenge of massive pilot signal overhead for CE suffered in RIS assisted networks with unstructured channels [32]. In recent studies, the timing for CE has been primarily determined based on the coherence time interval, which is dependent on the velocity of the UE. However, in this chapter we have identified that the effect of

the current channel condition and pathloss of the UEs can also be utilized to control the duration between successive CE to reduce the overhead while still maintaining the quality of service. Therefore, based on the throughput analysis on outdated CSI, an algorithm has been designed to dynamically predict the next time instant for CE after the current CSI acquisition. The contributions of this chapter are summraized as follows: Firstly, when CE is performed, the phase shift of the RIS is optimized using the CSI outdated by a delay due to channel estimation and feedback overhead. We propose to use either the semi-definite programming or a local search based phase shift optimization depending on the acceptable complexity constraints. Next we take into account the degradation in SINR of each UE that occurs when CSI becomes more outdated with passing time and propose a power allocation algorithm that maximizes the sum throughput per bandwidth while satisfying the minimum rate requirement of each UE. After power allocation, the total bandwidth is allocated optimally among UEs to maximize the sum throughput. Finally, we propose an algorithm that returns the number of consecutive time slots in which CE can be skipped. To compute this, the proposed algorithm allocates optimal power and bandwidth for each time slot after the last slot where CE was performed until a time slot is reached beyond which performing CE is unavoidable. We provide detailed complexity analysis and convergence proof for our proposed algorithm. We perform extensive system level simulations and show that the proposed algorithm outperforms the approach with coherence time based fixed inter CE duration [67], [13] and a dynamic CE strategy proposed in [70] in terms of sum throughput over the entire duration of communication. We also show the impact of hardware limitations on the performance of our proposed algorithm.

In chapter 5, we deal with the vital decision of whether or not to take the assistance of an RIS when URLLC service-based UEs switch connection from the current serving cell to a neighbouring cell. To this end, we propose a mechanism to select an appropriate BS or BS-RIS pair to maximise user throughput while satisfying the delay and reliability constraints of URLLC users. The contributions of this chapter is as follows: Firstly, the network selection problem in RIS has been formulated as a non-separable non-linear integer programming problem. Here the objective is to choose an appropriate BS or a BS-RIS to maximise user throughput while the reliability and latency constraints are satisfied. In the formulated non-separable non-linear integer programming problem, quantities like number of re-transmissions depends on channel qualities which are unknown in advance. To deal with such a scenario, a contextual adversarial bandit formulation for network selection has been proposed. The goal of this formulation is to enable instant decision making based on a

multi arm bandit (MAB) and to achieve the near optimal performance over time. Based on the formulation, a network selection strategy has also been proposed. Extensive system level simulations confirm that the proposed scheme outperforms the traditional received signal strength based handover scheme [83] in terms of reliability and delay.

In chapter 6 and chapter 7 we focus on RB allocation in RIS assisted networks. In chapter 6, we investigate RB allocation in orthogonal multiple access (OMA) networks. The objective of this chapter is to establish that the existing RB allocation mechanism considering only the direct BS-UE channel conditions are not suitable for RIS assisted networks. In an RIS assisted environment, the RB allocation based solely on the direct channel condition may not be optimal. This is because, a distant UE can achieve a high throughput through the indirect channel even if the direct channel condition is not good. In this chapter, first, we formulate the RB allocation problem in RIS assisted environment as a multi arm bandit (MAB) problem. Then based on the MAB formulation, we develop a two-phase ϵ-greedy algorithm which explicitly considers the throughput achievable through the indirect channel while selecting RBs. In exploitation phase, it selects the RB providing maximum reward with a probability $1-\epsilon$. In exploration phase, any available RB is selected randomly with a probability ϵ. Finally, through extensive system level simulations, we have shown that our proposed algorithm performs better than an widely adopted proportional fairness based RB allocation mechanism [84] which only utilises the direct BS-UE CSI. In chapter 7, a resource allocation algorithm is proposed in mmWave cellular NOMA systems, where each UE selects an appropriate RIS using the multi-agent multi-arm bandit framework accounting both channel gain and possibility of LoS blockage by the dynamic obstacles. The UEs are then grouped according to the selected RIS. Subsequently, RBs are allocated to UE groups with the aim to maximize the sum rate, ensuring that the UEs with the worst channel conditions receive the requested data rate, by solving the underlying maximum weight bipartite matching problem. By assigning each group of UEs to a single RIS and grouping their RB allocation accordingly, we eliminate the need to estimate every individual UE–RIS channel. Simulation results show that the proposed algorithm outperforms the UE clustering based algorithm [41] in terms of sum data rate and proportion of UEs achieving the required data rate. Our proposed RIS and RB pair allocation mechanism will be highly helpful for the mobile operators towards serving stringent data rate requirements of eMBB services in RIS assisted 5G systems.

1.5 Thesis organisation

In chapter 1, we formally introduce various operational challenges faced when using RISs for improving the performance of eMBB and URLLC services. In chapter 2, we address the challenge of RIS placement in mmWave D2D networks. In chapter 3, some major limitations involved in RIS selection for mmWave D2D have been identified and resolved. In chapter 4, a time-varying channel estimation algorithm considering outdated CSI has been developed to reduce massive pilot overhead and improve throughput. In chapter 5, a jont RIS-BS selection algorithm based on C-MAB has been developed to ensure successful handover of URLLC based UEs without violating latency constraints. Chapters 6 and 7 address the challenge of massive CSI overhead encountered during optimal resource block (RB) allocation in RIS-assisted networks. Chapter 6 establishes that both direct BS-UE and RIS assisted channel information are needed for optimal RB allocation in RIS assisted network. In chapter 7, a RIS-RB pair allocation algorithm has been proposed for mmWave NOMA systems that maximises the aggregate system throughput without incurring unessecarry pilot overhead. Finally, chapter 8 concludes the thesis and also provides a discussion on future research directions.

Chapter 2

RIS placement in mmWave D2D[1]

RISs, once deployed on the surfaces of buildings, remain stationary, while the UEs that utilise the RIS are mobile and may move to a location where the deployed RIS is no longer useful. In this chapter, we address the challenge that arises due to the stationarity of a RIS deployed in a D2D network where both transmitters and receivers are mobile. To mitigate this, we develop a strategy for placing a minimum number of RISs in an environment filled with obstacles such that any pair of devices in the environment without direct LoS can communicate via these RISs. We model the wireless environment by partitioning the network region into distinct, equal sized square zones. Then we construct a visibility graph to identify the pair of zones that do not have LoS with each other and mark them as blind pairs. We develop a near optimal strategy based on set cover to install poles/towers upon which RISs will be mounted. This strategy aims to minimize the number of poles or towers required for mounting RISs and determines their appropriate orientations. The objective is to ensure that any pair of regions that are blind to each other can still communicate via at least one RIS. This deployment is carried out as an offline preprocessing step, prior to the actual deployment of user devices. Finally, we propose an algorithm for RIS selection, which activates only a subset of the pre-deployed RISs that are necessary to support the current set of communicating device pairs. The remaining RISs are kept inactive to reduce overhead. Simulation results show the superiority of our proposed algorithm over the strategies that deploy RISs only on the walls of the obstacles and a random placement strategy.
The symbols used in this chapter and their respective meaning are given in Table 2.1.

[1]This chapter is based on the following publication:
Souvik Deb and Sasthi C. Ghosh, "An RIS deployment strategy to overcome static obstacles in millimeter wave D2D communication," **The 20th IEEE International Symposium on Network Computing and Applications (IEEE NCA 2021)**, Boston, MA, USA, pp. 1-8, 23-26 November 2021.

Table 2.1: Important notations for Chapter 2

Symbol	Meaning	Symbol	Meaning
TX	Transmitter	RX	Receiver
N	Number of grid rows	M	Number of grid columns
z	Zone index	$r_{\max}$	Maximum communication distance
Δt	Duration of one time slot	θ_b	Beamforming angle of a transmitter
ψ	Orientation of TX–RX line w.r.t. horizontal axis	$l = (z_1, z_2)$	Requesting zone pair (TX in z_1, RX in z_2)
Z	Set of all requesting zone pairs	n	Number of requesting pairs, $n = \|Z\|$
R	Set of RIS-mounted locations	m	Number of locations with at least one RIS
m_i	Number of RIS elements on RIS at i	$\mathcal{W}$	Total RIS elements
$\mathbf{g}_l^i$	Channel vector from TX of pair l to RIS i	$\mathbf{f}_r^i$	Channel vector from RIS i to RX of pair r
$\mathbf{g}_l$	Concatenated channel vector to all RISs	$\mathbf{f}_r$	Concatenated channel vector from all RISs
h_{lr}	Direct channel coefficient from TX of l to RX of r	$\mathbf{\Theta}$	Phase shift matrix
ϕ_i	Phase-shift angle for RIS element i	η	Reflection coefficient of each RIS element
P_l, P_i	Transmit powers of requesting pairs l and i	σ^2	Additive Gaussian noise power
z_l	SINR at receiver of pair l	$\mathbb{V}$	Set of all vertices in the visibility graph
P_z	Points in $\mathbb{V}$ within $r_{\max}$ from z	I	Set of blind zone pairs
L	Set of obstacle boundary segments	$A = (a_{ij})$	Visibility matrix
T_R	Range tree of segment endpoints	I_h	Interval tree for horizontal segments
I_v	Interval tree for vertical segments	$\mathcal{F}$	Segments returned by window query
k'	Number of segments intersecting query rectangle	$\mathbb{CL}$	Set of candidate RIS locations
$j\gamma$	Orientation angle of RIS	γ	Minimum tunable orientation step
C_{zj}	Blind pairs served by RIS at z with orientation $j\gamma$	C	Effective (location, orientation) pairs
$B_{z_1 z_2}$	All pairs that can serve blind pair (z_1, z_2)	B	Set of coverable blind pairs
$Cover_z$	Blind pairs coverable from location z		

2.1 System model

We assume that the region of interest is a rectangle and is subdivided into smaller square zones or grids of unit size as shown in Figure 2.1. We assume there are N rows and M columns of these grids or zones. The zones are identified by the co-ordinate of their centers and the bottom left most zone's center is considered the origin. We consider that there is a base station (BS) in the environment that knows the locations and channel state information (CSI) of the devices. The devices that are to operate in this environment are assumed to

be equipped with highly directional antennas. For practical purpose, it is also assumed that devices that are more than r_{max} (typically 30 to 40 meters) distance apart cannot communicate with each other even if a direct LOS exists between them as the mmWave signal would get highly attenuated and the received signal to interference plus noise ratio (SINR) will be below the required threshold. The time is considered to be discretized into slots each with a small Δt time span.

2.1.1 Mobility of the devices

The devices are assumed to be pseudo-stationary as in [85]. That is, during a time slot in which two devices communicate they do not move outside their zones. However, while remaining inside the zones, during a time slot, the devices may follow any mobility model. Such assumption of mobility has been widely used in many studies such as [86, 87, 88]. Since the data rate is huge (order of Gbps) and Δt is very small (order of milliseconds), this is not an impractical assumption in mmWave D2D communication. Position of a device in some unit zone is approximated by the center of the zone. Henceforth when we say a device is in zone z we will mean the device is located at the center of that zone and z represents the center point.

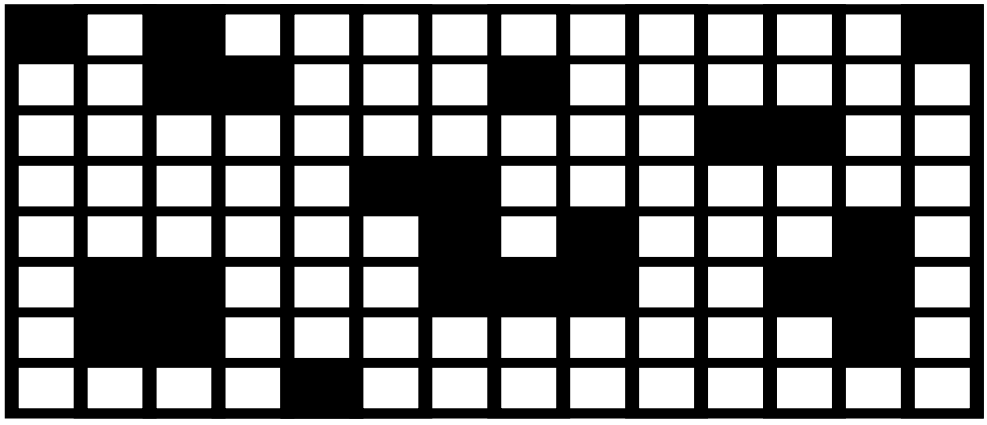

Figure 2.1: Environment subdivided into square zones and obstacles modelled as blacked-out zones

2.1.2 Obstacle model

Zones that consist of a part of the obstacles are marked black as shown in Figure 2.1 and are considered blocked or covered by an obstacle. No devices can be placed in blocked zones.

That is, we consider an outdoor environment. RISs cannot be placed in blocked zones which are surrounded by other blocked zones from all sides. Multiples such blocked zones together form the polygon approximating the shape and size of the obstacle. The location of these blocked zones are assumed to be known through satellite imagery [89]. The white zones in Figure 2.1 are free zones where there can be devices or which can be the candidate locations for setting up poles to mount RIS upon. RISs can also be mounted on the boundary wall shared between a blocked zone and free zone.

2.1.3 Critical Region

Let θ_b be the beam-forming angle of the transmitter. Let the line segment joining the transmitter and the receiver is in orientation ψ with respect to the horizontal x-axis. As shown in Figure 2.2, the sector with radius r_{max} centered at transmitter and bounded by line segments at angles $\psi - \frac{\theta_b}{2}$ and $\psi + \frac{\theta_b}{2}$ is the critical region of this transmitter, as defined in [86]. The transmitter can cause interference to any receiver that falls inside its critical region. When a device pair (a, b) communicates via an RIS c the critical region is a union of two regions. First region is the sector as defined above between a and c where a acts as the transmitter and c acts as the receiver. The second region is the sector where c acts as the transmitter and b acts as the receiver.

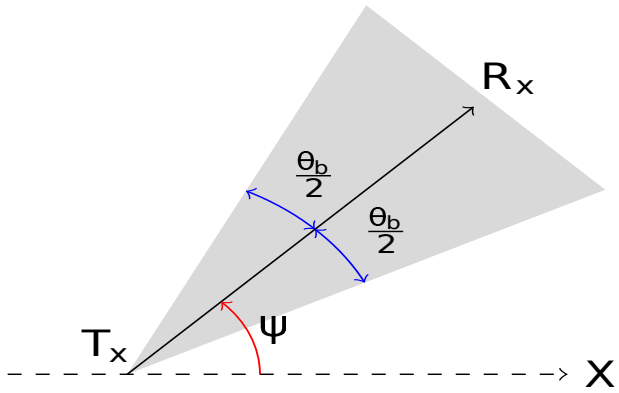

Figure 2.2: Critical region of interference

2.1.4 Channel model

Let there are n device pairs that want to communicate at a particular time slot. Suppose the transmitter and receiver of one such device pair lies in zone z_1 and z_2 respectively. Then

we say that the zone pair $l = (z_1, z_2)$ is a requesting zone pair. Let Z be the set of all such requesting zone pairs, where $n = |Z|$. Let R be the set of all locations that has at least one RIS installed, where $m = |R|$. An RIS may be installed either on a pole in a free zone or on the boundary wall shared between a blocked zone and free zone. Let i^{th} location has m_i elements combining all the RISs in that location and $\mathcal{W} = \sum_i m_i$. We consider $\mathbf{g^i}_l \in \mathbb{C}^{m_i}$ and $\mathbf{f^i}_r \in \mathbb{C}^{m_i}$ as the channel coefficients from transmitter of device pair l to the elements of the RISs in i^{th} location and from elements of the RISs in i^{th} location to receiver of device pair r respectively. The channel coefficient from the transmitter of device pair l to the receiver of device pair r is defined as $h_{lr} \in \mathbb{C}$ as in [48]. Hence the channel coefficient vectors from the transmitter of device pair l to all the RIS elements and from all the RIS elements to the receiver of device pair r are $\mathbf{g}_l = (\mathbf{g^1}_l, \mathbf{g^2}_l, ..., \mathbf{g^m}_l) \in \mathbb{C}^{\mathcal{W}\times 1}$ and $\mathbf{f}_r = (\mathbf{f^1}_r, \mathbf{f^2}_r, \mathbf{f^3}_r, ...\mathbf{f^m}_r) \in \mathbb{C}^{\mathcal{W}\times 1}$ respectively.

2.1.5 Calculating the channel coefficients

As the transmitters are highly directional in nature, two device pairs interfere with each other iff the receiver of one pair falls in the critical region of the transmitter of another. Hence, we calculate the channel coefficients accordingly as follows.

If l is a requesting pair communicating via an RIS of location i,

- $h_{ll} = 0$.
- $h_{jl} = 0 \,\forall\, j$ such that receiver of requesting pair l is not in critical region of the transmitter of requesting pair j.
- $\mathbf{f^k}_l = \mathbf{g^k}_l = \mathbf{0} \,\forall\, k \neq i$.
- $\mathbf{g}_j = \mathbf{0} \,\forall\, j$ such that requesting pair j does not choose any RIS of location i.

If l is a requesting pair communicating directly

- $\mathbf{g}_l = \mathbf{0}$.
- $\mathbf{g}_j = \mathbf{0} \,\forall\, j$ such that receiver of requesting pair l does not fall in critical region of the transmitter of requesting pair j.
- $h_{jl} = 0 \,\forall\, j$ such that receiver of requesting pair l is not in critical region of the transmitter of requesting pair j.

- $\mathbf{f^k}_l = \mathbf{0} \, \forall \, k$ such that receiver of requesting pair l does not fall in critical region of any transmitter that communicates via an RIS of location k.

All other non-zero channel coefficients are computed using standard channel estimation methods as described in [90].

2.1.6 Calculating the phase shifts

As stated in [48], the phase-shift matrix for the elements of all the RISs can be computed as the diagonal matrix $\mathbf{\Theta} = \sqrt{\eta} diag(\boldsymbol{\theta})$, where $\boldsymbol{\theta} = (\theta_1, \theta_2, \cdots, \theta_L)^H$. Each θ_i here is a complex number $e^{j\phi_i}$ where ϕ_i lies in the interval $[0, 2\pi]$ and is called the phase shift of i^{th} element [48]. Here $|\theta| = 1$ and η is the reflection coefficient of each element of the RISs.

2.1.7 Calculating the maximum sum throughput

The SINR z_l received at the receiver of requesting pair l is computed as given in [48]

$$z_l = \frac{|h_{ll} + f_l^T \mathbf{\Theta} g_l|^2 P_l}{\sigma^2 + \sum_{i=1(i \neq l)}^{n} \zeta_{il} |h_{il} + f_l^T \mathbf{\Theta} g_i|^2 P_i}. \tag{2.1}$$

Here P_l and P_i are transmission power of the transmitters of requesting pairs l and i respectively and σ^2 is the Gaussian noise factor. We set $\zeta_{il} = 1$ if the receiver of pair l falls inside the critical region of pair i. Using Shannon's capacity formula, we can get the throughput for a given requesting pair and adding over all pairs we get the system sum throughput. After calculating the channel coefficients as described in Subsection 2.1.5, we can compute the phase shifts as described in Subsection 2.1.6 and system sum throughput using Shannon's capacity formula using the algorithm in [48]. Given as input the set of requesting pairs Z and set of available RISs R, let us denote this procedure as *Max_Sum_Throughput(Z,R)*. We will make use of this procedure later.

2.2 Strategic deployment of RISs

Before actually deploying the devices we wish to do some pre-processing and find out the best locations where we can deploy the RISs. The RISs can be mounted either on a pole setup at the center in a free zone or can be placed on the boundary walls shared between a blocked zone and free zone. To begin with we first compute the *visibility graph* corresponding to

such locations where we mount the RISs in the considered region. Furthermore, we have also assumed that the location of a device in a free zone is approximated by the center point of that zone. After computing the visibility graph we can find pairs of location points which are blind to each other that is their LOS is blocked by obstacle and try to deploy the RISs such that most of these blind pairs are served by the RISs. We consider free zones along with boundary walls of obstacles because when the RIS is mounted on a boundary wall it can face only a fixed direction and thus it can cover only 180° region in front of it. This may lead to certain blind pairs to lie in such a position with respect to the RIS on the wall that they cannot be served by the said RIS. However, in a free zone more than one RISs can be mounted on a tall pole in different angles thus making it possible to have an RIS face any direction in the 360° region surrounding the free zone. This allows us to cover blind pairs that could not be covered by just RISs on the boundary walls.

2.2.1 The visibility graph

First we wish to construct the *visibility graph*. The vertices of the graph are location points which are the center points of the squares representing the free zones and the mid-points of the line segments sharing boundary between blocked and free zones. The mid-points of such line segments represent locations (walls of the buildings) on which RISs can possibly be mounted. The center points of free zones represent locations where a pole can be set up upon which RISs can be mounted. Let $\mathbb{V}$ be the set of all such vertices. An edge between two vertices represent that the corresponding location points are visible to each other. We compute the *visibility matrix* as described below. Let $L = \{l_1, l_2, \cdots, l_n\}$ be the set of horizontal and vertical line segments constituting the boundaries of the obstacles. We consider that two location points $z_1 = (x_1, y_1)$ and $z_2 = (x_2, y_2)$ are visible to each other iff the line segment z_1z_2 does not intersect any line segments in L. For a location point $z \in \mathbb{V}$ we consider a function *Finding Circle* for finding a set of location points in $\mathbb{V}$ called P_z which are at a max distance of r_{max} from the location point z. As the radius of the circle is fixed there can be at most a constant k number of elements in P_z. After computing P_z for a location point z, for each p in P_z, we check whether p is visible or not from z using a function *Not_Visible* as described below. If reported invisible and if both points are centers of free zones, we add that pair of points (p, z) in the set of blind pairs I. At the same time we also modify the $|\mathbb{V}| \times |\mathbb{V}|$ visibility matrix $A = (a_{ij})$ as follows: $a_{ij} = a_{ji} = 0$ if (i, j) is a blind pair and 1 if they are visible. Initially a_{ij} was set to -1 for

all pairs. Hence, if a_{ij} remains as -1 that means the zones are at a distance beyond r_{max} and hence cannot communicate regardless of whether they are visible or invisible. The method for constructing the visibility graph is formally stated in Algorithm 1.

Algorithm 1: The visibility graph.

Input: $L = \{l_1, l_2, \cdots, l_n\}$, T_R, I_h, I_v,$\mathbb{V}$
Output: Visibility matrix A and set of blind pairs I

```
Initialize A with a_ij = −1 ∀ij and set I = ∅;
for all z = (x_1, y_1) ∈ V do
    Set P_z =Finding Circle(z);
    for all p = (x_2, y_2) ∈ P_z do
        if Not_Visible(p, z)= True and a_pz ≠ 0 then
            Set a_pz = a_zp = 0;
            if z and p are center of a free zone then
                Set I = I ∪ (p, z);
            end
        end
        else
            if a_pz = −1 then
                a_pz = a_zp = 1;
            end
        end
    end
end
```

Now we describe the function *Not_Visible* to check the visibility of a given pair of points (z_1, z_2). We store end points of all line segments in L in a range tree T_R with fractional cascading [91]. The x coordinates of the end points of the horizontal segments and y coordinates of vertical segments form closed intervals. These intervals are stored in interval trees [92] I_h and I_v respectively along with their associated priority range tree [93] of the end points of segments as described in [94]. Given a rectangle we can use the windowing query algorithm [94] to report all segments which partly or fully lie inside the rectangle. For given segment z_1z_2, the function *Not_Visible* returns true if z_1z_2 intersects any segment in L else returns false. Querying complexity is $O(log^2(n) + k')$ time where k' is the number of segments lie inside the query rectangle. Hence, for all free zones the Algorithm 1 will run for $O(MN(log^2(n) + K))$ time in worst case where K is the maximum number of segments queried over any iteration.

Algorithm 2: Not_Visible(z_1=(x_1, y_1), z_2=(x_2, y_2))

Input: $L = \{l_1, l_2, \cdots, l_n\}$, T_R, I_v, I_h
Output: True or False

$Intersect = False$;
if z_1z_2 *is horizontal that is* $y_1 = y_2$ **then**
    Run horizontal query $[x_1, x_2] \times y_1$ on I_v;
    if *query is non empty* **then**
        $Intersect = True$;
if z_1z_2 *is vertical that is* $x_1 = x_2$ **then**
    Run vertical query $x_1 \times [y_1, y_2]$ on I_h;
    if *query is non empty* **then**
        $Intersect = True$;
if z_1z_2 *is neither vertical nor horizontal* **then**
    Run window query $[x_1, x_2] \times [y_1, y_2]$ using T_R, I_v, I_h and store result in $\mathcal{F}$;
    if $\exists\ f \in \mathcal{F}$ *that intersects with* z_1z_2 **then**
        $Intersect = True$;
Return $Intersect$;

2.2.2 Candidate locations

We now define the set of *candidate* locations. All location points $z \in \mathbb{V}$ in which RISs can be potentially deployed either upon a pole in case its a center point of a free zone or on the wall of an obstacle in case its the mid-point of a boundary segment shared between a blocked zone and a free zone are called *candidate* locations. We denote this set by $\mathbb{CL}$.

For each location point $z \in \mathbb{V}$ corresponding to the center of a free zone we want to know weather that point can be a potential location for placing a pole or tower to mount RISs on it. The poles to be placed are of a fixed height and the RIS is mounted on top of the pole. We mount the RIS having a tilt such that the plane of the ground and the plane of the flat surface of the RIS makes an acute angle. We assume that the RISs placed in such a location can be set to be mounted in any orientation angle around the axis parallel to the pole from the interval $(0^\circ, 360^\circ)$. We define the smallest tuned angle to be γ with respect to the horizontal axis. This means that an RIS can be now placed at such a location at a specific orientation $j\gamma$ where j runs from 0 to $\lfloor \frac{360^\circ}{\gamma} \rfloor - 1$. It is evident that an RIS has a *reflective side* and a *non-reflecting* side. Assume the x-y plane is parallel to the plane of the ground. If we take $z = (x, y)$ as the origin with the horizontal being the x-axis (aligned with the RIS)

and the vertical being the y-axis, we consider the side of the RIS facing the positive y-axis as the *reflective side*. If we consider a zone z_1 with co-ordinates of the center as (x_1, y_1) then by the rotation of axes $(x_1 - x)sin(j\gamma) + (y_1 - y)cos(j\gamma) > 0$ means that the zone z_1 faces the *reflective side* of the RIS placed at the center of zone z having co-ordinates (x, y). The subset of blind pairs I that can be served by an RIS placed at location point z with orientation $j\gamma$ can be computed as:

$$C_{zj} = \{(z_1, z_2) \in I | \text{ and criteria 1 and 2 are satisfied}\}$$

Criteria 1: Both z_1 and z_2 are visible from z.
Criteria 2: Both z_1 and z_2 are on the reflective side of the RIS with orientation $j\gamma$ placed at the center of z.

For $z \in \mathbb{V}$, corresponding to a mid-point of a boundary line segment shared between a blocked zone and a free zone an RIS can only be mounted on the boundary wall which is facing a free zone. So such an RIS can be mounted at a specific orientation $j\gamma$ coinciding with the orientation of the boundary line with respect to the x-axis. We can now compute C_{zj} as described above assuming that the RIS is placed at the mid-point of the line segment representing the boundary wall.

Note that $z \in \mathbb{V}$ and an orientation j pair can be considered for placing an RIS only if that pair can serve at least one blind pair. Let $C = \{(z, j) : |C_{zj}| \geq 1\}$ be the set of all such *effective* (location, orientation) pairs. Let z_1 and z_2 be center points of two free zones then, $B_{z_1 z_2} = \{(z, j) : (z_1, z_2) \in C_{zj}\}$ is the set of all (location, orientation) pairs which can serve the blind pair (z_1, z_2). It is evident that a blind pair (z_1, z_2) can be served only if $|B_{z_1 z_2}| \geq 1$. Let $B = \{(z_1, z_2) : |B_{z_1 z_2}| \geq 1\}$ be the set of all blind pairs which can be served by at lease one (location, orientation) pair. We call B as the set of *coverable* blind pairs. Let us define $Cover_z = \bigcup_j C_{zj}$ such that $(z, j) \in C$ to be the subset of the set of coverable blind pairs B whose elements can be covered by the RISs placed at location z. If we consider $Cover_z$ as the given subsets and B as the universal set, then our problem boils down to the problem of finding minimum number of subsets which can cover all the elements of B. That is, the RIS deployment problem under consideration is equivalent to the set cover problem, which is a well known NP-hard problem.

2.2.3 Strategic deployment of the RISs

The objective is very simple. We wish to cover as many blind pairs as possible by strategically deploying as small RISs as possible to get a cost effective deployment of RISs in the environment. As this is pre-processing stage, we are not considering the actual position, number and density of the devices that will be later deployed in the environment but our strategy for placing RISs is completely based on the position and distribution of obstacles in the environment. A subset of RISs will later be selected for operation depending on the set of device pairs that want to establish communication.

The RISs are themselves very cheap and cost effective. For $z \in \mathbb{CL}$ corresponding to a free zone, the real cost is setting up the poles upon which the RISs will be mounted. Again, in case z is a mid-point of a boundary segment as mentioned in Subsection 2.2.2 then we simply mount an RISs on the wall represented by that segment facing a free zone. Our objective therefore primarily focuses on minimizing the number of candidate locations to be selected to mount RISs. We define the following variables for our optimization problem.

$$x_{zj} = \begin{cases} 1, & \text{if } z \in \mathbb{CL} \text{ with orientation } j\gamma \text{ is selected} \\ 0, & \text{otherwise.} \end{cases} \tag{2.2}$$

$$y_z = \begin{cases} 1, & \text{if at least one RIS is placed at } z \in \mathbb{CL} \\ 0, & \text{otherwise.} \end{cases} \tag{2.3}$$

The optimization function then becomes as below:

$$\min \sum_{i \in \mathbb{CL}} y_i$$
$$\text{subject to:}$$

$$\sum_j x_{zj} \leq \lfloor \frac{360^\circ}{\gamma} \rfloor \, \forall \, z \in \mathbb{CL} \tag{2.4}$$

$$\sum_{(z,j):(z_1,z_2) \in C_{zj}} x_{zj} \geq 1 \, \forall \, (z_1, z_2) \in B \tag{2.5}$$

$$x_{zj} \leq y_z \, \forall \, (z, j) \in C \tag{2.6}$$

$$x_{zj} \in \{0,1\} \, \forall (z,j) \text{ and } y_z \in \{0,1\} \, \forall z \tag{2.7}$$

Constraint (2.4) gives an upper bound on the number of RISs to be installed in location z. Constraint (2.5) represents that a blind pair in B must be covered by at least one chosen RIS in some location z having some orientation $j\gamma$. Constraint (2.6) ensures that $y_z = 1$ if location z with some orientation $j\gamma$ is selected. We can clearly see that this formulation is actually a variation of the set cover problem with B as the universal set and $Cover_z = \bigcup_j C_{zj}$ as the subsets. Therefore, we adopt the well-known greedy algorithm (one of the best possible greedy algorithm for set cover in terms of the approximation ratio [95]) for set cover to get an approximate solution to the problem of strategic deployment of RISs. The approximation ratio is $O(\ln |B|)$, where $|B|$ is the cardinality of the set of coverable blind pairs B. The algorithm is formally stated in Algorithm 3. Algorithm 3 picks the location z that together with all its orientations covers the maximum number of uncovered blind pairs, marks the location z as chosen and marks the set $cover_z$ of all blind pairs which can be covered by RISs placed in that location z together with all its orientations as covered. The process is repeated until all blind pairs are covered.

Algorithm 3: Strategic deployment of RISs (SDR)

Input: The set of blind pairs B, C_{zj} for all $(z, j) \in C$
Output: Locations and orientations of the RISs.

$Selected = \phi$;
$CL = \{z : \exists\, j \text{ such that } (z, j) \in C\}$;
for *each* $z \in CL$ **do**
    $Cover_z = \{\bigcup_j C_{zj} : (z, j) \in C\}$;
while $B \neq \phi$ **do**
    Choose $z = \arg\max_x \{|B \cap Cover_x| : x \in CL\}$;
    $CL = CL \setminus \{z\}$;
    $B = B \setminus Cover_z$;
    $Selected = Selected \cup \{(z, j) : (z, j) \in C\}$;
Return $Selected$ and $Cover_z \, \forall\, z \in Selected$

The greedy Algorithm 3 runs in $O((MN)^3)$ time in the worst case.

2.3 Selecting RIS for operation

In the above section, as a pre-processing step, we have found the set of RISs that is necessary to cover all the *coverable* blind pairs existed in the environment. However, at a given time

slot, only a certain number of device pairs need to establish communications. Assume that the transmitter and receiver of one such device pair lies in zone z_1 and z_2 respectively. Then we say that the zone pair (z_1, z_2) is a requesting zone pair. Let Z be the set of all such requesting zone pairs. Given the visibility matrix $A = \{a_{ij}\}$ as computed by Algorithm 1 and the set of coverable blind pairs B, we can construct the set $D = \{(z_1, z_2) : (z_1, z_2) \in Z \cap B\}$ of requesting pairs which are coverable. Let $\mathcal{B} = \bigcup_{(z_1,z_2)\in D} B_{z_1 z_2}$ where $B_{z_1 z_2}$ is the set of all (z, j) pairs which can serve the blind pair (z_1, z_2).

For $(z_1, z_2) \in Z$ with $a_{z_1 z_2} = 1$, direct LOS exists and hence they communicate without the help of RISs. For $(z_1, z_2) \in Z$ with $a_{z_1 z_2} = -1$, the distance between z_1 and z_2 is more than r_{max} and hence they can not communicate. As a results, these requesting pairs are not in D. We can find the subset Sel_OP that would cover the blind pairs in D simply by calculating $\mathcal{B} \cap Selected$ where the set $Selected$ is returned by Algorithm 3. Then after calculating the channel coefficients as described in 2.1.5, we compute the phase shift matrix $\mathbf{\Theta}$ and system sum throughput for a given power of transmissions of the devices by calling the procedure *Max_Sum_Throughput*(D, Sel_OP) as described in Subsection 2.1.7. This procedure is formally described in Algorithm 4.

Algorithm 4: RISs selected for operation and phase shift optimization

Input: Set Z, D, $\mathcal{B}$, $Selected$ and $Cover_z \; \forall \, z \in Selected$

Output: Set of RISs selected for operation and their channel coefficients and phase shifts

$Sel\_OP = \mathcal{B} \cap Selected$;
for *each blind pair* $(z_1, z_2) \in D$ **do**
    Find location z such that $(z_1, z_2) \in Cover_z$;
    Choose location z to serve the blind pair (z_1, z_2);
Compute channel coefficient as in 2.1.5;
Call *Max_Sum_Throughput*(Z,Sel_OP);

2.4 Simulation results

For our simulation we consider a $1000m \times 1000m$ square area. We assume each zone is a square of size $10m$. The threshold distance r_{max} is considered to be $40m$ hence, receivers which are more than $40m$ away from transmitters or reflectors do not receive signals with enough power to overcome the SINR threshold for communication. We assume the D2D

Table 2.2: 3GPP Urban Macro (UMa) Parameter Assumptions for Simulation (Based on TR 38.901)

Parameter	**Value**	**Unit/Note**
Minimum BS-UE 2D Distance	35	m
Reference Distance for Path Loss	Implicit (close-in ≈ 1)	m
Shadow Fading Std. Dev. (σ_{SF}) - LOS	4	dB
Shadow Fading Std. Dev. (σ_{SF}) - NLOS	6	dB
Mobility Model	Random Waypoint or Uniform	(UEs move at constant speed)
Delay Spread ($\mu_{\lg DS}$) - NLOS	-6.83	$\log_{10}$(s)

communication to be in 60 GHz frequency and a bandwidth of 500 MHz as in [96]. The transmit power of the devices is considered to be 23 dBm as in [34]. The other channel parameters are assumed as below according to the two scenarios that we will compare. The simulation parameters are depicted in Tables 7.2 and 2.3.

Scenario 1: (*Proposed Strategy*): In this case the RISs are placed in the environment based on our strategy. Hence, we can either get direct LOS between the transmitter and receiver or an indirect LOS via an RIS. Here we consider a Rician fading channel with Rician factor β tending to infinity as we are considering the layout of the environment where LOS component dominates. We consider a path loss exponent $\alpha = 1.88$ for obstacle free LOS path and SINR threshold of 15 dB as used in [85]. The additive Gaussian noise at the receivers is taken as $\sigma^2 = -117\, dBm/Hz$ as in [48].

Scenario 2:(*Random Placement*): In this case the RISs are placed arbitrarily in geographically separated locations as considered in [48]. Here static obstacles are not mapped, the channels follow Rician fading with Rician factor 2 and path loss exponent is considered as 4 [48]. The SINR threshold is taken as 15 dB like in Scenario 1.

Scenario 3: (*Deployment only on walls*): In works such as [52, 81, 82] all RISs are deployed only on the walls of the obstacles, which is the most widely adopted convention. In these studies no particular idea on selecting walls to mount RISs has been proposed. In our study we place on walls the same number of RIS as computed by our proposed algorithm in such a way that it covers as many blind pairs as possible. In this scenario the parameters are

Table 2.3: Simulation parameters and values for chapter 2

Parameter	**Value**
Simulation Area	1000×1000 m (square area)
Zone Size	10×10 m (square zones)
Threshold Distance (r_{max})	40 m
D2D Communication Frequency	60 GHz
Bandwidth	500 MHz
Transmit Power	23 dBm
SINR Threshold	15 dB
Additive Gaussian Noise (σ^2)	-117 dBm/Hz
RIS Reflection Efficiency (η)	0.8
RIS Elements	4 (2-bit resolution) per RIS
Smallest Tuned Angle (γ)	10 degrees
Rician Fading Factor (β)	$\rightarrow \infty$
Rician Fading Factor (β) (Scenario 2)	2
Path Loss Exponent (α)	1.88
Path Loss Exponent (Scenario 2)	4

considered to be same as in Scenario 1 and all the walls of the obstacles are considered as candidate locations for placing RISs.

The RIS reflection efficiency in all scenarios is taken as $\eta = 0.8$ and we assume that each RIS has 4 elements with 2-bit resolution. We also assume that the value of smallest tuned angle $\gamma = 10^{\circ}$.

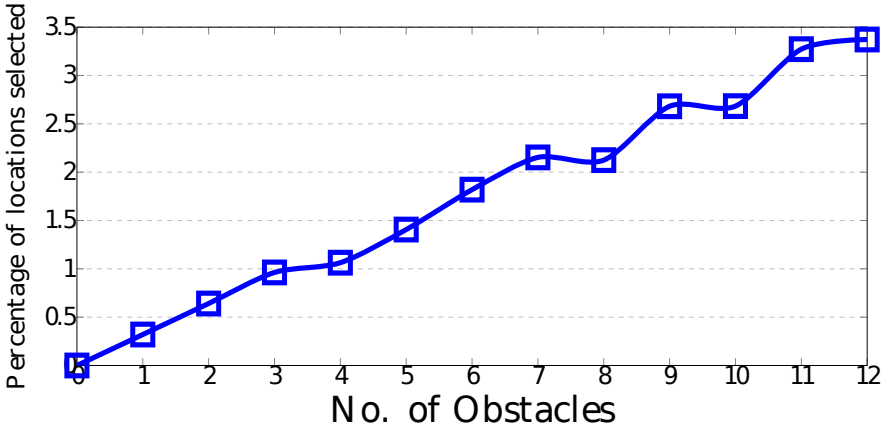

Figure 2.3: Percentage of locations selected vs. number of obstacles

Figure 2.3 shows the percentage of locations selected out of total number of candidate locations for placing RISs for varying number of obstacles. We see that when the number

of obstacles is low we need only a few locations to cover all the blind spots and hence only about 0.2%-1% of candidate locations are used. As the number of obstacles rises we do see an increase in the percentage but we can also see that it increases to only a mere 3%-4%. It is to be noted that, as the numbers of obstacles rise higher and higher the total number of candidate locations also reduces, as most of the area is covered by obstacles in that case. Thus, even if the proportion rises the number of selected locations does not increase significantly.

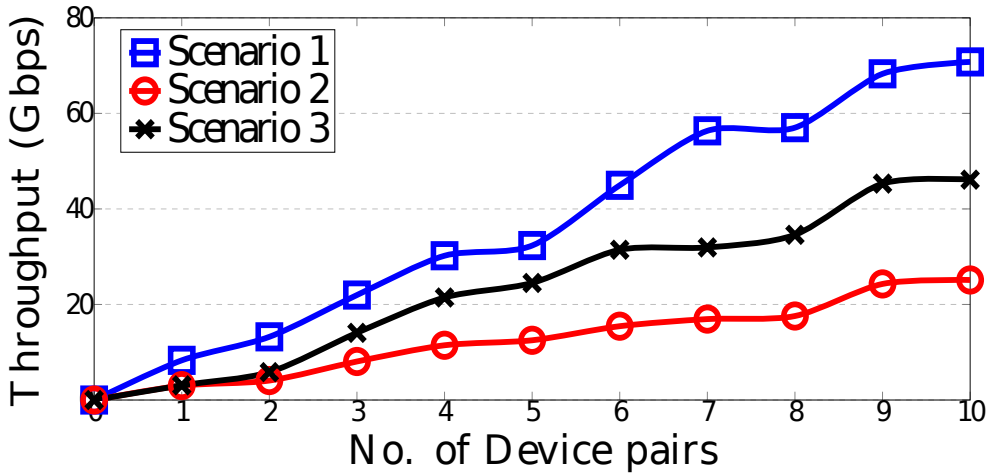

Figure 2.4: Throughput vs. number of device pairs

Figure 2.4 shows how the throughput of the system behaves as the number of device pairs increases in the environment with 10 obstacles randomly placed. We can clearly see that our scenario provided the highest throughput in comparison to other scenarios. This is because obstacle walls are not always the optimal location for an RIS. Furthermore, the RIS orientation is also fixed once placed on the walls. We see the trend that the throughput rises and then gets saturated; as with large number of devices not all devices can be served. Overall, we can see that our strategy performs better as more links can be established using RISs compared to Scenarios 2 and 3, resulting in improved throughput.

From Figure 2.5 we can clearly see that Scenario 1 gives higher throughput compared to Scenarios 2 and 3 for a given number of obstacles in the environment. Here we have considered 15 device pairs and measured the throughput with varying number of obstacles. In Scenario 1 more device pairs are served by the strategically placed RISs and also the channel have much higher gain due to either direct or indirect LoS. But the system throughput falls with rising number of obstacles because with more obstacles the LOS between more number of device pairs are blocked in all scenarios.

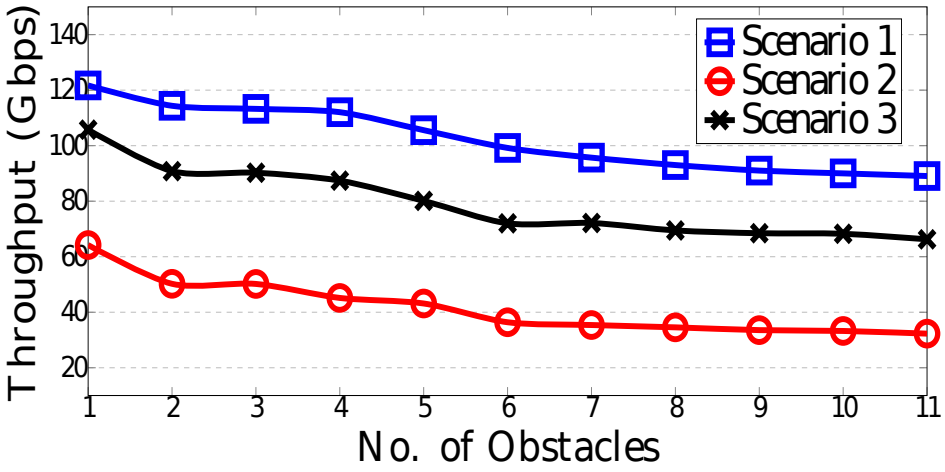

Figure 2.5: Number of obstacles vs. throughput

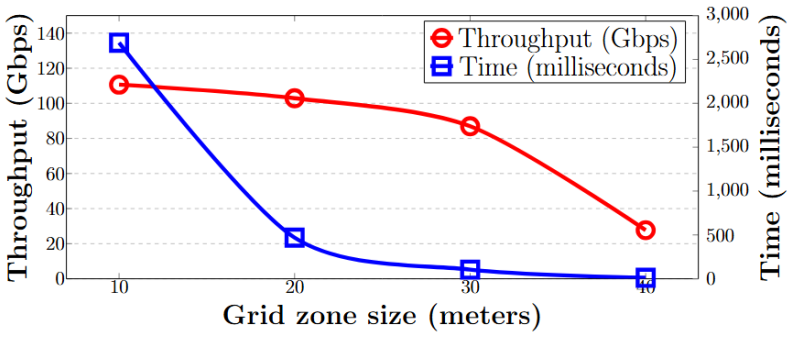

Figure 2.6: Throughput and time vs. grid size

In Figure 2.6 we see how the throughput and time for prepossessing change with zone size. By zone size we mean the length of the side of the square representing the zone. Here we consider 15 device pairs. We can clearly see that as the zone size increases the prepossessing time reduces drastically as the number of zones reduces. But due to high approximation involved in higher zone size, the throughput also falls. Note that the position of a device is approximated to the center of the corresponding zone. Thus with large zone size the actual distance between two devices can become very large in comparison to the distance between their respective zone centers, causing huge fall in gain. In some cases the actual distance between a device pair may even be beyond the threshold distance calculated based on their approximate position. Hence we get good approximation for small zone size only.

Finally, we observe that the proposed set cover based RIS placement algorithm achieves a maximum throughput gain of 66% relative to Scenario 3 (Deployment only on walls [52, 81]) and 200% relative to Scenario 2 (Random Placement [48]), for a total of 10 D2D pairs and 10 obstacles under the considered simulation set-up. Furthermore, the margin of error at 95% confidence for the measured throughput is less than 0.049, indicating high accuracy of the results.

2.5 Conclusion

We have given a strategy to place RISs in minimum number of locations to cover all the coverable blind pairs. In our strategy, the RISs can be mounted on top of poles set up in free zones, as well as on the walls of obstacles. Then, after actually deploying devices in the region, we select a subset of these locations to serve them. Simulation results show how our RIS deployment strategy gives better performance over the widely adopted strategy of deployment on obstacle walls as well as a random deployment strategy. However, in many real world scenarios the optimally computed location for RIS placement may not be accessible due to reasons like third party ownership of the specific location. In such a case, the UEs must choose the best RIS to serve them among the sub optimally placed RISs. We address this challenge in the next chapter.

Chapter 3

RIS selection in mmWave D2D[1]

In this chapter, we address the problem of selecting an optimal RIS among multiple RISs in a mmWave D2D network underlying a cellular network. We present a novel deterministic RIS selection algorithm based on the concept of visibility polygons. A visibility polygon with respect to an RIS, in this context, represents the region of points which have an LOS with the reflective side of the RIS. Our approach begins with a preprocessing step where the visibility polygon for each RIS is computed and its segments are efficiently stored using a segment tree. This structure enables fast prediction of the RIS-UE LoS status for several future time slots, significantly reducing both the signaling overhead and computational complexity by avoiding frequent UE location updates. Utilizing the preprocessed data structure, we propose a selection strategy that identifies a common RIS visible to both UEs in a D2D pair, choosing the one that offers the minimum pathloss for the cascaded transmitter-RIS-receiver channel. If no common RIS is found, communication falls back to the BS, with or without RIS assistance depending on visibility. Extensive system-level simulations demonstrate that our method outperforms both CSI-based and location-based RIS selection schemes.
The symbols used in this chapter and their respective meaning are given in Table 3.1.

[1]This chapter is based on the following publication:
Souvik Deb and Sasthi C. Ghosh, "Visibility polygon-based obstacle aware RIS selection for millimeter wave D2D communication", **The 5th IEEE International Mediterranean Conference on Communications and Networking (IEEE MEDITCOM 2025)**, Nice, France, 7-10 July 2025 (Accepted for publication).

Table 3.1: Important notations for Chapter 3

Symbol	Meaning	Symbol	Meaning
U	Number of single-antenna UEs	$\mathcal{U}$	Set of UEs
b	Macro-BS index	K	Number of RISs
R	Number of reflecting elements per RIS	$\mathcal{K}$	Set of RISs
δ	Duration of one TTI	ΔT	Superslot duration
Z	Number of TTIs in one superslot	$\mathcal{D}_t$	Set of D2D pairs scheduled at time slot t
d	Maximum distance threshold for viable links	M	Number of static obstacles
B_1	Bandwidth per RB for mmWave band	B_2	Bandwidth per RB for sub-6 GHz band
$\mathbf{\Phi}_k$	Diagonal phase-shift matrix of RIS k	η	Reflection efficiency of RIS elements
ϕ_r	Phase shift of reflecting element r	$\mathbf{g}_{pk}$	Channel vector from p to RIS k
$\mathbf{f}_{kq}$	Channel vector from RIS k to q	κ	Rician factor for all channels
ρ_1, ρ_2	Path-loss at 1 m for direct and RIS-links	d_{xy}	Distance between nodes x and y
α, β	Path-loss exponents for direct and RIS-links	T_p	Transmit power of node p
σ_q^2	AWGN power at receiver q	γ_{pq}	SNR at q from p via RIS k
δ_p	CE duration for transmitter p	$\mathbf{A}^u(s)$	Visibility matrix for UE u in superslot s
P	Polygonal region of interest	$\mathcal{E}$	Set of all edges of P
N	Total number of reflex vertices in P	$\mathcal{V}_k$	Edge set of visibility polygon for point k
S_k	Visibility edges not in $\mathcal{E}$	$\mathcal{S}$	Set of all visibility segments
$\mathcal{L}_l$	Labels of segment l	$\mathcal{T}$	Segment tree on $\mathcal{S}$
$\mathbf{PL}^p(t)$	Path-loss vector for UE p at slot t	$PL_k^p(t)$	kth entry of $\mathbf{PL}^p(t)$
$\mathbf{CPL}^{ij}(t)$	Hadamard product $\mathbf{PL}^i(t) \odot \mathbf{PL}^j(t)$	$\mathbf{0}$	Zero vector

3.1 System model and assumptions

We consider that the network has one single antenna sub 6 GHz macro BS denoted by b. Inside the coverage of the BS there are U single antenna UEs with equal antenna height indexed by the set $\mathcal{U} = \{1, 2, \cdots, U\}$ [34]. A total of K RISs with R passive reflecting elements each are mounted on the walls of different buildings in the coverage region of the BS indexed by $\mathcal{K} = \{1, 2, \cdots, K\}$. The time is discritized into transmission time intervals (TTI) of fixed duration δ [97]. The UEs move throughput the coverage region each with different speeds and direction. We make the following practical assumptions regarding the *channel coherence time* and motion of the UEs:

- *Assumption 1:* The channel coherence time for an RIS-assisted channel is equal to the TTI of duration δ. It is assumed that the CSI does not vary during the channel coherence time [11].

- *Assumption 2:* There exists a duration ΔT for which the trajectory of a UE can be approximated as a straight line. Therefore, the number of TTIs making up the duration ΔT is computed as $Z = \lceil \frac{\Delta T}{\delta} \rceil$. The duration of ΔT is termed as the *superslot*.
- *Assumption 3:* The BS is updated with the location and velocity vectors of the UEs at the beginning of each superslot ΔT [98, 99]. This can be obtained using easily accessible technology like global positioning system.

Let $\mathcal{D}_t = \{(i,j) \mid i \in \mathcal{U}$ is the transmitter and $j \in \mathcal{U}$ is the receiver$\}$ be the set of D2D pairs that are scheduled to communicate at time slot t. The D2D pair (i,j) communicates using both the direct i-j channel and the reflected channel via an RIS $k \in \mathcal{K}$. Due to high propagation loss of mmWaves the the distance between UEs in the D2D pair and between the RIS and UEs must be below a threshold d. In the case when both the channels are blocked by obstacles or distance between the concerned nodes is greater than a threshold distance d, pair (i,j) communicates via the BS. When communicating via the BS, half the TTI is utilized for uplink from UE i to the BS and the remaining half for downlink from BS to UE j [100]. Such uplink and downlink communication is assisted by an RIS if it is visible to both the UEs and the BS.

3.1.1 Obstacle modeling

The region in which the UEs roam is a rectangular area with M static obstacles that are uniformly spread throughout the region. The static obstacles are represented using polygonal holes in the rectangle. The static obstacles in an urban area are primarily buildings. Moreover, given the propagation loss suffered by mmWave, the RISs need to deployed at low heights so that they are in proximity to the UEs. Therefore, it is considered that the height of all buildings is taller than the deployment height of all RISs.

3.1.2 Channel model

We consider an orthogonal frequency division multiple access (OFDMA) based multi-user communication in both mmWave and sub 6 GHz frequency bands where each UE communicates using orthogonal resource blocks (RB) [97]. The bandwidth of each RB for mmWave band is denoted by B_1 and that for sub 6 Ghz frequency band is denoted by B_2. The phase shift matrix of RIS $k \in \mathcal{K}$ is denoted by the $R \times R$ diagonal reflection matrix $\mathbf{\Phi}_k = \eta \; diag\{e^{j\phi_1}, e^{j\phi_2}, \ldots, e^{j\phi_R}\}$ where, $\eta \in [0,1]$ and ϕ_r are the reflection efficiency and

phase shift induced upon the incident wave by the reflecting element r respectively and $j = \sqrt{-1}$.

Let $p, q \in \{i,\ j,\ k,\ b\}$. For a transmitter p and a receiver q communicating using RIS k at time slot t, we denote by $h_{pq} \in \mathbb{C}$, the channel coefficient of the direct p-q channel and by $\mathbf{g}_{pk} \in \mathbb{C}^{R\times 1}$ and $\mathbf{f}_{kq} \in \mathbb{C}^{1\times R}$ the channel coefficients of RIS assisted p-k and k-q channels respectively. We assume all channels experience Rician fading with Rician factor κ [97]. Furthermore, the pathloss factor is computed as $\rho_1 d_{pq}^{\alpha}$, $\rho_2 d_{pk}^{\beta}$ and $\rho_2 d_{kq}^{\beta}$ for the p-q channel, p-k channel and k-q channel respectively [97]. Here, $d_{xy}\ \forall x, y \in \{p,\ q,\ k\}$ is the distance between x and y with α and β being the pathloss exponents and ρ_1 and ρ_2 being the pathloss at 1 meters. Computing the optimal phase shift of the RIS using phase shift optimization in [101], the received SNR at q from p is computed as:

$$\gamma_{pq} = \frac{T_p \left| h_{pq}^H \sqrt{\rho_1 d_{pq}^{-\alpha}} + \mathbf{f}_{kq}^H \mathbf{\Phi}_k \mathbf{g}_{pk} \sqrt{\rho_2^2 (d_{pk} d_{kq})^{-\beta}} \right|^2}{\sigma_q^2}. \tag{3.1}$$

Here, σ_q^2 is the power of additive white Gaussian noise and T_p is the transmit power of p. Finally, let δ_p be CE duration, then the data rate for D2D communication of $(i,j) \in \mathcal{D}_t$ is $(1 - \frac{\delta_p}{\delta}) B_1 \log_2(1+\gamma_{ij})$. However, when (i,j) communicates via the BS, the rate is $\frac{1}{2}\min\{(1 - \frac{\theta\delta_p}{\delta}) B_2 \log_2(1+\gamma_{ib}),\ (1 - \frac{\theta'\delta_p}{\delta}) B_2 \log_2(1+\gamma_{bj})\}$ [58] where, $\theta = \theta' = 1$ if RIS used for uplink and downlink respectively and 0 otherwise.

3.2 Proposed visibility polygon based RIS selection

In this section we develop a RIS visibility query (RVQ) algorithm that can determine the visibility of all RISs to any UE for a given period without using CE. At the beginning of a superslot s of duration ΔT current locations and velocity information of UEs is updated at the BS. The proposed algorithm generates a $K \times Z$ matrix $\mathbf{A}^u(s)$ for each UE u, where the entry at the k^{th} row representing RIS and c^{th} column representing time slot within the superslot s is denoted by $A_{kc}^u(s)$ and defined as follows:

$$A_{kc}^u(s) = \begin{cases} 1, & \text{RIS } k \text{ is visible to } u \text{ at slot } c \text{ of superslot } s \\ 0, & \text{otherwise} \end{cases} \tag{3.2}$$

Furthermore, no location information needs to be sent for the duration of ΔT thereby, reducing additional signaling overhead. It is to be noted that the c^{th} column of the matrix $\mathbf{A}^u(s)$ is a vector that represents the visibility state of each RIS for UE u and is denoted by $A_c^u(s)$. Finally an algorithm is designed that either finds an optimal RIS for a D2D pair or decide to use the BS in the absence of such an RIS. In the following subsection we propose the pre-processing required to perform the visibility query.

3.2.1 The pre-processing

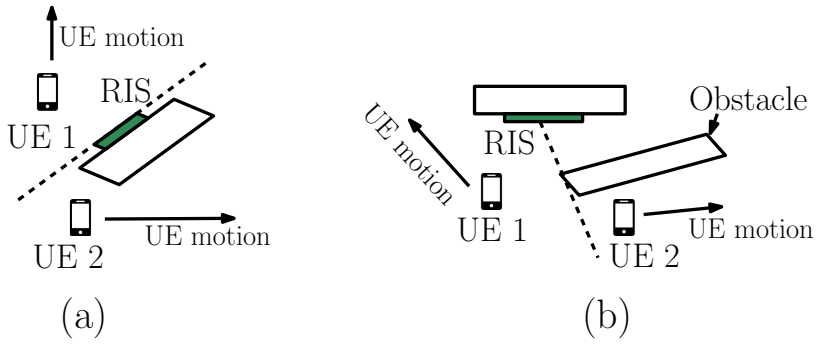

Figure 3.1: Cases when RIS ahs no LOS with the UE

We consider the region of interest to be a rectangle with holes denoted by P, where the holes represent static obstacles such as buildings. Let $\mathcal{E}$ be the set of edges of the considered polygon with holes and the total number of reflex vertices be N. An RIS attached to a building is represented as a rectangle that has one of its long sides adjacent to the edge of a hole as shown in Fig. 3.1. The RIS is identified by the mid-point on the reflecting side of the RIS. Consider each point $k \in \mathcal{K}$ as a query point and construct a visibility polygon for that query point using the visibility query algorithm for a polygon with holes [102]. A UE has LoS with an RIS k if it lies inside the visibility polygon for $k \in \mathcal{K}$. Therefore, if the UE trajectory crosses the boundary segment it signifies that the LoS status of RIS k has changed. The set of edges of the visibility polygon be denoted by $\mathcal{V}_k$. The time complexity for computing the visibility polygon is $O(N \log N)$ [102]. Let $S_k = \mathcal{V}_k \setminus \mathcal{E}$ be the set of line segments that are part of the edges of the visibility polygon excluding the edges in $\mathcal{E}$ and let $\mathcal{S} = \cup_{k \in \mathcal{K}} S_k$. For a line segment $l \in \mathcal{S}$ we define a set of labels $\mathcal{L}_l$ as follows:

$$\mathcal{L}_l = \{k \in \mathcal{K} \mid l \in S_k \}. \tag{3.3}$$

Set $\mathcal{L}_l$ identifies the RISs associated with segment l. The set of all such labeled edges is denoted by the labeled line segments of $\mathcal{S}$ are stored in a segment tree $\mathcal{T}$ [94]. Segment tree is a data structure that stores the line segments on a plane in such a way that the set of line segments contained in or intersecting a given rectangle can be queried in logarithmic time.

We now show that the segment tree $\mathcal{T}$ can be built in $O(KN \log KN)$ time and storage space complexity. At first, we find the maximum number of line segments in S_k. A segment in the visibility polygon $\mathcal{V}_k$, is either a part of the original rectangle with holes P or a line segment between the query point k and a reflex vertex in P which has an LoS with the query point k. Since, $S_k = \mathcal{V}_k \setminus \mathcal{E}$, there can be $O(N)$ such segments in S_k. Therefore the total number of segments in $\mathcal{S} = \cup_{k \in \mathcal{K}} S_k$ is upper bounded by $O(KN)$. Hence, both the time and storage complexity of the segment tree $\mathcal{T}$ is $O(KN \log KN)$.

3.2.2 Computing RIS visibility matrix

In this subsection we design an algorithm to compute the RIS visibility matrix $\mathbf{A}^u(s)$ of a UE u at superslot s after $\mathbf{A}^u(s-1)$ was computed for previous superslot. It is to be noted that $\mathbf{A}^u(0)$ is the visibility matrix before communication in the network begins. This can be computed by standard CE process [1]. Note that this is the only time that CE for all RIS have to be conducted by the UEs. Let at the beginning of a superslot s the position vector of a UE u be $\mathbf{A}$. If the velocity vector of UE u is $\mathbf{v}_u$ with magnitude v_u, the next position vector $\mathbf{B}$ of UE u after a duration of ΔT is computed as $\mathbf{B} = \mathbf{A} + \mathbf{v}_u \times \Delta T$. Therefore, we obtain a line segment $\overline{\mathbf{AB}}$ which approximates the trajectory of the UE over time duration ΔT. If segment $\overline{\mathbf{AB}}$ is not parallel to the sides of P, we compute the vertices of an axis parallel rectangle with $\overline{\mathbf{AB}}$ as its main diagonal. For the case where $\overline{\mathbf{AB}}$ is parallel to the sides of P we consider the segment $\overline{\mathbf{AB}}$ itself as a rectangle with a predefined width $\epsilon > 0$. In this construction, the longer side of the rectangle remains parallel to $\overline{\mathbf{AB}}$ and the segment $\overline{\mathbf{AB}}$ bisects the rectangle. We denote this axis parallel rectangle by W. Using the segment tree $\mathcal{T}$ and the above-computed rectangle W, a rectangular window query is run to determine the set of edges ($\subset \mathcal{S}$) that lie in this query rectangle. Finally, we check for the intersection of segment $\overline{\mathbf{AB}}$ with the queried segments. Let a total of $\mathcal{L} = \{1,\ 2,\ \cdots\ L\}$ segments intersect $\overline{\mathbf{AB}}$. Let I_l be the distance between A and the point of intersection of segment l with $\overline{\mathbf{AB}}$. We define the set $\mathcal{Q}(s) = \{(\mathcal{L}_l, I_l) |\ l \in \mathcal{S}\}$. Now we sort the entries of $\mathcal{Q}(s)$ in increasing order of I_l. From the entries in $\mathcal{Q}(s)$ we compute the time slot t_l when the UE

would intersect the segment l as follows:

$$t_l = \lfloor \frac{I_l / v_u}{\delta} \rfloor. \tag{3.4}$$

Let $\{t_1,\ t_2\ \cdots\ t_L\}$ be the time slots in superslot s where $\overline{\mathbf{AB}}$ intersects a segment. The index of the slots are arranged in increasing order. Now we are ready to update the RIS

Algorithm 5: RIS visibility query (RVQ) algorithm for UE u

Data: $\mathcal{T}$, A, $\mathbf{v}_u$, ΔT, δ
Result: $\mathbf{A}^u(s)$

```
Compute the segment AB;
Construct axis parallel rectangle W;
Run window query with window W on T;
Construct Q(s) = {(L_l, I_l)| l ∈ S} ;
if Q(s) ≠ φ then
    Sort Q(s) in increasing order I_l;
    Compute intersection time slots t_l using (3.4);
    Compute A^u(s) based on (3.5), (3.6) and (3.7);
else
    A^u(s) = A^u(s − 1);
return A^u(s);
```

visibility matrix $\mathbf{A}^u(s)$. Since the starting position of the UE at the beginning of superslot s is the same as the final position of UE at the end of superslot $s-1$ we have:

$$A^u_Z(s-1) = A^u_1(s). \tag{3.5}$$

Now when $\overline{\mathbf{AB}}$ intersects line segment l at time slot t_l we update the RIS visibility matrix as follows:

$$A^u_{kt_l}(s) = \begin{cases} 1, & \text{If } A^u_{k(t_l-1)}(s) = 0\ \forall k \in \mathcal{L}_l \\ 0, & \text{If } A^u_{k(t_l-1)}(s) = 1\ \forall k \in \mathcal{L}_l \\ A^u_{k(t_l-1)}, & \forall k \in \mathcal{K} \setminus \mathcal{L}_l \end{cases} \tag{3.6}$$

Now for all time slots $c > 1$ other than $t_l \forall\ l \in L$ we have:

$$A^u_{kc}(s) = A^u_{k(c-1)}(s)\ \forall k \in \mathcal{K}. \tag{3.7}$$

If $\mathcal{Q}(s) = \phi$ then $\mathbf{A}^u(s) = \mathbf{A}^u(s-1)$. The complete procedure is depicted in Algorithm 5. Line 3 takes $O(\log_2^2(KN) + o)$ time where o is the number of segments queried. Line 6 takes $q \log_2 q$ time where $q = |\mathcal{Q}(s)|$. Finally, line 8 has complexity $O(KZ)$ for updating the matrix $\mathbf{A}^u(s)$. All other lines are executed in constant time. Therefore, the time complexity of Algorithm 5 for all UEs is $O(U(\log_2^2 KN + o + q \log_2 q + KZ))$. It should be noted that, since the UEs are moving throughout a large outdoor urban area, there exists superslots where a UE does not intersect any visibility polygon segments and $q = 0$. In such a case, no update is needed for the visibility matrix and the complexity of Algorithm 5 reduces to $O(\log_2^2(KN))$.

3.2.3 RIS-UE association

The RIS visibility matrix computed at the beginning of each superslot s provides the visibility status of all RISs for each UE over all time slots $1 \leq t \leq Z$ within the duration ΔT. Let at time slot t the set of D2D pairs that are scheduled to communicate be $\mathcal{D}_t$. Consider the D2D pair $(i, j) \in \mathcal{D}_t$ corresponding to transmitting UE i and receiving UE j. The visibility status of all RISs for UE i and UE j are given by the vectors $A_t^i(s)$ and $A_t^j(s)$ respectively. Let d_{ik} and d_{jk} be the distance of UE i and UE j from RIS $k \in \mathcal{K}$ respectively. Utilizing the visibility status vectors for UE $p \in \{i,\ j\}$, we compute the corresponding pathloss vector $\mathbf{PL}^p(t)$ for time slot t as follows:

$$PL_k^p(t) = \begin{cases} 0, & \text{If } A_{kt}^p(s) = 0 \text{ OR } d_{pk} > d \\ \rho_2 d_{pk}^{-\beta} & \text{If } A_{kt}^p(s) = 1 \end{cases} \quad \forall k \in \mathcal{K}. \tag{3.8}$$

Here, $PL_k^p(t)$ is the k^{th} component of $\mathbf{PL}^p(t)$ which corresponds to the RIS k. Now if we compute the Hadamard product of $\mathbf{PL}^i(t)$ and $\mathbf{PL}^j(t)$, the product vector will only have non-zero entries corresponding to components for which both $\mathbf{PL}^i(t)$ and $\mathbf{PL}^j(t)$ have non-zero entries. Therefore, the Hadamard product of vectors $\mathbf{PL}^i(t)$ and $\mathbf{PL}^j(t)$ is computed to obtain the vector $\mathbf{CPL}^{ij}$ as follows:

$$\mathbf{CPL}^{ij}(t) = \mathbf{PL}^i(t) \odot \mathbf{PL}^j(t). \tag{3.9}$$

The non-zero components in $\mathbf{CPL}^{ij}(t)$ correspond to the RISs that are visible to both UEs i and j. Therefore, the optimal RIS is the RIS corresponding to the least non-zero component.

On the other hand, if $\mathbf{CPL}^{ij}(t) = \mathbf{0}$, it implies that there are no RISs that are visible to both UE i and UE j at time slot t. In such a case, the D2D pair (i, j) communicate using the BS. Furthermore, the BS and RISs are stationary, the visibility status of all RISs and pathloss vector $\mathbf{PL}^{b}(t)$ with respect to the BS b is always known and remains unchanged. To select the optimal RIS for assisting the uplink communication from UE i to BS b and for downlink communication from BS b to UE j, the vector $\mathbf{CPL}^{pq}(t)$ can be computed as discussed above, where $p,\ q \in \{i,\ j,\ b\}$. If no uplink or downlink RIS is found, communication with BS continues without RIS assistance. The Algorithm 6 formally describes the RIS selection process and runs for each UE in each time slot. Therefore, it has a computational complexity of $O(UK)$ in each time slot.

Algorithm 6: Selecting optimal RIS for D2D pair $(i, j) \in \mathcal{D}_t$ for superslot s

Data: $\mathbf{A}^{u}(s)$, $\mathbf{PL}^{b}(t)$, $(i, j) \in \mathcal{D}_t$
Result: Optimal RIS

```
Compute PL^i(t), PL^j(t) and CPL^ij(t) from (3.8) and (3.9);
if CPL^ij(t) ≠ 0 then
    RIS = argmin_{k∈K} {CPL_k^ij(t) | CPL_k^ij(t) ≠ 0} ;
else
    Compute CPL^ib(t) and CPL^bj(t);
    if CPL^ib(t) ≠ 0 then
        RIS = argmin_{k∈K} {CPL_k^ib(t) | CPL_k^ib(t) ≠ 0};
    else
        No optimal uplink RIS
    if CPL^bj(t) ≠ 0 then
        RIS = argmin_{k∈K} {CPL_k^bj(t) | CPL_k^bj(t) ≠ 0};
    else
        No optimal downlink RIS;
```

Remark 1. *In our proposed algorithm, the obstacles, such as buildings, are considered as polygons. In such a case, if any polygon intersects the line connecting an RIS and the user, the particular RIS is considered to be invisible to the user. However, if the elevation difference and tilting are taken into account, an RIS which is marked as invisible in the 2D geometry may be actually visible to the user. This is because an obstacle that lies below*

the 3D line segment joining the user and the RIS will not intersect that line. Therefore, our proposed algorithm overestimates the number of invisible RISs corresponding to an user.

3.3 Simulation results

In this section, we perform system level simulations to evaluate the performance of our proposed visibility polygon based RIS selection algorithm with varying number of UE, obstacles and RISs in terms of sum data rate. We compare our algorithm with the following state of the art deterministic approaches for RIS selection:

- **CSI based RIS selection:** In this approach the perfect CSI knowledge is used to select the RIS which provides maximum SNR [53, 54, 1]. If the SNR of the best RIS is less than an acceptable threshold then the BS is selected for communication.
- **Location based RIS selection:** In this approach the location of both the transmitter and receiver is known at each time slot and the RIS providing the minimum pathloss for the cascaded transmitter-RIS-receiver channel is selected [55]. If the pathloss for all RISs in the environment are above an acceptable threshold the device pairs communicate with the BS.

Table 3.2: 3GPP Urban Macro (UMa) Parameter Assumptions for Simulation (Based on TR 38.901)

Parameter	**Value**	**Unit/Note**
Minimum BS-UE 2D Distance	35	m
Reference Distance for Path Loss	Implicit (close-in $\approx$ 1)	m
Shadow Fading Std. Dev. (σ_{SF}) - LOS	4	dB
Shadow Fading Std. Dev. (σ_{SF}) - NLOS	6	dB
Mobility Model	Random Waypoint or Uniform	(UEs move at constant speed)
Delay Spread ($\mu_{\lg DS}$) - NLOS	-6.83	$\log_{10}$(s)

Table 3.3: Simulation parameters and values for chapter 3

Parameter	**Value**
Simulation Area	1000 × 1000 m (square area)
maximum velocity	20 m/s
Number of UEs	100 to 160
UE Antenna Height	1 m above ground level
Threshold Distance (d)	50 m
BS carrier frequency	5 GHz
BS position	(0,0)
Obstacles shape	Non-overlapping rectangular
Obstacle side length	10-50 m
Number of obstacles	50-90
Height of BS and RIS	10 m above ground level
RIS Elements	100 per RIS
Transmit Power (UEs and BS)	24 dBm
Thermal Noise	-174 dBm/Hz
mmWave Carrier Frequency	28 GHz
mmWave Bandwidth	1 GHz (total)
Sub-6 GHz Bandwidth	100 MHz
Path Loss Exponent (mmWave)	4
Path Loss Exponent (Sub-6 GHz)	2
Rician Factor	4 dB (all channels)
SNR Threshold	5 dB

3.3.1 Simulation setup

In our simulation setup, the UEs move in a 1000 m × 1000 m square area [103] following random waypoint mobility model with a maximum velocity of 20 m/s. The number of UEs range from 100 to 160. All UE antennas height are 1 m above ground level. Threshold distance $d = 50$ m. At each time slot, UEs are grouped into exclusive D2D pairs, ensuring that the separation between the UEs in each pair does not exceed d m. A sub 6 GHz BS operating with a carrier frequency of 5 GHz [35] is positioned at the center of the square region which is considered to be the origin $(0,0)$. The obstacles are modeled as non overlapping rectangular holes uniformly randomly distributed across the square region with the length and breadth of the sides lying uniformly between 10 m and 50 m. The number of obstacles ranges from 50 to 90. Multiple RISs are positioned on the walls of a predefined percentage of obstacles (shown in results) chosen at random at each iteration of the simulation. The height of the BS and the RIS are set to 10 m above ground level.

Each RIS is considered to have 100 elements. The transmit power of the UEs and BS is set at 24 dBm and the thermal noise is set at -174 dBm/Hz [103]. The carrier frequency for the mmWave band is set to 28 GHz [53] with a total bandwidth of 1 GHz [56]. The bandwidth of the BS for the sub 6 GHz band is 100 MHz [104]. The pathloss exponent for the mmWave band communication is 4 and for the sub 6 Ghz is 2 [97, 105]. The Rician factor is set to 4 dB for all channels [34]. The SNR threshold is set as 5 dB [55]. All results are generated after averaging over 10000 independent runs of the simulation. All simulation parameters have been described in Tables 7.2 and 3.3

3.3.2 Performance evaluation

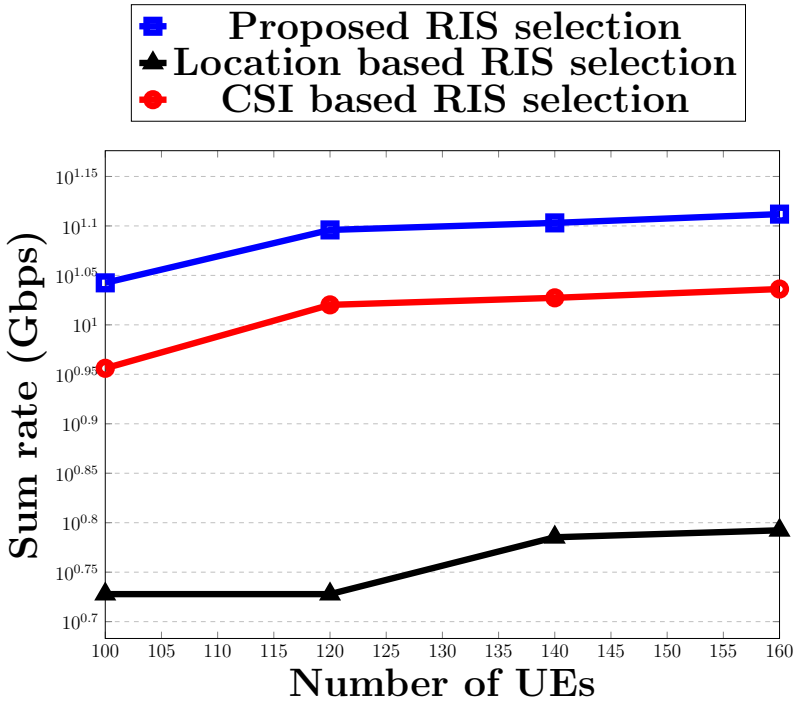

Figure 3.2: Sum rate vs. No. of UEs

Fig. 3.2 shows the relationship between the sum rate and the number of UEs. The number of UEs varies from 100 to 160 at a step of 20 UEs. A total of 80 static obstacles are considered to be uniformly spread across the simulation region. At each iteration, 50% of the obstacles were chosen to mount RISs. This implies that a total of 40 RISs were mounted randomly on walls of different obstacles. It can be observed that the sum rate for our proposed algorithm

is the highest compared to both CSI based and location based RIS selection schemes. For the case of CSI based selection scheme, full CSI knowledge is used to obtain the optimal RIS. Furthermore, both the proposed algorithm and the CSI based algorithm can determine if there are no RISs visible to both the transmitter and receiver pair and decide to use the BS for communication. However, the UEs need to send $O(K \times U \times R)$ pilots to determine the CSI of all the RIS assisted channels before making any decision. This massive overhead consumes a significant portion of the TTI leaving little time for actual data communication. On the other hand, our proposed algorithm is able to predict the visibility status of all RISs for each UE and for all time slots in a superslot. As a result, each UE only needs to acquire CSI for its chosen RIS thereby reducing the pilot overhead to $O(U \times R)$. This allows more time in a TTI for actual data communication resulting in a higher sum data rate. For the case of location based RIS selection, even though the locations of the transmitter, receiver and the RISs is utilized to compute the the pathloss of the cascaded channel, the visibility status of the RIS is not considered as opposed to our proposed algorithm. As a consequence, the RIS chosen by the location based selection often may not be visible to either the transmitter or the receiver or both, leading to a drop in data rate as the chosen RIS cannot be utilized.

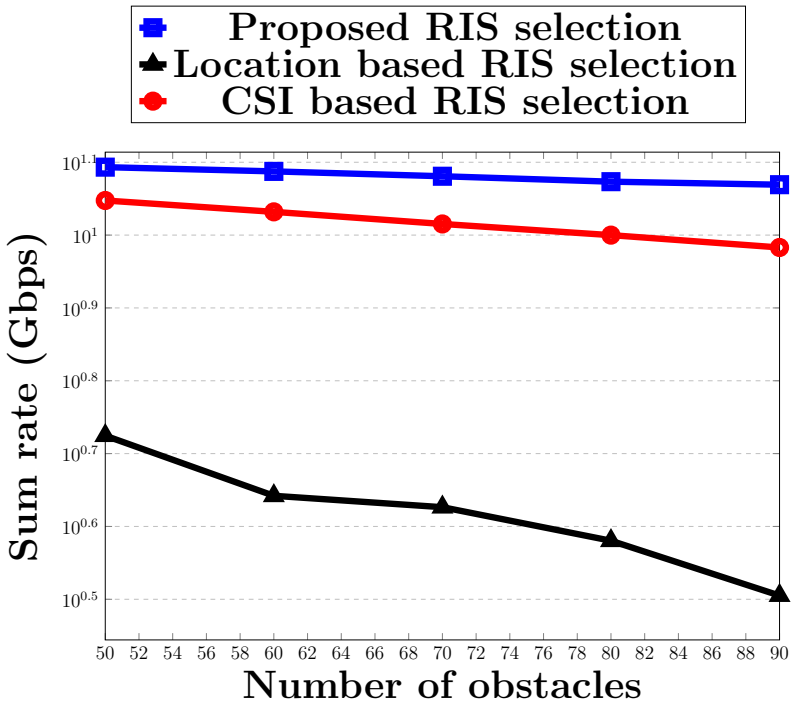

Figure 3.3: Sum rate vs. No. of obstacles

Fig. 3.3 shows the effect of the number of obstacles in the network environment on the sum data rate. Here, the number of obstacles vary from 50 to 90 at a step of 10 obstacles. The number of UEs considered here is 120. At each iteration of the simulation, 50% of the obstacles were chosen to mount RISs. It can be observed that the sum rate decreases with more obstacles despite an increase in the actual number of RISs. However, the visibility region of an RIS shrinks with increasing number of obstacles. Therefore, UEs move outside the visibility region of RISs more often during the period of communication. However, our proposed algorithm perform better than the both the CSI based RIS selection scheme and location based selection scheme for the same reason as described for Fig. 3.2.

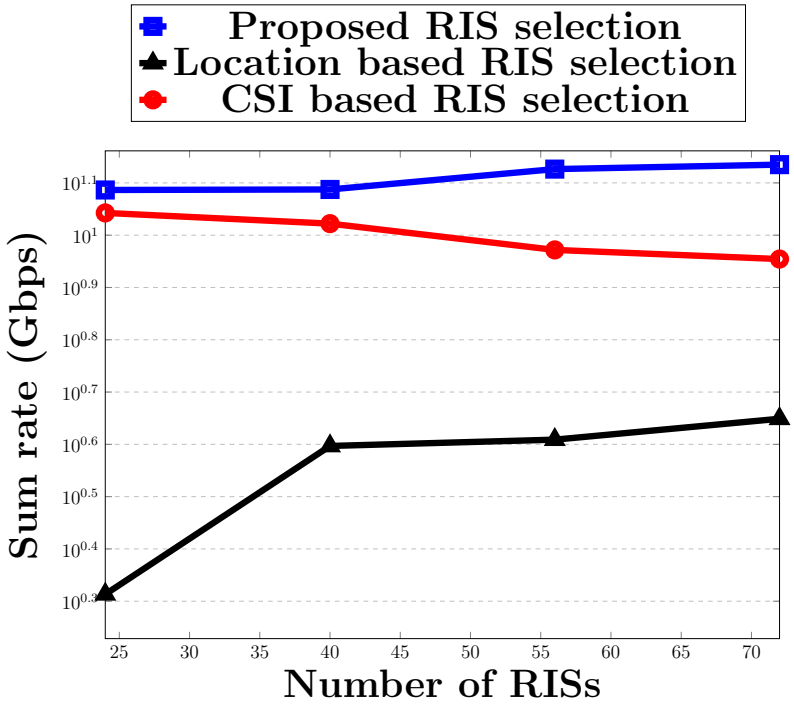

Figure 3.4: Sum rate vs. No. of RISs

Fig. 3.4 shows effect of the percentage of obstacles mounted with RISs on the sum rate. Here we have fixed the number of obstacles to 80 and the number of UEs to 120. Therefore, the sum rate has been measured for the following number of RISs (I) 24 ($\sim$ 30%) (II) 40 ($\sim$ 50%) (III) 56 ($\sim$ 70%) and (IV) 72 ($\sim$ 90%). The sum rate for the proposed algorithm and the location based algorithm increases monotonically with the increasing number of RISs as expected. However, the sum rate for the case of CSI based selection algorithm decreases with the number of RIS. This is because with more RISs the pilot overhead for

measuring CSI increases thereby reducing time for actual data communication in a TTI. Furthermore, it can be observed that our proposed algorithm perform better than the both the CSI based RIS selection scheme and location based selection scheme for the same reason as described for Fig. 3.2.

Finally, we observe that the visibility polygon based algorithm achieves a maximum throughput gain of 25% relative to channel state information (CSI) based RIS selection algorithm [53] for a total of 120 UEs, 80 static obstacles and 40 RISs. Moreover, a throughput gain of 254% is achieved relative to location based RIS selection algorithm [55], for 120 UEs, 90 obstacles and 45 RISs. Furthermore, the margin of error at 95% confidence for the measured sum rate is less than 0.038, demonstrating the high accuracy of the reported results.

3.4 Conclusion

It is essential to consider the RIS-UE LoS status and to mitigate CSI overhead when determining appropriate RIS in D2D communication. We propose a visibility polygon based algorithm that selects either the best RIS for D2D links or opts for BS assisted communication when no RIS is available for use. Simulation results show its superiority over CSI based and location based approaches.

Chapter 4

Dynamic channel estimation to mitigate CSI overhead[1]

The focus of our study in the previous chapters was to address the limitations of using RIS in D2D mmWave communication by optimally placing and selecting the RISs. We now shift our focus to some of the major challenges that arise when RIS is used in 5G cellular networks. In this chapter, we specifically deal with the massive CSI overhead required to acquire the accurate CSI for RIS configuration in a network with unstructured channels having multipath propagation. The channel estimation (CE) overhead for unstructured multipath-rich channels increases linearly with the number of reflective elements of RIS. This results in a significant portion of the channel coherence time being spent on CE, reducing data communication time. Furthermore, due to the mobility of the UE and the time consumed during CE, the estimated CSI may become outdated during actual data communication. In recent studies, the timing for CE has been primarily determined based on the coherence time interval, which is dependent on the velocity of the UE. However, the effect of the current channel condition and pathloss of the UEs can also be utilized to control the duration between successive CE to reduce the overhead while still maintaining the quality of service. Furthermore, for multi-user systems, the appropriate coherence time intervals of different users may be different depending on their velocities. Therefore, CE carried out ignoring the difference in coherence time of different UEs may result in the estimated CSI

[1]This chapter is based on the following publication:
Souvik Deb, Sasthi C. Ghosh, "Time varying channel estimation for RIS assisted network with outdated CSI: Looking beyond coherence time", **Computer Communications (Elsevier)**, Volume 240, August 2025, 108202, ISSN 0140-3664, https://doi.org/10.1016/j.comcom.2025.108202.

being detrimentally outdated for some users. In contrast, others may not have sufficient time for data communication. To this end, based on the throughput analysis on outdated CSI, an algorithm has been designed to dynamically predict the next time instant for CE after the current CSI acquisition. In the first step, optimal RIS phase shifts to maximise channel gain is computed. Based on this and the amount of degradation of SINR due to outdated CSI, transmit powers and bandwidth are allocated for the UEs and finally the next time instant for CE is predicted such that the aggregated throughput is maximized. Simulation results confirm that our proposed algorithm outperforms the coherence time-based strategies and an existing algorithm that adaptively changes inter CE duration.
The symbols used in this chapter and their respective meaning are given in Table 4.1.

Table 4.1: Important notations for Chapter 4

Symbol	Meaning	Symbol	Meaning
U	No. of UEs	$\hat{\mathbf{g}}_u$	Outdated channel from RIS to UE u
$\hat{h}_{u0}$	Outdated channel from gNB to UE u	$\mathbf{h}$	Channel from gNB to RIS
$\mathcal{U}$	Set of UEs	P_{tot}	Total transmit power allowed
σ_{uf}^2	Outdated CSI noise at UE u	n_{u0}	Additive white Gaussian noise
W	Total available bandwidth	ρ_{u0}	Correlation coefficient between outdated and actual direct channel
$\hat{h}_{u0}$	Outdated direct channel from gNB to UE u	ρ_u	Correlation coefficient between outdated and actual cascaded channel
D	BS-RIS center distance	V_u	velocity of UE u
R	Range of RIS service	f_c	Carrier frequency
M	No. of RIS elements	f_{ud}	Doppler spread for UE u
Ψ	Coherence time based inter CE duration	c	Speed of light
G_u	Throughput gain for UE u	Ω_0, Ω_1, Ω_2	Mean of Rician variables $\lvert\hat{h}_{u0}\rvert$, $\lvert h_m\rvert$ and $\lvert\hat{g_{u}}_m\rvert$ $\forall m$
$\mathbf{g}_u$	Channel from RIS to UE u	Δ_u	Expected SINR at UE u
h_{u0}	Channel from gNB to UE u	G_n	Aggregate throughput gain at time slot $l+n$
$\mathbf{\Phi}$	Phase shift matrix of RIS	$\mathbf{L}$	Pathloss matrix : gNB-RIS-UE
Σ_u	Standard deviation of interference	N_{max}	Smallest integer at which channel correlation becomes 0
β_0	Pathloss : gNB-UE	ρ^{th}	Time correlation threshold
β_u	Pathloss : gNB-RIS-UE u	T_c	Time slot duration
$\mathbf{I}_u$	Interference from neighboring cells	T_p	CE overhead time
δ_u	Actual SINR at UE u	$\mathbf{P}$	Transmit power vector

4.1 System model

4.1.1 Environment model

We consider a downlink wireless network with a single gNB providing ubiquitous coverage to a set $\mathcal{U} = \{1,\ 2,\ \cdots\ U\}$ of eMBB UEs. The UEs adopt orthogonal frequency division multiple access (OFDMA). Each UE is assigned a bandwidth $b_u \in [0, W]$ satisfying $\sum_{u \in \mathcal{U}} b_u \leq W$, where W is the total available bandwidth [106]. The total allowed transmit power at the gNB is P_{tot}. Moreover, the gNB communicates with the UEs over discrete time slots. The UEs receive interfering signals from neighbouring cells. The gNB communicates with the UEs utilizing the assistance of an RIS with M passive reflective elements. The gNB is at a distance D from the centre of the RIS. The service range of the RIS is considered to be R meters. We consider a 2-D scenario where the UEs roam on the ground level plane with the same antenna height at all positions. The coherence time for UE u denoted by T_{uc} is defined as the maximum time interval over which the time correlation of the channel is above a predefined threshold ρ^{th} [12, 13]. Let $f_{ud} = f_c V_u / c$ be the maximum Doppler spread, f_c is the carrier frequency, c is the velocity of light and V_u is the velocity of the UE u then T_{uc} is approximately computed as follows [13]:

$$T_{uc} = \frac{c \cos^{-1}(\rho^{th})}{2\pi V_u f_c}. \tag{4.1}$$

We consider that time is discritized into time slots of length $T_c = \min_{u \in \mathcal{U}} \{T_{uc}\}$.

4.1.2 Outdated channel and SINR model

We consider that the UEs lie in the far-field of the RIS. The phase shift induced by the reflective elements of the RIS is represented through a diagonal matrix as follows [46]:

$$\mathbf{\Phi} = diag(e^{j\phi_1},\ e^{j\phi_2},\ \ldots,\ e^{j\phi_M}), \tag{4.2}$$

where, $\phi_m \in [0, 2\pi]$ for all $m = 1,\ 2,\ \cdots,\ M$. Let $x_u(t)$ be the Gaussian transmitted signal from the gNB to the UE u at time t. Let $h_{u0} \in \mathbb{C}^1$, $\mathbf{h} = [h_1,\ h_2, \cdot\cdot, h_m \cdots, h_M]^T \in \mathbb{C}^M$ and $\mathbf{g}_u = [g_{u1},\ g_{u2}, \cdot\cdot, g_{um}, \cdots,\ g_{uM}] \in \mathbb{C}^{1\times M}$ be the channel vectors from gNB to UE u, gNB to RIS and from RIS to UE u respectively, following Rician fading models [35]. A schematic of the system model is presented in Fig. 4.1. It may be

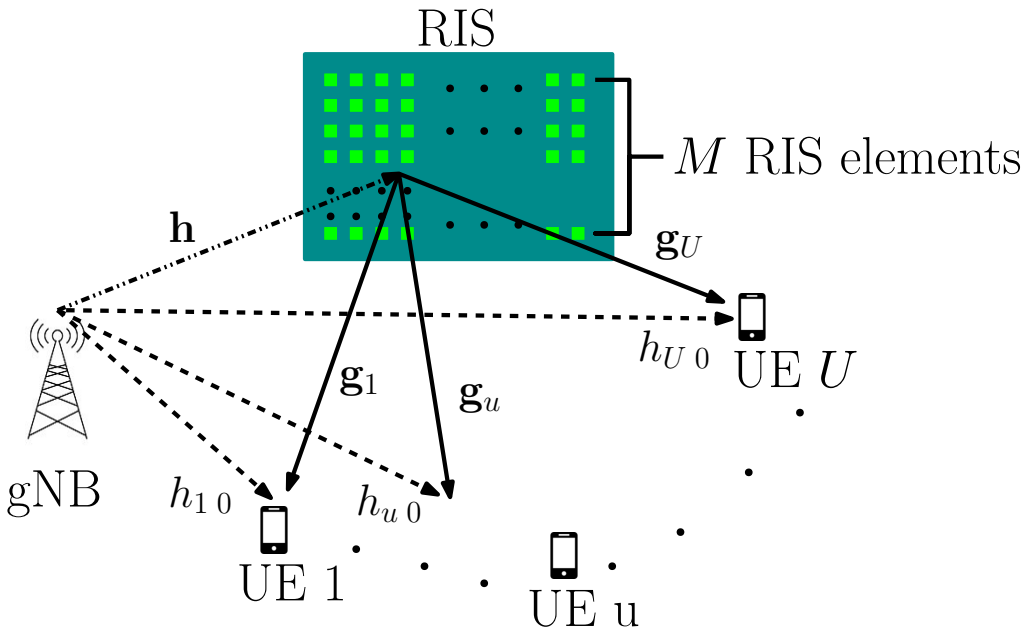

Figure 4.1: System model

observed that,$\hat{\mathbf{g}}_u = \hat{\mathbf{g}}_{uI} + j\hat{\mathbf{g}}_{uQ}$, and $\mathbf{h} = \mathbf{h}_I + j\mathbf{h}_Q$ are complex Gaussian vectors and $\hat{h}_{u0} = \hat{h}_{u0I} + j\hat{h}_{u0Q}$ is a complex Gaussian random variable. Here, $\hat{\mathbf{g}}_{uI}$, $\mathbf{h}_I$ and $\hat{h}_{u0I}$ are Gaussian random variables denoting the in-phase components of the corresponding channels. Similarly, $j\hat{\mathbf{g}}_{uQ}$, $\mathbf{h}_Q$ and $\hat{h}_{u0Q}$ are Gaussian random variables denoting the quadrature components of the corresponding channels. The in-phase and quadrature components are independent to each other. Let the i^{th} component of the vectors $\hat{\mathbf{g}}_u$ and $\mathbf{h}$ be $\hat{g}_u^i$ and h^i respectively. The random variables $|\hat{g}_u^i|$, $|h^i|$ and $|\hat{h}_{u0}|$ follows Rician distribution signifying the existence of a line of sight channel from RIS to UE, gNB to RIS and gNB to UE respectively. Due to the mobility of UEs and the delay caused by the massive number of pilot transmissions during CE [107, 61], it is considered that the CSI for the direct gNB-UE channel and RIS-UE channel is outdated with T_p being the respective estimation delays. Here, T_p is total time consumed for CE including pilot transmission to all UEs, processing delay and feedback from gNB to the RIS. We adopt the widely accepted first order Gauss-Markov fading channel [108, 67],[63]. The relation between the actual channels h_{u0} and $\mathbf{g}_u$ and the outdated channels $\hat{h}_{u0}$ and $\hat{\mathbf{g}}_u = [\hat{g}_{u1}, \hat{g}_{u2}, \cdots, \hat{g}_{um}, \cdots, \hat{g}_{uM}] \in \mathbb{C}^{1\times M}$ is as follows [35]:

$$h_{u0} = \rho_{u0}\hat{h}_{u0} + \widetilde{\rho}_{u0}\omega_0, \tag{4.3}$$

$$\mathbf{g}_u = \rho_u\hat{\mathbf{g}}_u + \widetilde{\rho_u}\boldsymbol{\omega}. \tag{4.4}$$

Here, $0 \leq \rho_{u0} \leq 1$ and $0 \leq \rho_u \leq 1$ are the correlation coefficients between the outdated channel estimate and the actual channel for the direct gNB-UE channel and the RIS-UE channel respectively. The correlation coefficients are computed as $\rho_{u0} = \rho_u = J_0\left(2\pi f_{ud} T_p\right)$ [35], where $J_0(.)$ is the zeroth order Bessel's function of the first kind. Moreover, $\boldsymbol{\omega} = [\omega_{u1},\ \omega_{u2},\ \cdots,\ \omega_{uM}] \in \mathcal{C}^{1\times M}$ where $\omega_{ui} \sim \mathcal{CN}(0, \sigma^2_{\hat{g}_{ui}})$ and $\omega_0 \sim \mathcal{CN}(0, \sigma^2_{\hat{h}_{u0}})$. Furthermore, $\widetilde{\rho}_{u0} = \sqrt{1-\rho^2_{u0}}$ and $\widetilde{\rho_u} = \sqrt{1-\rho^2_u}$. Therefore the received signal for the outdated CSI is as follows [35]:

$$
\begin{aligned}
y_u(t) = \sqrt{P_u}\Big(&(\rho_u \hat{\mathbf{g}}_u \mathbf{L}_u \boldsymbol{\Phi} \mathbf{h} + \rho_{u0}\sqrt{\beta^{-1}_{u0}}\hat{h}_{u0}) x_u(t) \\
&+ (\widetilde{\rho}_u \boldsymbol{\omega} \mathbf{L}_u \boldsymbol{\Phi} \mathbf{h} + \widetilde{\rho}_{u0}\sqrt{\beta^{-1}_{u0}}\omega_0) x_u(t)\Big) + n_{u0} + \mathbf{I}_u,
\end{aligned} \tag{4.5}
$$

where $n_{u0} \in \mathcal{N}(0, \sigma^2_u)$ is the additive white Gaussian noise (AWGN) with 0 mean and variance σ^2_u and P_u is the power associated with $x_u(t)$ allocated to UE u. Here β_{u0} is the pathloss of the direct channel from gNB to UE u and the pathloss of the cascaded gNB-RIS-UE channel is represented using the diagonal matrix $\mathbf{L}_u = diag(\sqrt{\beta^{-1}_u},\ \sqrt{\beta^{-1}_u}, \cdots,\ \sqrt{\beta^{-1}_u}) \in \mathbb{R}^{M\times M}$ [35]. However, the power consumed by the reflecting elements of the RIS has been ignored. The first order Gauss-Markov fading channel mathematically characterizes the temporal correlation by using channel state transitions. The correlation coefficient computed by Jake's model explicitly characterizes the dependence of the temporal correlation of the channel on the velocity of the UE. Well accepted closed form expressions for signal to interference plus noise ratio (SINR) have been derived using this model [66, 35]. These expressions enable us to study the impact of outdated CSI on the sum throughput when channel estimation is skipped at any time slot. The above cited reasons justify the use of the first order Gauss-Markov fading channel for our study.

Adopting from [109], $\mathbf{I}_u \sim \mathcal{LN}(\mu_u, \Sigma^2_u)$ is the interference suffered by UE u from neighbouring cells and follows log normal distribution with mean μ_u and standard deviation Σ_u. We have assumed that the serving gNB is surrounded by neighboring gNBs uniformly in all directions. Furthermore, we assume that the interferences from the neighboring cells experience independent large scale and small scale fading. It is well known [110, 109] that interference power with large scale fading usually follows the log-normal distribution. Therefore, the aggregate interference power can be regarded as a sum of randomly weighted log-normal variables, which can also be modeled as a log-normal distribution.

Denoting the mean of the Rician random variables $|\hat{h}_{u0}|$, $|h_m|$ and $|\hat{g}_{um}|$ by Ω_0, Ω_1 and

Ω_2 respectively, the effective noise (outdated CSI noise + AWGN noise) is computed as follows:

$$\sigma_{uf}^2(\rho_{u0},\rho_u) = \frac{P_u M\widetilde{\rho}_u^2\left(1-\Omega_2^2\right)}{\beta_u} + \frac{P_u\widetilde{\rho}_{u0}^2\left(1-\Omega_0^2\right)}{\beta_{u0}} + \sigma_u^2. \tag{4.6}$$

Therefore, adopting the interference computation from [109], $\mathbb{E}(\mathbf{I}_u) = \exp(2\mu_u + 2\Sigma_u^2)$, and the received SINR at UE u for the channel correlation coefficients ρ_u and ρ_{u0} is computed as follows:

$$\delta_u(\rho_{u0},\rho_u) = \frac{P_u|\rho_u\hat{\mathbf{g}}_u\mathbf{L}_u\mathbf{\Phi}\mathbf{h} + \rho_{u0}\sqrt{\beta_{u0}}^{-1}\hat{h}_{u0}|^2}{\sigma_{uf}^2 + \exp(2\mu_u + 2\Sigma_u^2)}. \tag{4.7}$$

The reflection phase of the RIS can be optimized using algorithms presented in [36]. To compute the expected SINR at any time t for the channel correlation coefficients ρ_u and ρ_{u0} we adopt the value of phase difference in the received signal for optimized phase shift values of the RIS from [67] and the expected SINR defined as Δ_u is given as follows [35]:

$$\begin{aligned}\Delta_u(\rho_{u0},\rho_u) =& \Delta_{uf}\big(M(\rho_u)^2/\beta_u + M(M-1)(\rho_u\Omega_1\Omega_2)^2/\beta_u \\ &+ 2M\rho_u\rho_{u0}\Omega_0\Omega_1\Omega_2/\sqrt{\beta_{u0}\beta_u} + \rho_{u0}^2\beta_{u0}^{-1}\big),\end{aligned} \tag{4.8}$$

where $\Delta_{uf} = \frac{P_u}{\sigma_{uf}^2(\rho_{u0},\rho_u)+\mathbb{E}(\mathbf{I}_u)}$.

For a given time slot l, we use (4.7) to compute the actual throughput of a UE at time slot l. Had CE been performed at the beginning of the time slot l, we compute the expected throughput the UE would achieve assuming outdated CSI using (4.8).

4.2 The proposed time varying CE

In this section, for a given time slot, we first compute the throughput gain achieved by a UE without CSI acquisition as opposed to the same after CSI acquisition. Then we compute the optimal phase shift of the RIS to maximize the channel gain at each UE and based on it we formulate the power allocation problem as a convex optimization problem which maximizes the aggregate throughput gain of all the UEs in the network. Finally, utilizing the gain computed for consecutive future time slots after the last slot in which CE was performed, an algorithm is proposed to compute the number of consecutive future time slots where CE can be skipped.

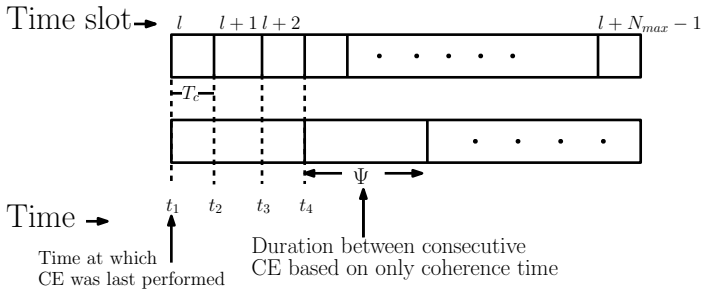

Figure 4.2: Time slot division

4.2.1 Throughput gain

In this subsection, we define the gain achieved by a UE at given time slot when the UE decided to skip CE process at the particular slot and utilizing the time spent on CE overhead for actual data communication.

Let T_p denote is total time consumed for CE including pilot transmission, processing delay and feedback for all UEs. It may be observed that the number of pilot signals required to obtain CSI for U UEs using an RIS with M reflective elements is $O(MU)$. If T_c is the duration of a single time slot then we define $s = \lceil \frac{T_p}{T_c} \rceil$. It should be noted that data communication can take place only after CE has been performed. Therefore, it takes a minimum of s time slots before actual data communication begins immediately after CE. Therefore, the fraction of time left for actual data communication over a duration of s time slots is $(1 - \frac{T_p}{sT_c})$. Moreover, due to the massive pilot overhead for large RISs and mobility of the UE, the CSI acquired by the UE becomes outdated by a time delay of at least T_p. Therefore, the correlation coefficient between the estimate of the channel and the actual channel during data communication right after CE at slot l for UE u is denoted by $\rho_{u0}[T_p]$ for the direct gNB-UE channel and $\rho_u[T_p]$ for the cascaded gNB-RIS-UE channel. Let l be the last time slot when CE was performed. We index this particular time slot as $l+0$. Furthermore, let $V = \max_{u \in \mathcal{U}} V_u$ be the maximum velocity achieved by a UE in the network and $f_d = f_c V/c$ be the corresponding maximum Doppler spread. Hence, $\rho_{u0}[T_p] = \rho_u[T_p] = J_0(2\pi f_d T_p)$. The n^{th} time slot greater than s after l is denoted by $l+n$. Therefore, the delay between the actual channel at time slot $l+n$ and the outdated channel estimated at time slot l is $T_p + nT_c$ for all $n \geq s$. The time correlation of the channel corresponding to f_d is computed as $\rho_u[T_p + nT_c] = \rho_{u0}[T_p + nT_c] = J_0(2\pi f_d(T_p + nT_c))$. It may be noted that when $\rho'_u = \rho'_{u0} = 0$, it means that the time delay between the current channel and the estimated channel is long enough for them to

become completely uncorrelated and hence CE has to be performed again to estimate the new channel which is completely independent of the previously estimated channel. We define $N_{max} = \min\{n \in \mathbb{Z}^+ |\ J_0\left(2\pi f_d^u (T_p + nT_c)\right) \leq 0\}$. This means that $l + N_{max}$ is the first time slot after l where $\rho'_u = \rho'_{u0} = 0$. Furthermore, since the time delay between l and $l + N_{max}$ is in the order of milliseconds, we assume the location of the UE to be approximately the same during slot l. Finally, we denote the set of consecutive time slots after the slot l upto the time slot $l + N_{max} - 1$ as $\mathcal{T} = \{1,\ 2,\ 3\ \cdots\ N_{max} - 1\}$. For time slots after $l + N_{max} - 1$, the SINR values computed in (4.7) and (4.8) become too erroneous to be useful. Now, from (4.7) and (4.8) the throughput per unit bandwidth for UE u is computed using Shannons's capacity formula as follows:
When CE is not performed at time slot $l + n$,

$$R_u(l+n) = \log_2\left(1 + \delta_u(\rho_{u0}[T_p + nT_c], \rho_u[T_p + nT_c])\right). \tag{4.9}$$

When CE is performed at time slot $l + n$,

$$\widetilde{R}_u(l+n) = \left(1 - \frac{T_p}{sT_c}\right) \log_2(1 + \Delta^u(\rho_{u0}[T_p], \rho_u[T_p]). \tag{4.10}$$

In recent works, such as [60, 58, 111, 64, 67] the time duration between two consecutive CE processes is determined solely based on coherence time and channel time correlation threshold $\bar{\rho}^{th} \leq \rho^{th}$ [112, 13]. Let such a time duration be denoted by Ψ and $z = \lceil \frac{\Psi}{T_c} \rceil$. The throughput gain when $n \leq z$ is defined as the difference between cumulative throughput obtained over s slots after performing CE at $l + n$ and the cumulative throughput obtained by skipping CE at slot $l + n$. This indicates the gain in throughput achieved if CE is performed before the fixed duration Ψ. Here, the cumulative throughput obtained over s time slots is defined as follows:

$$\mathcal{R}_u(l+n) = (1 - \alpha_n) \sum_{i=0}^{s-1} b_u^{n+i} R_u(l+n+i) + \alpha_n b_u^n \widetilde{R}_u(l+n). \tag{4.11}$$

Here, b_u^n is bandwidth allocated to to UE u at slot $l + n$ and α_n is the binary variable which indicates CE is performed as slot $l + n$ when set to 1. Mathematically, throughput gain G_u for UE u is defined as:

$$G_u = \max\left(\sum_{j=0}^{s-1} b_u^{n+j} R_u(l+n+j) - b_u^n \widetilde{R}_u(l+n), 0\right). \tag{4.12}$$

For the case when $n = m \times z$ where $m \in \{1, 2, 3, \cdots\}$, the throughput gain is the difference between the cumulative throughput obtained over the entire duration Ψ by skipping CE and the cumulative throughput obtained over z slots after performing CE at slot $l+n$. A positive gain indicates that CE can be skipped for all z slots. So for this case, throughput gain G_u for UE u is defined as:

$$G_u = \max\Big(\sum_{j=0}^{z-1} b_u^{n+j} R_u(l+n+j) - b_u^n \widetilde{R}_u(l+n) - \sum_{j=s}^{z-1} \log_2(1+\Delta^u(\rho_{u0}[T_p+jT_c], \rho_u[T_p+jT_c]), 0\Big). \tag{4.13}$$

Therefore the aggregate throughput gain for all UEs at time slot $l+n$ is defined as

$$G_n = \sum_{u=1}^{U} G_u. \tag{4.14}$$

4.2.2 Phase shift optimization

The correlation coefficient between the channel estimated at time slot l and the actual channel at slot $l+n$ for UE u be $\rho_0^u[l+n]$ for the direct gNB-UE channel and $\rho^u[l+n]$ for the cascaded gNB-RIS-UE channel. We first determine the phase shift of the RIS elements in order to maximize the channel gain at each UE. We adopt the same optimization strategy presented in [36] to compute the optimal phase shifts. However, [36] does not consider outdated CSI. In order to compute the optimal phase shifts for outdated CSI, the channel gain at UE u at time slot $l+n$ where $n \in \mathcal{T}$ in (4.7) is given by

$$|\rho_u[l+n]\hat{\mathbf{g}}_u \mathbf{L}_u \mathbf{\Phi} \mathbf{h} + \rho_{u0}[l+n]\sqrt{\beta_{u0}^{-1}} h_{u0}|^2 = |\rho_u[l+n]\hat{\mathbf{g}'}_u \mathbf{\Phi} \mathbf{h} + \rho_{u0}[l+n]\sqrt{\beta_{u0}^{-1}} h_{u0}|^2.$$

Here $\hat{\mathbf{g}'}_u = [\sqrt{\beta_u^{-1}}\hat{g}_{u1}, \sqrt{\beta_u^{-1}}\hat{g}_{u2}, \cdots, \sqrt{\beta_u^{-1}}\hat{g}_{uM}] \in \mathbb{C}^{1\times M}$. Let $s_m = e^{\phi_m}$ and $\mathbf{s} = [s_1, s_2, \cdots, s_M]^T \in \mathbb{C}^M$. The channel gain can be rewritten as

$$|\mathbf{s}^H \mathbf{\Theta} + \rho_{u0}[l+n]\sqrt{\beta_{u0}}^{-1} \hat{h}_{u0}|^2.$$

Here $\mathbf{\Theta} = diag(\rho_u[l+n]\hat{\mathbf{g}'}_u)\mathbf{h} \in \mathbb{C}^M$.

The first step is to find the optimal phase shift vector $\mathbf{s}$ such that the minimum channel gain among all UEs is maximised. This can be formulated as the optimization problem as follows:

$$\max_{\mathbf{s}} \min_{u \in \mathcal{U}} |\mathbf{s}^H \boldsymbol{\Theta} + \rho_{u0}[l+n]\sqrt{\beta_{u0}}^{-1}\hat{h}_{u0}|^2 \tag{4.15}$$

$$\text{s.t. } |s_n| = 1 \; \forall 1 \leq n \leq M. \tag{4.16}$$

Consider the following matrix as defined in [36]:

$$\mathbf{X}_u = \begin{bmatrix} \boldsymbol{\Theta}\boldsymbol{\Theta}^H & \boldsymbol{\Theta}\rho_{u0}[l+n]\sqrt{\beta_{u0}^{-1}}\bar{\hat{h}}_{u0} \\ \rho_{u0}[l+n]\sqrt{\beta_{u0}^{-1}}\hat{h}_{u0}\boldsymbol{\Theta}^H & 0 \end{bmatrix}. \tag{4.17}$$

where $\bar{(.)}$ is the complex conjugate. Let $\bar{\mathbf{s}} = [s_1,\ s_2,\ \cdots,\ s_M, x]^T$, where x is an auxiliary variable. Defining $\mathbf{S} = \bar{\mathbf{s}}\bar{\mathbf{s}}^H$, adding an auxiliary variable ξ and adopting the transformation in [36], we can rewrite the optimization formulation in (4.15) as a semi-definite programming (SDP) as follows:

$$\max_{\xi,\, \mathbf{S}} \xi \tag{4.18}$$

s.t.

$$tr(\mathbf{X_u S}) + |\rho_{u0}[l+n]\sqrt{\beta_{u0}}^{-1}\hat{h}_{u0}|^2 \geq \xi \; \forall u \in \mathcal{U} \tag{4.19}$$

$$\mathbf{S}_{m,m} = 1 \; 1 \leq m \leq M+1 \tag{4.20}$$

$$\mathbf{S} \succeq 0 \tag{4.21}$$

$$\xi \geq 0 \tag{4.22}$$

Here $tr(.)$ denotes the trace of a matrix. The SDP in (4.18) can easily be solved using CVX [113] followed by Gaussian randomization step to obtain the rank 1 optimal solution [**?** 48].

In our study, the objective of the phase shift optimization is to maximize the poorest channel gain among all UEs. It may be observed that finding such an optimal phase shifts at the RIS is a non-convex problem [36]. SDP has long been a theoretically powerful tool for solving such a non-convex optimization problem. Moreover, it is easier to mathematically formulate the optimization problem with our desired objective using SDP. In addition, tools

to solve SDP such as CVX is openly available. This strongly motivates us to use SDP in our case. However, the SDP based approach requires $O(M^{3.5})$ complexity [114] and therefore, is suitable only when the M is significantly small. On the other hand, in the real world

Algorithm 7: Local search for phase shift optimization

```
for RIS element m ∈ {1, 2, ··· , M} do
    Keep phase shift values of RIS elements other than m fixed;
    Find quantization bit q* such that minimum channel gain among UEs is maximized;
```

hardware, the RIS elements can induce only a finite set of discrete quantized phase shifts. The phase shift response at an RIS element is e^{ϕ}. Let q be the number of quantization bits, then each RIS element can generate 2^q phase shift values. Therefore the phase shift values are computed as $\phi = \frac{2i\pi}{2^q-1}$ where $i \in \{0,\ 1,\ 2,\ \cdots,\ 2^q-1\}$. Therefore, considering this hardware limitation, an $O(MU)$ local search based phase shift optimization algorithm [34] described below may be adopted, when M is large.

4.2.3 Power and bandwidth allocation

Optimal power allocation: Let the time slot l be the latest slot at which CE was performed. After determining the phase shifts of the RIS, we first optimally distribute the power across UEs to maximize the sum throughput per bandwidth by ensuring that the minimum rate requirement of all UEs is satisfied for time slot $l+n$. For a given time slot $l+n$, we need to find the power allocation to all UEs such that both $\sum_{u\in\mathcal{U}} R_u(l+n)$ and $\sum_{u\in\mathcal{U}} \widetilde{R}_u(l+n)$ are maximized. From (4.9) and (4.10) we observe that $R_u(l+n)$ and $\widetilde{R}_u(l+n)$ are functions of $\delta_u(\rho_{u0},\rho_u)$ and $\Delta_u(\rho_{u0},\rho_u)$ respectively. Furthermore, $\Delta_u(.)$ and $\delta_u(.)$ are of the form $\frac{A_uP_u}{B_uP_u+C_u}$ where, A_u, B_u, and C_u are positive real numbers, explicitly described as follows:

$$A_u = |\rho_u[T_p+nT_c]\hat{\mathbf{g}}_u\mathbf{L}_u\mathbf{\Phi}\mathbf{h} + \rho_{u0}[T_p+nT_c]\sqrt{\beta_{u0}^{-1}}\hat{h}_{u0}|^2 \quad \text{for } R_u(l+n)$$

$$A_u = \frac{M\rho_u^2}{\beta_u} + \frac{M(M-1)(\rho_u[T_p]\Omega_1\Omega_2)^2}{\beta_u} + \frac{2M\rho_u[T_p]\rho_{u0}[T_p]\Omega_0\Omega_1\Omega_2}{\sqrt{\beta_{u0}\beta_u}}$$

$$+\rho_{u0}[T_p]^2\beta_{u0}^{-1} \quad \text{for } \widetilde{R}_u(l+n)$$

$$B_u = \frac{M\widetilde{\rho}_u[T_p+nT_c]^2\left(1-\Omega_2^2\right)}{\beta_u} + \frac{\widetilde{\rho}_{u0}[T_p+nT_c]^2\left(1-\Omega_0^2\right)}{\beta_{u0}} \quad \text{for } R_u(l+n)$$

$$B_u = \frac{M\widetilde{\rho}_u[T_p]^2\left(1-\Omega_2^2\right)}{\beta_u} + \frac{\widetilde{\rho}_{u0}[T_p]^2\left(1-\Omega_0^2\right)}{\beta_{u0}} \quad \text{for } \widetilde{R}_u(l+n)$$
$$C_u = \sigma_u^2 + \exp(2\mu^u + 2(\Sigma^u)^2).$$

Let $\mathbf{P} = [P_1,\ P_2,\ \cdots,\ P_U]$ denote the transmit power vector for U UEs at time slot to compute $\boldsymbol{\tau_n}(l+n)$ at slot $l+n$ where $\boldsymbol{\tau}_u(l+n) \in \{R_u(l+n),\ \widetilde{R}_u(l+n)\} \quad \forall l, n \in \mathbb{N}$ and $n \geq s$. In order to compute the aggregate throughput gain, we need to optimize power allocation to maximize both $\sum_{u\in\mathcal{U}} R_u(l+n)$ and $\sum_{u\in\mathcal{U}} \widetilde{R}_u(l+n)$. This is because, the gain is measured as the difference between the maximum achievable throughput without CE and the maximum expected throughput had CE been performed at time slot $l+n$. Now, to formulate the optimization problems, we define two auxiliary variable vectors $\boldsymbol{\eta} = [\eta_1,\ \eta_2\ \cdots,\ \eta_U]$. Therefore, the optimal power allocation problems can be formulated as follows:

$$\max_{\boldsymbol{\eta}} \sum_{u=1}^{U} \eta_u \tag{4.23}$$

s.t.

$$\eta_u - \boldsymbol{\tau}_u(l+n) \leq 0,\ u \in \mathcal{U} \tag{4.24}$$

$$\sum_{u=1}^{U} P_u \leq P_{tot} \tag{4.25}$$

$$P_u \geq 0,\ u \in \mathcal{U} \tag{4.26}$$

$$\eta_u \geq 0,\ u \in \mathcal{U} \tag{4.27}$$

It may be observed that $R_u(l+n)$ and $\widetilde{R}_u(l+n)$ are concave function in $\mathbf{P}_n$ and $\bar{\mathbf{P}}_n$ respectively which can be easily observed from the Hessian matrix for these functions. Therefore the optimization problem (4.23) is separable convex optimization problems. Let R_u^{th} is the minimum throughput per bandwidth requirement for UE u. Therefore to satisfy this requirement, we must have the following:

$$R_u^{th} - \boldsymbol{\tau}_u \leq 0,\ u \in \mathcal{U}. \tag{4.28}$$

We can expand (4.28) and solve for the minimum power required to satisfy the required

throughput by UE u denoted by P_u^{min} as follows:

$$\frac{A_u P_u}{B_u P_u + C_u} \geq 2^{R_u^{th}} - 1$$
$$P_u \geq \frac{(2^{R_u^{th}-1})C_u}{A_u - (2^{R_u^{th}-1})B_u}$$
$$\implies P_u^{min} = \frac{(2^{R_u^{th}-1})C_u}{A_u - (2^{R_u^{th}-1})B_u}$$

After determining the minimum required power, the following feasibility cases need to be verified before deciding to skip CE in slot $l+n$.
Case 1: If $A_u - (2^{R_u^{th}-1})B_u < 0$ or $\sum_{u=1}^{U} P_u^{min} > P_{tot}$ then no feasible solution is possible. Hence channel needs to estimated again.
Case 2: If $\sum_{u=1}^{U} P_u^{min} = P_{tot}$, this becomes the only possible solution.
Case 3: If $\sum_{u=1}^{U} P_u^{min} < P_{tot}$, it may be easily observed that the constraint (4.24) and (4.25) satisfy the Slater's condition. Therefore the convex optimization problems follows strong duality. We solve the dual of the above convex optimization to obtain a closed form expression for P_u.

The Lagrangian for the objective function (4.23) and the constraints (4.24) and (4.25) is as follows:

$$\mathcal{L}(\boldsymbol{\eta},\ \mathbf{P},\ \boldsymbol{\zeta},\ \boldsymbol{\nu}) = \sum_{u=1}^{U} \eta_u + \sum_{u=1}^{U} \zeta_u \left(\boldsymbol{\tau_u}(l+n) - \eta_u\right)$$
$$+\nu \left(P_{tot} - \sum_{u=1}^{U} P_u\right) - \sum_{u=1}^{U} \nu_u \left(P_{min} - P_u\right). \tag{4.29}$$

Here, $\boldsymbol{\zeta}[\zeta_1,\ \zeta_2,\ \cdots,\ \zeta_U]$ and $\boldsymbol{\nu} = [\nu,\ \nu_1,\ \cdots,\ \nu_U]$ are the Lagrangian dual variables. Therefore, the Lagrangian dual of (4.23) is formulated as follows:

$$\min_{\nu>0,\,\zeta} \mathcal{G}(\boldsymbol{\nu},\boldsymbol{\zeta}) = \sup_{\boldsymbol{\eta},\mathbf{P}} \mathcal{L}(\boldsymbol{\eta},\mathbf{P},\boldsymbol{\zeta},\nu), \tag{4.30}$$

where $\mathcal{G}(\boldsymbol{\nu},\boldsymbol{\zeta}) = \inf_{\boldsymbol{\eta},\mathbf{P}} \mathcal{L}(\boldsymbol{\eta},\mathbf{P},\boldsymbol{\zeta},\boldsymbol{\nu})$ is the Lagrangian dual objective. Now, (4.29) is convex, continuous and differentiable in $\mathbf{P}_n$ and $\boldsymbol{\eta}$. The critical points of the Lagrangian can be

computed from the following equations:

$$\frac{\partial \mathcal{L}}{\partial \eta_u} = 0,\ \forall u \in \mathcal{U} \tag{4.31}$$

$$\frac{\partial \mathcal{L}}{\partial P_u} = 0,\ \forall u \in \mathcal{U} \tag{4.32}$$

From (4.31) we compute the values of $\zeta_u\ \forall u \in \mathcal{U}$ as follows:

$$\begin{aligned}
&\frac{\partial \mathcal{L}}{\partial \eta_u} = 0,\ \forall u \in \mathcal{U} \\
&\implies 1 - \zeta_u = 0,\ \forall u \in \mathcal{U} \\
&\implies \zeta_u = 1,\ \forall u \in \mathcal{U}
\end{aligned}$$

Substituting ζ_u in (4.29) and for a given value of ν, the closed form expression of $P_u\ \forall u \in \mathcal{U}$ is obtained from (4.32) as follows:

$$\begin{aligned}
&\frac{\partial \mathcal{L}()}{\partial P_u} = 0, \\
&\implies (A_u + B_u)B_u P_{un}^2 + P_{un}C_u(A_u + 2B_u) + \\
&C_u^2 - \frac{SA_uC_u}{\nu - \nu_u} = 0.
\end{aligned} \tag{4.33}$$

Here, $S = \left(1 - \frac{T_p}{sT_c}\right)$. Considering $a_u = (A_u + B_u)B_u$, $b_u = C_u(A_u + 2B_u)$ and discarding the negative root, we find the value of P_u as follows:

$$P_u^{\nu} = \frac{-b_u + \sqrt{b^2 - 4a(C_u^2 - \frac{SA_uC_u}{\nu - \nu_u})}}{2a}. \tag{4.34}$$

Therefore, for $\boldsymbol{\nu}^{(.)*} = \text{argmin}\ \mathcal{G}(\boldsymbol{\nu})$ we obtain the the optimal power allocated for UE u at time slot $l + n$ denoted by P_u^* is obtained as follows:

$$P_u^* = \frac{-b + \sqrt{b^2 - 4a(C_u^2 - \frac{SA_uC_u}{\nu^* - \nu_u^*})}}{2a}. \tag{4.35}$$

Furthermore, $\mathcal{G}(\boldsymbol{\nu})$ is convex in $\boldsymbol{\nu}$ since it is the point-wise supremum of an affine function.

Hence, we can obtain $\boldsymbol{\nu}^{(.)*}$ iteratively by simple gradient descent after substituting P_u from (4.34) in (4.29). The entire optimization process has been formally described in Algorithm 8.

Algorithm 8: Power allocation at slot $(l+n)$

Data: Gradient descent step χ, Acceptable error margin ϵ
Result: Optimal power allocation $\mathbf{P}^*$

1 Initialize $i=0$, $\nu^i = 100$, $\mathbf{P} = \mathbf{0}$;
2 Compute $\mathbf{P}$ according to (4.34) for $\boldsymbol{\nu}^i$;
3 **for** $P_u^i \in \mathbf{P}^i$ **do**
4 **if** $P_u^i \leq P_u^{min}$ **then**
5 Set $P_u^i = P_u^{min}$;
6 Substitute $\mathbf{P}^i$ in (4.29);
7 **for** $\hat{\nu}^i \in \boldsymbol{\nu}^i$ **do**
8 $\hat{\nu}^{i+1} = \left(\hat{\nu}^i - \chi\left(\frac{\partial \mathcal{L}(\mathbf{P}_n^i, \nu)}{\partial \hat{\nu}}|_{\hat{\nu}=\hat{\nu}^i}\right)^+\right)^+$;
9 Compute $\mathbf{P}_n^{(.)i+1}$ according to (4.34) for ν^{i+1};
10 **for** $P_{un}^{i+1} \in \mathbf{P}_n^{i+1}$ **do**
11 **if** $P_u^i \leq P_u^{min}$ **then**
12 Set $P_u^i = P_u^{min}$;
13 **if** $|\mathbf{P}_n^{i+1} - \mathbf{P}_n^i| \leq \epsilon$ **then**
14 $\mathbf{P}_n^* = \mathbf{P}_n^{i+1}$;
15 **else**
16 $i = i+1$ and go to line 2;
17 **Return** $\mathbf{P}_n^*$

Optimal bandwidth allocation to maximize sum throughput: After the optimal power allocation across UEs having different throughput requirement, we find the optimal bandwidth allocation to maximize the sum throughput. We denote by $\mathbf{b}^n = [b_1^n,\ b_2^n, \cdots\ b_U^n]$ as the resource vector where, b_u^n is the bandwidth allocated to UE u out of a total bandwidth of W at time slot $l+n$. Now the optimal resource allocation can be computed by solving the following optimization problem:

$$\max_{\mathbf{b}} \sum_u b_u^n . \log_2\left(1 + \frac{A_u P_u / b_u^n}{B_u P_u / b_u^n + C_u}\right) \tag{4.36}$$

$$\text{s.t.} \tag{4.37}$$

$$\sum_{u=1}^{U} b_u^n \leq W \tag{4.38}$$

$$b_u^n \geq 0,\ u \in \mathcal{U} \tag{4.39}$$

It is evident from the double derivative test that (4.36) is concave. This implies (4.36) a convex optimization problem. The optimal closed form expression for resource allocation can therefore be obtained by adopting the Karush-Kuhn-Tucker conditions (KKT) based method from [106]. The Lagrangian is given as follows:

$$\mathcal{L}(\mathbf{b}, \nu_1) = \sum_u b_u^n . \log_2 \left(1 + \frac{A_u P_u / b_u^n}{B_u P_u / b_u^n + C_u}\right) - \nu_1 \left(\sum_{u=1}^{U} b_u^n - B\right). \tag{4.40}$$

Therefore, from the KKT conditions we solve the equation $\frac{\partial \mathcal{L}}{\partial b_u^n} = 0$ for all $u \in \mathcal{U}$. Expanding the equation we get:

$$\log_2 \left(1 + \frac{A_u P_u}{C_u b_u^n + B_u P_u}\right) - \frac{A_u P_u}{B_u P_u + A_u P_u + C_u b_u^n} + \frac{B_u P_u}{A_u P_u} \left(\frac{(A_u P_u / (C_u b_u^n + B_u P_u))^2}{1 + A_u P_u / (C_u b_u^n + B_u P_u)}\right) = \nu_1. \tag{4.41}$$

To satisfy (4.41), we define a variable $x > 0$ as below:

$$\frac{A_u P_u}{C_u b_u^n + B_u P_u} = 1/x \quad \forall \quad u \in \mathcal{U}. \tag{4.42}$$

Therefore, we obtain the closed form expression for b_u^n as follows:

$$b_u^n = \frac{x A_u P_u - B_u P_u}{C_u}. \tag{4.43}$$

Furthermore, from constraint (4.38) we have $x = \frac{W + \sum_u B_u P_u / C_u}{\sum_u A_u P_u / C_u}$.

4.2.4 Algorithm for skipping CE phase

Considering that the last CE was done at time slot l and the coherence time based fixed interval be Ψ we need to find the number of consecutive time slots where CE can be skipped such that the aggregate throughput gain G_n defined in Subsection 4.2.1 is maximised. The first step is to compute the RIS phase shifts by either solving the optimization problem (4.18)

or using Algorithm 7. It may be observed that the RIS phase shifts will not be optimized again before the next CE is performed. The RIS is configured using outdated CSI estimates delayed by T_p immediately after CE. As shown in (4.7), when computing SINR, the phases of the channel coefficients remain invariant and the degradation in SINR with CSI aging is mathematically captured through the effective noise and the decreasing value of the channel correlation. Furthermore, the channel correlation coefficient is determined exclusively by the UE's velocity and the delay between the estimated and actual channels, and is independent of the channel coefficients' phase. Therefore, the drop in SINR of each UE is combated by optimal allocation of power and bandwidth across UEs without the need to update the RIS phase-shift configuration for time slots where CE is skipped, yielding a significant reduction in algorithmic complexity. Let us denote by S, the number of consecutive time slots that can be skipped. We need to check if CE needs to be formed at slot $l+n$ or not where $n < N_{max}$. If $n < z = \lceil \frac{\Psi}{T_c} \rceil$, we compute the optimal power and bandwidth allocation to maximize $\sum_{u \in \mathcal{U}} R_u$ and $\sum_{u \in \mathcal{U}} R_u$ for s consecutive time slots from slot $l+n$. If the power allocation is feasible and $G_n > 0$ we update $S = \min(S+s, z)$ and $n = \min(n+s, z)$. On the other hand, if the power allocation is not feasible or $G_n \leq 0$ we return the value of S updated thus far. We follow the same process when $n > z$, however here S is updated as $S = S + z$ and n is changed to $n+z$. The process terminates when either $n \nleq N_{max}$ or the optimal power allocation is not feasible or $G_n \leq 0$. After the process is completed, all UEs refrain from engaging in CE for S consecutive time slots and then communicate using the optimal power and bandwidth allocation determined during the process. The algorithm is formally described as follows in Algorithm 9. A schematic diagram to explain the entire process is given in Figure 4.3

Remark 2. *It may be observed that in our proposed algorithm the phase shifts are optimized only at the time slot when CE is performed. The optimal power and bandwidth allocation to maximize the sum throughput are computed accordingly. Therefore, the RIS need not be reconfigured repeatedly at all the slots where CE is skipped. Therefore, our proposed algorithm also helps to cope with the challenge posed by the limitations of phase adjustment speed to some degree.*

Remark 3. *It may be observed that the Gauss-Markov fading channel used in the proposed algorithm relies on the Markov property, which may not always accurately capture the complex temporal dynamics of real-world channels. In case the channel characteristics deviates from the adopted Gauss-Markov fading model but the deviation remains within*

Algorithm 9: CE skipping prediction algorithm

Data: Time slot l when CE was last performed; $z = \lceil \frac{\Psi}{T_c} \rceil$
Result: The number of consecutive time slots where CE can be skipped

Optimize phase shift at RIS;
Set $S = 0$;
while $n < N_{max}$ **do**
  if $n < z$ **then**
    for *n to* $n + s$ **do**
      Compute **P** to maximize $\sum_{u \in \mathcal{U}} R_u$ and $\sum_{u \in \mathcal{U}} R_u$ by Algorithm 8;
      if **P** *is not feasible* **then**
        return S;
      else
        Allocate optimal bandwidth using (4.43);
    if $G_n > 0$ **then**
      $S = \min(S + s, z)$;
      $n = \min(n + s, z)$;
    else
      return S;
  else
    for *n to* $n + z$ **do**
      Compute **P** to maximize $\sum_{u \in \mathcal{U}} R_u$ and $\sum_{u \in \mathcal{U}} R_u$ by Algorithm 8;
      if **P** *is not feasible* **then**
        return S;
      else
        Allocate optimal bandwidth using (4.43);
    if $G_n > 0$ **then**
      $S = S + z$;
      $n = n + z$;
    else
      return S;

acceptable margins, the algorithm may be modified to utilize real measurements of SINR in each skipped slot. Such technique may result in lower sum data rates compared to the proposed algorithm due to an increase CE frequency. This may shorten the difference between the sum rates obtained by the proposed method and that obtained by performing

CE at fixed time intervals. However, the advantage of skipping multiple time slots over performing CE after every fixed interval duration still exists.

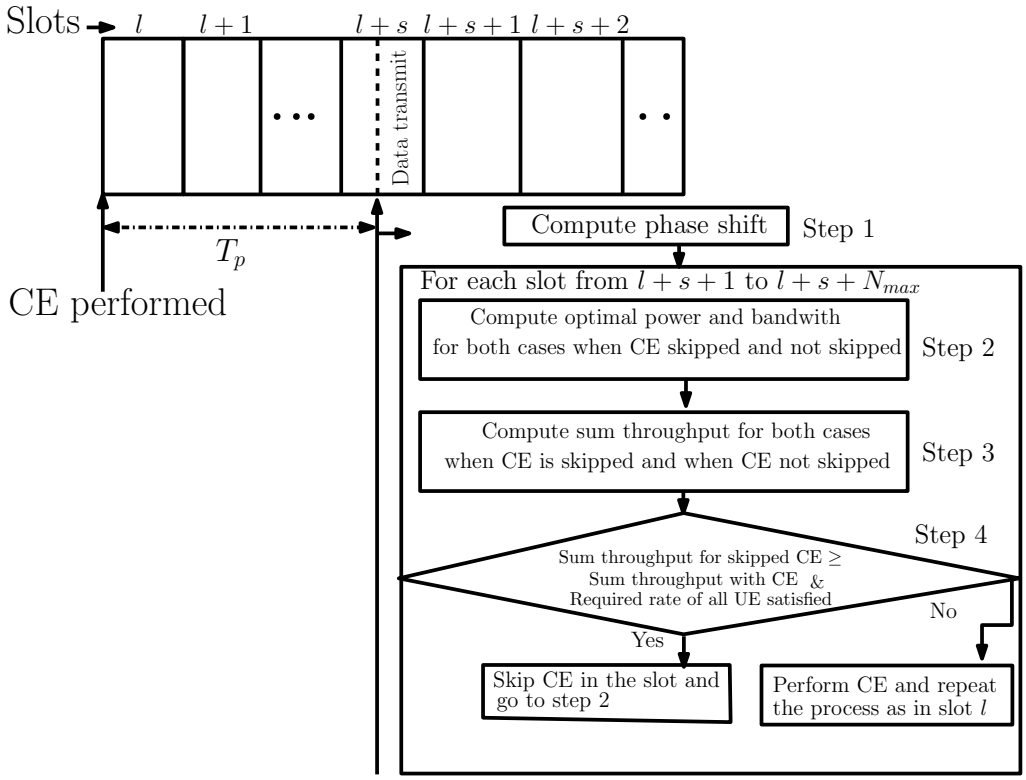

Figure 4.3: Overview of the proposed algorithm

4.2.5 Convergence and complexity analysis

In this subsection, we prove the convergence of the proposed iterative Algorithm 2 and discuss the computational complexity of proposed CE skipping algorithm.

Convergence: Note that in our proposed technique, the dual variables $\boldsymbol{\nu} = [\nu,\ \nu_1,\ \cdots,\ \nu_U]$ are updated at the i^{th} iteration as follows:

$$\nu^{i+1} = \left(\nu^i - \chi\left(\frac{\partial \mathcal{L}(\mathbf{P}^i, \nu)}{\partial \nu}|_{\nu=\nu^i}\right)\right)^+ \tag{4.44}$$

$$\nu_u^{i+1} = \left(\nu_u^i - \chi\left(\frac{\partial \mathcal{L}(\mathbf{P}^i, \nu_u)}{\partial \nu_u}|_{\nu_u=\nu_u^i}\right)\right)^+ \tag{4.45}$$

where χ is the step size, $\mathbf{P}^i$ is the transmit power vector and $(x)^+ = \max(0, x)$. We now show that $[\frac{\partial \mathcal{L}(\mathbf{P}_n^i, \nu)}{\partial \nu}, \frac{\partial \mathcal{L}(\mathbf{P}_n^i, \nu)}{\partial \nu_1}, \cdots, \frac{\partial \mathcal{L}(\mathbf{P}_n^i, \nu)}{\partial \nu_U}]_{\boldsymbol{\nu}=\boldsymbol{\nu}^i}$ is a subgradient of $\mathcal{G}(\nu)$.

$$
\begin{aligned}
\mathcal{G}(\boldsymbol{\nu}) =& \sup_{\boldsymbol{\eta}, \mathbf{P}} \mathcal{L}(\boldsymbol{\eta}, \mathbf{P}, \boldsymbol{\zeta}, \boldsymbol{\nu}) \\
=& \sup_{\boldsymbol{\eta}, \mathbf{P}} \sum_{u=1}^{U} R_u(l+n) + \nu \left(P_{tot} - \sum_{u=1}^{U} P_u \right) - \sum_{u=1}^{U} \nu_u \left(P_{min} - P_u \right) \quad \text{[Substituting } \boldsymbol{\eta} \text{ and } \boldsymbol{\zeta}\text{]} \\
& \text{By substituting the value of } P_u \text{ with } P_u^i \text{ and } R_u \text{ with } R_u^i \text{ obtained} \\
& \text{in the } (i-1)^{th} \text{ iteration, we get} \\
\geq& \sum_{u=1}^{U} R_u^i(l+n) + \nu \left(P_{tot} - \sum_{u=1}^{U} P_u^i \right) - \sum_{u=1}^{U} \nu_u \left(P_{min} - P_u \right) \\
=& \sum_{u=1}^{U} R_u^i(l+n) + (\nu + \nu^i - \nu^i) \left(P_{tot} - \sum_{u=1}^{U} P_u^i \right) - \sum_{u=1}^{U} (\nu_u + \nu_u^i - \nu_u^i) \left(P_{min} - P_u \right) \\
=& \mathcal{G}(\boldsymbol{\nu}^i) + \left(P_{tot} - \sum_{u=1}^{U} P_u^i \right) (\nu - \nu^i) + \sum_{u=1}^{U} \left(P_{min} - P_u \right) (\nu_u - \nu_u^i) \\
=& \mathcal{G}(\boldsymbol{\nu}^i) + \left(\frac{\partial \mathcal{L}(\mathbf{P}^i, \boldsymbol{\nu})}{\partial \nu} |_{\nu=\nu^i} \right) (\nu - \nu^i) + \sum_{u=1}^{U} \left(\frac{\partial \mathcal{L}(\mathbf{P}^i, \boldsymbol{\nu})}{\partial \nu_u} \right) (\nu_u - \nu_u^i)
\end{aligned}
$$

This implies that the dual variable ν is updated following the subgradient decent method, which is guaranteed to converge by setting $\chi = \frac{Z}{i}$ for an appropriate constant Z [115, 116, 117]. In our study, we have set $Z = 0.1$.

Complexity analysis: The proposed algorithm is executed in the first slot and then only at those slots when CE is required to be performed. In the first step, the proposed algorithm optimizes the phase shift of the RIS elements based on the estimated CSI. This can be done in $O(MU)$ computational complexity by considering the hardware limitations and subsequently using the local search based phase shift optimization algorithm (Algorithm 7), where M is the number of RIS elements and U is the number of UEs. The algorithm then iteratively predicts the number of consecutive future time slots out of $N_{max} - 1$ slots where CE can be skipped. To do so, it computes the optimal power and bandwidth allocation for each such future slot iteratively. Optimal power allocation (Algorithm 8) can be computed in $O(KU)$ complexity, where K is the number of iterations it takes to converge. The optimal bandwidth allocation requires $O(U)$ complexity. In the worst case, the proposed algorithm runs for $N_{max} - 1$ iterations, where $N_{max} - 1$ is the maximum

number of slots that can be skipped. Hence the worse case complexity of the proposed algorithm is $O((N_{max}-1)(KU+U)+MU)$. In other words, for fixed number of RIS elements, it scales linearly with the number of UEs and for a fixed number of UEs, it scales linearly with number of RIS elements.

4.3 Numerical results

In this section, we evaluate the performance of our proposed algorithm through extensive system-level simulations. It is to be noted that with the best of our knowledge we are the first to develop an algorithm to dynamically perform CE for an RIS assisted multi user scenario explicitly considering outdated CSI. The study closest to our proposed algorithm has been explored in [70]. Herein, the authors have proposed an algorithm that jointly optimizes the adaptive CE interval and passive beamforming of the RIS by modeling the problem as a bi-level partially observable Markov decision process (POMDP). At each time step, past observations are leveraged to first decide weather or not to skip CE in that time slot. Next the action corresponding to the passive beamforming at the RIS is chosen. However, their proposed algorithm is designed only for a single UE. Furthermore, the normalized mean square error of the proposed algorithm increases significantly with increase in channel correlation coefficient, as demonstrated therein. Our proposed algorithm is specifically designed for multi user scenario. In order to apply their POMDP model in our multi user scenario, we assume that each UE is associated with an independent POMDP agent. Subsequently each agent chooses a passive beamforming configuration at the RIS that is best suited for its corresponding UE. Since an RIS can only implement one configuration at a time, at each time slot, we choose the configuration that maximizes the sum throughput. Therefore, we now compare the simulation results obtained by our proposed algorithm with coherence time based fixed inter CE duration based approach [64, 35, 67] and a dynamic CE strategy proposed in [70]. In [64, 35, 67], the fixed interval duration is defined as $\Psi = \frac{c\cos^{-1}(0.5)}{2\pi V f_c}$. Here V is the maximum velocity achieved by any UE [13]. Through simulations, we show the impact of UE velocity, number of UEs and number of RIS elements on the sum throughput over the entire duration of communication.

The sum throughput is the sum of the aggregate throughput obtained by all users in all

time slots T, calculated as follows:

$$\sum_{t=1}^{T}\sum_{u=1}^{U} R_u(t), \tag{4.46}$$

where $\sum_{u=1}^{U} R_u(t)$ the aggregate throughput obtained by all users at a particular time slot t. The advantage offered by the proposed algorithm lies in the fact that CE is avoided in multiple time slots over the entire duration of communication. This reduces the CE overhead and boosts the throughput of the UEs over the entire duration of communication. This justifies our choice for the metric defined in (4.46) for analyzing the performance of the proposed algorithm.

4.3.1 Simulation setup

Table 4.2: 3GPP Urban Macro (UMa) Parameter Assumptions for Simulation (Based on TR 38.901)

Parameter	**Value**	**Unit/Note**
Minimum BS-UE 2D Distance	35	m
Reference Distance for Path Loss	Implicit (close-in $\approx$ 1)	m
Shadow Fading Std. Dev. (σ_{SF}) - LOS	4	dB
Shadow Fading Std. Dev. (σ_{SF}) - NLOS	6	dB
Mobility Model	Random Waypoint or Uniform	(UEs move at constant speed)
Delay Spread ($\mu_{\lg DS}$) - NLOS	-6.83	$\log_{10}$(s)

The parameters of the simulation environment have been adopted from [109, 36, 35, 13, 105]. The simulation has been performed using custom python code using python version 3.11.11. The following libraries were used to compute the expected values of the Rician random variables using Laguerre function: from scipy.special import genlaguerre and from scipy.special import eval_genlaguerre. The values for the bessel function was computed using the library tensorflow and the function tensorflow.math.special.bessel_j0(.). Random numbers following uniform distribution are generated using the library function

Table 4.3: Simulation parameters for Chapter 4

Parameters	**values**
Radius of gNB coverage	100 meters
Velocity range	20 m/s to 26 m/s
gNB coordinate	$(50, 0, 10)$
RIS coordinate	$(25, 30, 10)$
No. of RIS elements	200 to 500
P_{tot}	20 dBm
Carrier frequency	5 Ghz
Noise power	-120 dBm
Pathloss exponent gNB-RIS-UE channel	3.5
Pathloss exponent direct channel	2
Rician factors	$K_1 = K_2 = 1$ dB, $K_0 = 0$
Total Bandwidth	17 MHz
Background interference	-95 dBm
R^{th}	256 Mbps
Total communication time	50 seconds

random.uniform and following standard normal distribution are generated using the standard_normal() function of the numpy.random library. The UEs are considered to move in a circular region of radius 100 meters. Random way point mobility model has been adopted to simulate the motion of the UEs. The center of the circular region is considered to be the origin. The initial positions of the UEs are chosen uniformly randomly inside the circular region. The UEs move linearly in arbitrary directions with a velocity ranging from 20 m/s to 26 m/s throughout the simulation time. It is to be noted that when a UE reaches the boundary of the considered simulation region, the direction of motion of the UE changes such that the UE stays within the boundary throughout the simulation time. The gNB is placed at $(50, 0, 10)$ and the coordinate of the RIS center is $(25, 30, 10)$. The simulation models a sub-6 GHz gNB equipped with single isotropic antenna. The antenna height is set at 10 meters above ground level. Each UEs is also modeled with a sub-6 GHz single isotropic antenna. The UE antenna height is set at 2 meters above ground level for all UEs. The antenna gain is set at 0 dBi. All distances are in meters. The total allowable transmission power of the gNB is set at $P_{tot} = 46$ dBm. The carrier frequency is set at 5 GHz [35]. The noise power is -120 dBm. Moreover, the gNB and UE antenna gains are 20 dB and 0 dB respectively [35]. The pathloss exponent of the cascaded gNB-RIS-UE channel is set at 3.5,

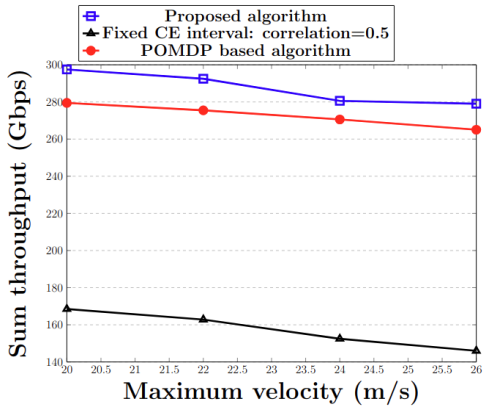

Figure 4.4: Sum throughput vs. maximum allowed velocity

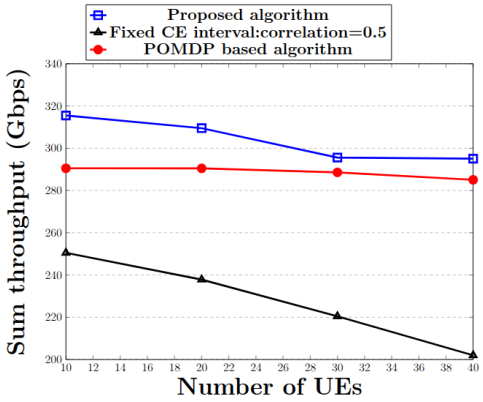

Figure 4.5: Sum throughput vs. number of UEs

and the direct gNB-UE channel is set at 2 [105]. We set the Rician factors as $K_1 = K_2 = 1$ dB and $K_0 = 0$ [105]. Total bandwidth is 17 MHz [36]. The background interference from neighbouring cells is set at a value of -95 dBm [109]. The default number of RIS elements is $M = 300$. The minimum required throughput is set at $R^{th} = 256$ Mbps. Finally, the total time of communication is 50 seconds. The results have been generated by averaging over 1000 independent runs of the simulation. Important parameters are summarized in Tables 7.2 and 4.3

4.3.2 Evaluating sum throughput

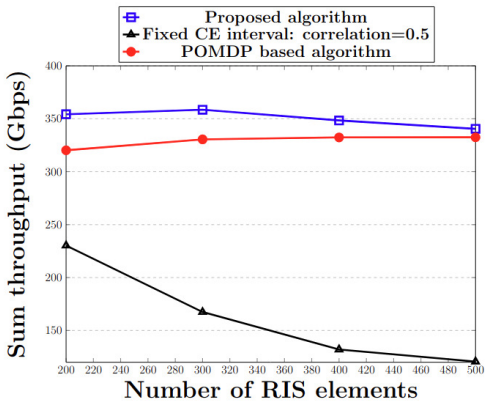

Figure 4.6: Sum throughput vs. number of RIS elements

Figure 4.4 shows the effect of the velocity of UE on the sum throughput for the cases where inter CE duration is determined by our proposed algorithm, the POMDP based

algorithm and the fixed time interval based algorithm. The number of UEs is 30 and the number of RIS elements is 300. The minimum velocity of each UE is set at 10 m/s. The maximum velocity allowed for UEs ranges from 20 m/s to 26 m/s with a step of 2 m/s. The sum throughput monotonically decreases for all three cases which can be explained as follows. The channel coherence time and the temporal channel correlation is inversely proportional to the velocity. As a consequence, the frequency of CSI acquisition increases with increasing maximum allowable velocity thereby increasing pilot overhead and reducing sum throughput. However, the sum throughput for our proposed strategy is higher as compared to both the POMDP based and fixed time interval based approaches. This can be explained as follows. When comparing with the fixed time interval based approach, our algorithm performs better because it can adaptively change the inter CE duration according to the channel conditions and velocity distribution among the UEs. Therefore, when channel conditions are good, more time slots are skipped thereby reducing pilot overhead. However, when the channel conditions are poor, impact of the outdated CSI degrades the SINR significantly. In such a case, our approach may perform CE even before the fixed duration Ψ simply to boost the throughput of each UE.

As oppose to the POMDP based algorithm, our algorithm is designed specifically for multi user scenario. Each POMDP agent determines its own passive beamforming configuration at the RIS best suited for its corresponding UE. However, the RIS can implement only one such configuration at a given time. The configuration that maximizes the sum throughput is chosen. However, this results in non-optimal beamforming for UEs other than the UE whose corresponding RIS configuration was chosen. This greatly reduces their throughput. Furthermore, with increasing velocity the temporal correlation between the channel decreases and the normalized mean square error increases. This further results in poorer performance by the POMDP based algorithm with increasing velocities of the UEs.

Figures 4.5 and 4.6 show the effect of number of UEs and number of RIS elements on the sum throughput. When the number of UEs vary, the number of RIS elements are fixed at 300 and the maximum allowed velocity is 20 m/s. For the case when the number of RIS elements vary, the number of UEs is fixed at 30 and the maximum allowed velocity is 20 m/s. The sum throughput decreases with number of UEs for both the case of our proposed algorithm and the fixed time interval based algorithm. The power and bandwidth resource allocated to each UE decreases with increasing UE. Furthermore, the complexity of estimating the channel also increases. This results in increased delay and faster degradation of the SINR and increases the frequency of CE. On the other hand the sum throughput

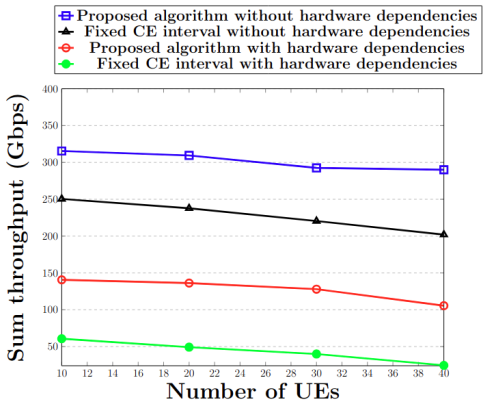

Figure 4.7: Sum throughput vs. number of UEs

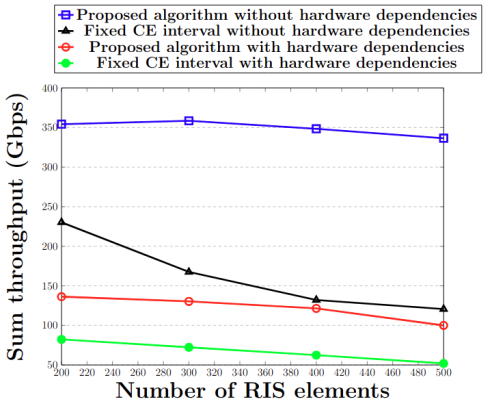

Figure 4.8: Sum throughput vs. number of RIS elements

initially increases with the number of RIS elements upto 300 elements and then decreases beyond 300 elements. This is because with increasing RIS elements the gain at the UEs increases however, the pilot overhead also increases which in turn increases time consumed for CE and reduces time left for data communication. This eventually decreases the sum throughput. Our proposed algorithm performs better than the other two algorithms for the same reasons as elaborated for Figure 4.4.

Finally, we observe that the proposed dynamic channel estimation algorithm achieves a maximum throughput gain of 12% relative to the partially observable Markov decision algorithm [70] for 10 UEs, 300 reflective elements and a UE maximum UE velocity of 20 m/s. Moreover, a throughput gain of 250% is achieved relative to fixed channel estimation interval based approach [64, 35] for 30 UEs, 500 reflective elements and a maximum UE velocity of 20 m/s. Furthermore, the margin of error at 95% confidence for the measured sum throughput is less than 0.053, which signifies a high level of accuracy in the obtained results.

4.3.3 Evaluating proposed algorithm under hardware limitations

In this subsection we evaluate the performance of our algorithm under certain practical hardware dependencies. We primarily consider the following hardware limitations.

1. **Discrete quantized phase shifts at the RIS:** The reflective element of a real world RIS hardware is not capable of continuous phase shifts. Therefore, the RIS elements can only generate finite phase shift values. This results in an error between the actual

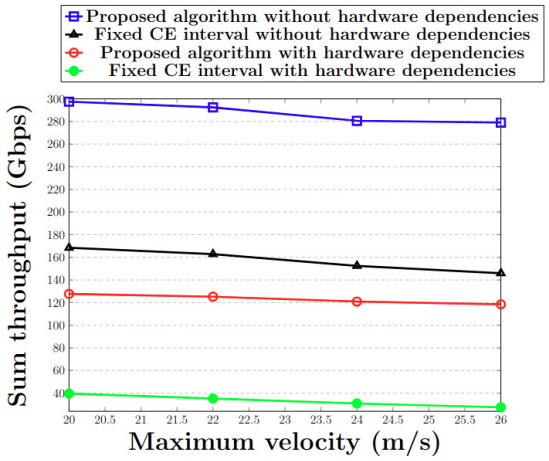

Figure 4.9: Sum throughput vs. maximum allowed velocity

optimal phase shift value of the RIS elements and the discrete value that is closest to the optimal value. In this regard, the phase shift optimization at the RIS is computed based on the local search based $O(MU)$ algorithm as discussed before.

2. **Limitation of channel capacity due to modulation coding:** In real world hardware the gNB transmits data based on channel adaptive modulation coding [118]. Therefore the throughput achieved generally does not follow the Shannon's capacity and it is dependent on the modulation coding scheme adopted by the gNB during transmission. Let c_{ur} be the modulation scheme for an UE u out of C available modulation schemes, then the corresponding throughput is $R_{ur} = \log_2(c_{ur})$. The modulation scheme selected for UE u depends on the SNR experienced by the UE and the acceptable bit error rate (BER).

The adaptive modulation scheme is incorporated in our proposed algorithm as follows: After computing the optimal power allocation for each UE, we calculate the SINR using (4.7) and (4.8). This SINR is then used to select the appropriate modulation scheme and determine the throughput, which replaces Shannon's capacity formula based throughput computation used in our proposed CE skipping algorithm. Note that the interference experienced is treated as noise in the expression for SINR in (4.7). The M-ary quadrature amplitude modulation (M-QAM) technique with a BER 10^{-6} is adopted [118] and depicted in Table 4.4. Using the M-QAM technique and discrete quantized phase shifts, the following new simulation results have been generated to

Table 4.4: Transmission Modes for BER $= 10^{-6}$.

SNR interval (dB)	Modulation	Rate (bits/symbol)
$(-\infty, 9.8554)$	No transmission	0
$[9.8554, 12.8657)$	BPSK	1
$[12.8657, 14.6266)$	QPSK	2
$[14.6266, 15.8760)$	8-QAM	3
$[15.8760, 16.8451)$	16-QAM	4
$[16.8451, 17.6369)$	32-QAM	5
$[17.6369, 18.3063)$	64-QAM	6
$[18.3063, 18.8863)$	128-QAM	7
$[18.8863, +\infty)$	256-QAM	8

show the impact of hardware limitations on the performance of the proposed algorithm. Figures 4.7, 4.8 and 4.9 show the sum throughput with respect to varying number of UEs, RIS elements and different maximum allowable velocities respectively. It is observed that the sum throughput considering hardware limitations is less than that achieved by not considering the hardware limitations. However, our proposed algorithm still performs better than the fixed time interval based CE scheme [67, 13] even when hardware limitations are taken into account. Here the fixed CE interval is computed as the the channel coherence time for the fastest UE for a correlation threshold of 0.5.

Remark 4. *The log-normal distribution assumes that interference from different cells is independent. In reality, interference can be correlated due to factors like spatial proximity and shared resources. However, during the simulation for generating results in Figure 4.7, Figure 4.8 and Figure 4.9, we have computed the actual interference power from randomly placed base stations in the neighborhood of the gNB at each time slot. We observe our proposed algorithm still performs better than the fixed time interval based CE strategy.*

4.3.4 Evaluating signaling overhead

Figure 4.10 and Figure 4.11 show the signaling overhead with respect to the number of UEs and the number of RIS elements respectively. The number of UEs range from 10 to 40 with a step of 5 UEs and the number of RIS elements range from 200 to 500 with a step of

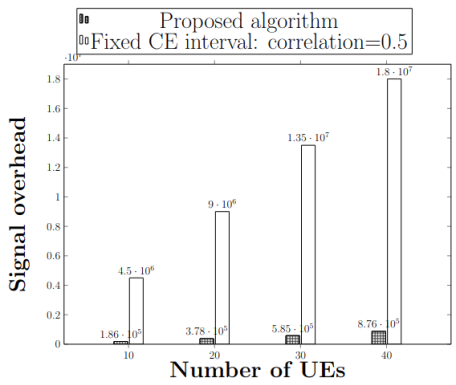

Figure 4.10: Signal overhead vs. number of UEs

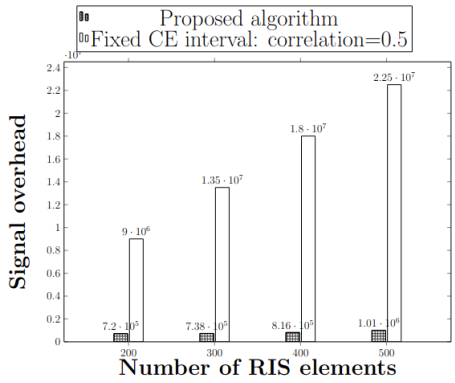

Figure 4.11: Signal overhead vs. number of RIS elements

100 elements. The maximum velocity of of the UEs is 20 m/s. Here, signaling overhead is defined as the sum of the following signals over the entire duration of communication: 1) the number of pilot signals, 2) the feedback signal to the RIS, and 3) the signal broadcasted to the UEs informing them about the slots where CE can be skipped. It can be observed that the signaling overhead increases with the number of UEs and number of RIS elements, as expected. However, the signaling overhead for our proposed algorithm is lower than that for a fixed time interval based CE scheme [13] by a factor of at least 12. Here the fixed time interval is computed as the coherence time for the fastest UE for a correlation threshold of 0.5. In [13], CE is performed consecutively after a fixed time duration of length Ψ, where Ψ is a function of the velocity of the UE. Whereas, in our proposed algorithm, multiple such intervals may be skipped by optimally allocating power and bandwidth to the UEs.

4.3.5 Evaluating impact of key parameters on algorithm performance

We have set the minimum velocity with which a UE can move to 10 m/s. The range of maximum allowable velocity of the UEs is 20 m/s to 26m/s with a step of 2 m/s. Such a range of user speed allows the existence of UEs with diverse moving speeds during the simulation starting from slow moving vehicles such as (bikes and electric scooters) to fast moving vehicles such as cars and buses. The quantity of RIS elements vary from 200 to 500 with a step of 100 elements which is the standard in most recent studies on RIS assisted networks such as [60, 59] to capture the effect of the number of RIS elements on the performance of the algorithm. We varied the number of UEs from 20 to 40 with a step

of 10 UEs within a circular region of 100m which allows us capture the effect of both low density and high density of UEs.

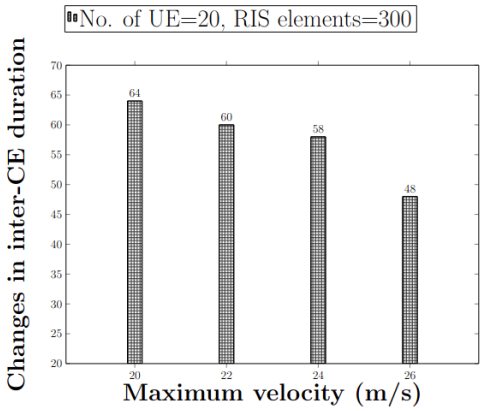

Figure 4.12: Time slots skipped between consecutive CE vs. maximum velocity

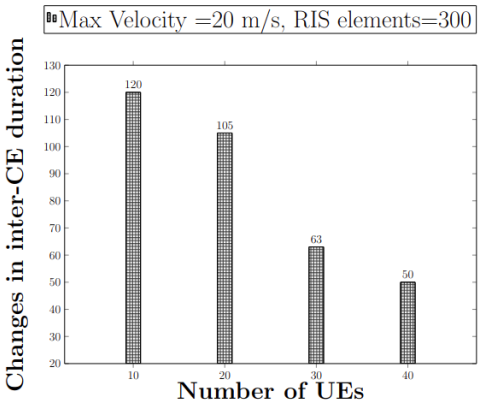

Figure 4.13: Frequency of change in inter-CE duration vs.number of UEs

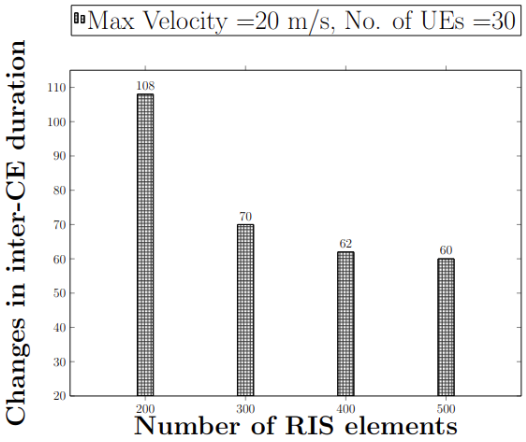

Figure 4.14: Frequency of change in inter-CE duration vs. number of RIS elements

The proposed algorithm outputs the number of time slots that can be skipped before CE is performed again. Figures 4.12, 4.13 and 4.14 show the frequency of changes in the inter-CE duration with respect to maximum allowable velocity of UEs, number of UEs and number of RIS elements respectively. These figures measure how the output of the proposed algorithm is effected by the different values of the key parameters given an idea on the sensitivity of the performance of the algorithm. It can be observed that the variation in the value of the number of times slots skipped decreases monotonically with the value of the key parameters. The value of SINR computed by the adopted models used in the

algorithm decreases monotonically with velocity. Therefore, the degradation in SINR due to delay between the actual CSI and the estimated CSI increases with velocity. This causes the algorithm to output smaller number of time slots to be skipped. Moreover, an increase in the maximum allowable velocity increases the disparity in magnitude of velocity between a slow moving UE and the fast moving UE. Since all UEs need to satisfy their rate requirement when deciding to skip a time slot, the duration of time over which CE needs to be avoided is heavily impacted by the high velocity UEs as compared to the low velocity UEs. Therefore, as the maximum allowable velocity increases the variation in output of the algorithm reduces around a value best suited for the fast moving UEs. In Figure 4.13, the primary reason for the decrease in frequency of changes in the inter-CE duration is due to the drop in data rate suffered by UEs as the number of UEs increases. With more UEs each UE gets a lesser share of the total power and bandwidth. As the data rate falls the algorithm outputs smaller values of the number of time slots skipped and the variation in these values reduces.

From Figure 4.14, it can be observed that there is a sharp drop in the variation in the inter-CE duration upto a threshold value of 300 RIS elements. This is because of the rise in CE overhead which increases the delay between estimated and outdate channel. The degradation of SINR rises with rising delay causes the maximum value of the inter-CE duration to decrease reducing the disparity between the smallest duration and the largest one. However beyond 300 RIS elements the rate of decrease in the variation drops with increasing number of RIS elements. The fraction of time in time slot consumed during CSI acquisition increases monotonically with the number of RIS elements. This negatively impacts the data rate. On the other hand, the SINR increases with increasing number of RIS elements which balances the negative impact of the increase in RIS elements. As a result the inter-CE duration is predominantly effected by the velocity, resource share and location of the UEs which change frequently over time. This in turn slows down the rate of decrease in the fluctuations of the algorithm's output.

In Figure 4.15, we show the number of time slots skipped between CE by the proposed algorithm with respect to the maximum allowable velocity. We observe that the average of the number of skipped slots between CEs decreases monotonically. This is because higher velocity leads to faster degradation of the SINR as the CSI becomes more outdated over time. As a consequence the average frequency of CE over time increases. We also observe that the rate of decrement in the average time slot skipped between CEs also falls with increasing velocity. This is because the duration of individual time slot decreases with velocity. As a

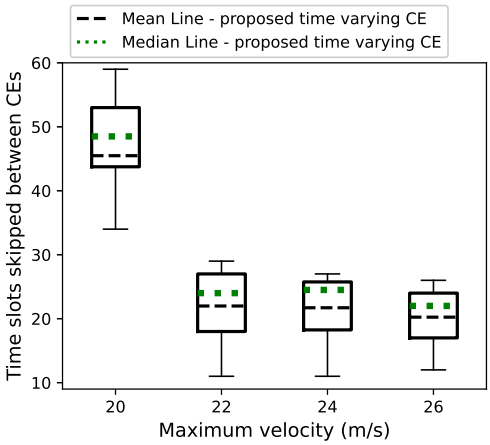

Figure 4.15: Time slots skipped between consecutive CE vs. maximum velocity

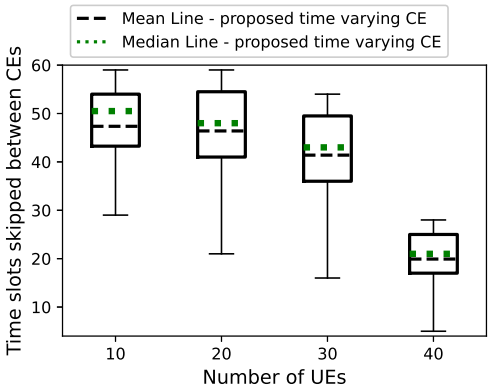

Figure 4.16: Time slots skipped between consecutive CE vs. number of UEs

result, even though the duration between consecutive CE reduces the number of time slots that make up for that duration does not reduce significantly.

In Figure 4.16, we show the number of time time slots skipped between CE by the proposed algorithm with respect to the number of UEs. We observe that the average of the number of skipped slots between CEs decreases monotonically. This is because higher number of UEs strains the power and bandwidth resources leading to smaller share of power and bandwidth for each. As a consequence, the SINR drops quicker with time when CE is skipped and thereby leading to and increase in the average frequency of CE.

In Figure 4.17, we show the number of time time slots skipped between CE by the proposed algorithm with respect to the number of RIS elements. We observe that the rate of decrease in the average of the number of skipped slots between CEs drops with increasing number of RIS elements. This is because the channel gain and the SINR improves along with increasing number of RIS elements. However, the pilot overhead also increases with the number of RIS elements. This creates a balancing effect thereby stabilizing the value of average number of slots skipped between CE.

4.3.6 Evaluating computation time of the proposed algorithm

In this subsection we evaluate the practical applicability of the proposed algorithm by measuring the time consumed during the execution of the algorithm. In Figures 4.18 and

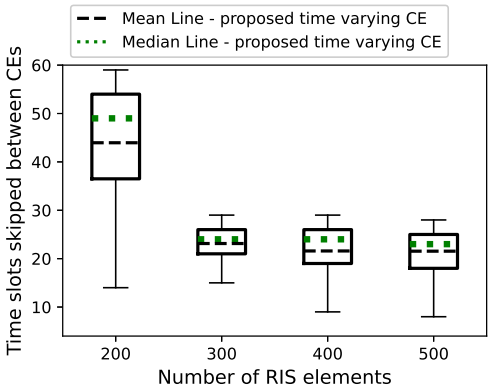

Figure 4.17: Time slots skipped between consecutive CE vs. number of RISs

4.19, we have shown the average percentage of time consumed for running the proposed algorithm out of the total duration of communication before the next CE operation with respect to varying number of UEs and RIS elements respectively. The algorithm is executed using a 64-bit and 4 GHz 12th Gen Intel(R) Core(TM) i7-12700 processor with 12 cores. The results have been averaged over 1000 runs of the algorithm. The number of UEs range from 10 to 40 with a step of 10 UEs and the number of RIS elements range from 200 to 500 with a step of 100 elements. The local search based phase shift optimization was used to find optimal RIS configuration. The values of the channel correlation coefficients are precomputed and stored in a table with the i^{th} row corresponding to the delay $T_p + iT_c$ and the j^{th} column corresponds to velocity $10 + j$ m/s. The maximum velocity of of the UEs is 26 m/s. It can be seen that a maximum of 4% of the duration communication after is consumed for execution of the algorithm. This makes the algorithm implementable in real-world system.

4.4 Conclusion

This chapter attempts to answer the question of when to conduct CE given outdated channel estimates in an RIS-assisted wireless network. The channel estimation overhead in RIS assisted network with unstructured multi-path rich channels render the estimates to become outdated during actual communication within a communication slot and also significantly

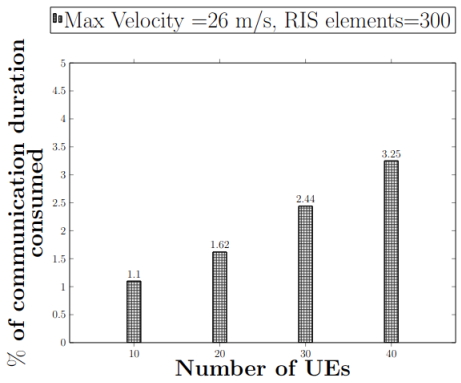

Figure 4.18: Average percentage of communication duration consumed vs. number of UEs

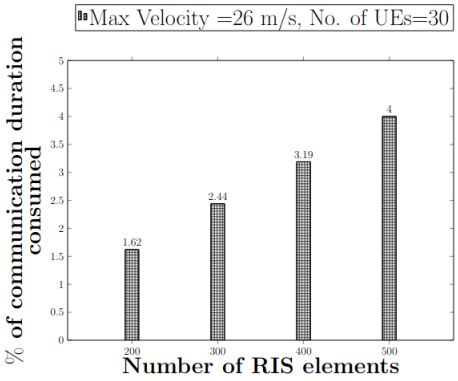

Figure 4.19: Average percentage of communication duration consumed vs. number of RIS elements

reduces the time left for actual data communication. Here, we propose an algorithm that dynamically determines the duration between consecutive CE periods by explicitly considering the velocities, channel conditions of different UEs in the network. Extensive simulations show that our proposed time varying CE achieves higher throughput in comparison to coherence time based fixed CE interval [13, 67] dynamic CE estimation algorithm proposed in [70]. A minimum of 90% and a maximum of 100% in sum throughput has been observed in comparison to the coherence time based fixed inter-CE duration. Moreover, a minimum of 10% and a maximum of 30% gain in sum throughput has been observed in comparison to the POMDP based adaptive CE duration algorithm. The proposed algorithm greatly reduces the CE overhead in RIS assisted multi-user wireless networks and increases the sum throughput. However, the strict latency constraints for the URLLC based UEs has not been considered here. In the next chapter, we develop a RIS selection such that the latency constraints are not violated during handovers for URLLC based UEs.

Chapter 5

Joint RIS-Network selection in URLLC[1]

This chapter deals with the limitation of violating strict latency constraints for URLLC based UEs caused by the time consumed to estimate the channel and configure the RIS during handover. Relying on outdated channel state information (CSI) for short packet URLLC based communication increases BER beyond the permitted thresholds and deteriorates reliability of transmission. Therefore, the RIS needs to be configured with CSI as accurate as possible. However, the pilot overhead to acquire precise CSI may often violate the strict delay constraints of URLLC based UEs. To mitigate this, a network selection mechanism for RIS assisted network has been proposed. The goal of the proposed mechanism is to select appropriate gNodeB (gNB) or gNB-RIS pair to maximize user throughput while satisfying the delay and reliability constraints of URLLC users. First, the network selection mechanism for RIS assisted network has been formulated as multi arm bandit MAB problem. Then, based on the formulation, a network selection strategy has been proposed. Finally, through extensive system level simulations, it has been shown that the proposed scheme outperforms the widely implemented A3 based handover scheme in terms of reliability and user throughput.

The symbols used in this chapter and their respective meaning are given in Table 5.1.

[1]This chapter is based on the following publication:
Souvik Deb, Shankar K. Ghosh and Sasthi C. Ghosh, "MAB based network selection mechanism for URLLC users in RIS assisted network," **The 21st IEEE International Symposium on Network Computing and Applications (IEEE NCA 2022)**, Boston, MA, USA, pp. 173-179, 14-16 December 2022.

Table 5.1: Important Notations for Chapter 5

Symbols	Meaning
$\mathbf{K}$, $\mathbf{N}$, $\mathcal{A}, \mathcal{C}_k$	Set of BSs, RISs, Actions, Contexts
U	No. of URLLC UEs
$\mathbf{\Phi}$	RIS phase shift matrix
ϕ_m	m^{th} Phase shift
$\mathbf{f}_{kn} \in \mathbb{C}^{m\times 1}$	gNB-RIS channel vector
$\mathbf{g}_{ni} \in \mathbb{C}^{m\times 1}$	RIS-UE channel vector
h_{ki}	gNB-UE channel coefficient
p_i^{tran}	Transmission power for UE i
$x_i(t)$	Data signal at time t
I	interference
$u_i(t)$	Additive white Gaussian noise
γ_i	SINR at UE i
Γ_i	Datarate of UE i
$\overline{\Gamma}_i$	Normalized datarate
$T_{\mathbf{\Phi}}$	Time for optimizing $\mathbf{\Phi}$
T_{trans}	Total transmission time
σ_{SINR}	Threshold for SINR
Ψ	Maximum allowed retransmissions
α	Threshold probability of transmission failure
τ	Delay threshold
$\mathbf{C_{jk}}$	Context j for gNB k
$\mathbf{P}^i_{jk}$	Probability vector of UE i, context j, gNB k
p_l^{jk}	Probability for action l, context j, gNB k

5.1 System model and assumptions

5.1.1 System Model

A downlink radio access network with K new radio (NR) gNB is considered along with a total of U URLLC UEs. Let $\mathbf{K} = \{1, 2, \ldots, K\}$ denote the set of BSs. The environment has M RISs with m elements in each. Let $\mathbf{M} = \{1, 2, \ldots M\}$ denote the set of RISs. The time is discretized into slots of duration 1ms each [36].

It is assumed that one UE can be served by at most one RIS [11]. The phase shift matrix of the RIS is:

$$\mathbf{\Phi} = diag(e^{j\phi_1}, e^{j\phi_2}, \ldots, e^{j\phi_m}) \in \mathbb{C}^{m\times m} \tag{5.1}$$

Here, *diag* means the diagonal matrix and $j^2 = -1$. It is to be noted that $\phi_n \in [0, 2\pi)$ is the phase shift of the n^{th} element.

5.1.2 Channel model

We assume that the channel state information (CSI) is perfectly known using standard techniques such as [90] [119]. In this study, $\mathbf{f}_{kn} \in \mathbb{C}^{m\times 1}$, $\mathbf{g}_{ni} \in \mathbb{C}^{m\times 1}$ and h_{ki} are used to denote the channel vectors from gNB k to RIS n, from RIS n to UE i and from gNB k to UE i respectively. The gNB to RIS and RIS to UE links are assumed to be Rician and all other channels are flat fading Rayleigh channels as considered in [36].

For UE i, the received signal at slot t from gNB k via n^{th} RIS can be written as:

$$y_i(t) = (h_{ki} + \mathbf{g}_{ni}^H \mathbf{\Phi}_n \mathbf{f}_{kn}) \sqrt{p_i^{tran}} x_i(t) + I + u_i(t) \tag{5.2}$$

where $x_i(t)$ is the data signal at time t, p_i^{tran} is the transmission power and $u_i(t)$ is the additive Gaussian noise which is assumed to be complex normal $\mathcal{CN}(0, \sigma)$. Here, $\mathbf{x}^H$ represents the conjugate transpose of the vector $\mathbf{x}$. The phase shift matrix of a chosen RIS n is optimized to maximize the gain $|h_{ki} + \mathbf{g}_{ni}^H \mathbf{\Phi}_n \mathbf{f}_{kn}|^2$ right at the beginning of a time slot using URLLC-RIS phase shift optimization method in [36]. The signal to interference and noise ratio (SINR) is then calculated as [36]:

$$\gamma_i = \frac{p_i^{tran} |h_{ki} + \mathbf{g}_{ni}^H \mathbf{\Phi}_n \mathbf{f}_{kn}|^2}{I + \sigma^2}, \tag{5.3}$$

where, $I = \sum_{n=1}^{M} \sum_{u=1 u\neq i}^{U} p_u^{tran} |h_{ku} + \mathbf{g}_{nu}^H \mathbf{\Phi}_n \mathbf{f}_{kn}|^2$ is the interference received due to signal transmitted to other UEs as well as corresponding reflections from other RISs in the environment. Then by Shannon capacity formula the achievable rate is

$$\Gamma_i = B log_2(1 + \gamma_i) \tag{5.4}$$

where B is the bandwidth. Let $\Delta = B log_2(1 + \frac{p_i^{trans}}{\sigma})$ be the highest achievable datarate assuming there is no interference and power loss.

We denote $\overline{\Gamma}_i = \frac{\Gamma_i}{\Delta}$ as the normalized datarate for UE i where $\overline{\Gamma}_i \in [0, 1]$.

5.1.3 Handover policy

When a URLLC UE approaches the edge of its serving cell, it must initiate a handover to a suitable neighboring cell to ensure ultra-reliable and low-latency connectivity is maintained. For URLLC traffic, the handover process must be fast, seamless, and highly reliable to prevent service interruption or latency spikes. As per the 3GPP technical specifications the URLLC based UEs follow the make before break handover mechanism [120, 121] also known as the dual active protocol stack (DAPS) handover. In the DAPS handover mechanism UE establishes a connection with the target cell before releasing the source cell, enabling seamless and near-zero interruption handovers. The UE receives data from both the serving cell and the chosen target cell in parallel until handover completion ensuring reliable connectivity for URLLC based UEs.

The mobile UE uses the measured reference signal received power (RSRP) value to determine when it is at the edge of the serving cell and is moving within the intersection of the coverage of multiple neighboring cells. When the measured RSRP from the serving cell fall below A2 threshold defined by the 3GPP technical specification 38.331 [122] it alerts the network of a possible handover. The subset of candidate BSs among the neighboring cells is chosen based on the A4 threshold defined in 3GPP technical specification 38.331 [122]. The A4 event is triggered when the neighboring cell RSRP is better than a predefined threshold. Therefore, the neighboring cells whose RSRP measurements are above the A4 threshold are the candidate BSs for handover.

5.2 Problem formulation

In this section, we formulate the network selection problem in RIS-assisted network as a non-linear programming problem (QPP). During its motion the UE moves into the intersection of the coverage of multiple BSs which it can detect based on the RSRP measurements. As the UE moves within the intersection area, it can either stay with its current gNB or perform a handover, choosing either a conventional gNB or a BS–RIS pair to maintain optimal connectivity. The choice of a gNB-RIS pair results in increased signal strength and reduced packet loss, making the connection reliable. However, CSI overhead and RIS phase shift optimisation complexity may increase the delay during packet delivery. The delay thus introduced adds up with the delay of the subsequent data packets in the gNB buffer. Therefore, if the chosen RIS is not optimally located to boost signal strength sufficiently, it

may deteriorate the performance of the URLLC based services. It may choose to directly communicate with a gNB when the channel quality is good and the signal is strong as there is minimum delay because the direct link results in a single hop communication. If the UE is at the cell edge, the packet error rate will be high resulting in higher number of re-transmissions which in turn may increase the delay. In this study, the UE must decide to choose between an RIS-BS pair or simply a new gNB without the assistance from an RIS by carefully balancing the trade off between reliability and delay.

Thus, the UE i at any time t must make an optimal choice based on the channel conditions, delay and reliability constraints to get the maximum throughput.

The UEs have a strict reliability and latency constraint target (typically $< 1ms$) [27]. We define reliability using the success probability for end to end link establishment between two network devices. Let the UE i choose gNB k and RIS n at time t. We denote p_{ki}, p_{kn} and p_{ni} to be the probability for end to end link failure between the gNB k and UE i, the gNB k and RIS n and between the RIS n and UE i respectively. Thus, reliability can be measured as the probability of successful communication denoted by $(1-p_{ki})+(1-p_{kn})(1-p_{ni})$. The total transmission time is the sum of $T_{\mathbf{\Phi}}$ (Time to optimize the phase shift matrix) and T_{trans} (Time to transmit data packet). Assuming an automatic repeat request (ARQ), the number of blind retransmissions before the arrival of an ACK/NACK within a time out interval determines the delay and the reliability of the channel. Then we denote maximum threshold probability of transmission failure as α.

We define the following binary variables:

$$x_k = \begin{cases} 1, & \text{gNB } k \text{ is selected} \\ 0, & \text{otherwise} \end{cases} \tag{5.5}$$

$$y_n = \begin{cases} 1, & \text{RIS } n \text{ is selected} \\ 0, & \text{otherwise} \end{cases} \tag{5.6}$$

We also define the integer variable R which denotes the number of retransmitions allowed after the first transmission. Let Ψ be the threshold on maximum allowable number of retransmissions.

We formulate the following optimization problem for network selection for a UE i:

$$\max \sum_{k=1}^{K} log_2(1 + \frac{p_i^{tran} x_k |h_{ki} + (\sum_{n=1}^{M} y_n) \mathbf{g}_{ni}^H \mathbf{\Phi} \mathbf{f}_{kn}|^2}{I + \sigma^2}) \tag{5.7}$$

Subject to:

$$\sum_{k=1}^{K} x_k = 1 \tag{5.8}$$

$$\sum_{n=1}^{M} y_n \leq 1 \tag{5.9}$$

$$\sum_{k=1}^{K} \frac{p_i^{tran} x_k |h_{ki} + (\sum_{n=1}^{M} y_n) \mathbf{g}_{ni}^H \mathbf{\Phi} \mathbf{f}_{kn}|^2}{I + \sigma^2} \geq \sigma_{SINR} \tag{5.10}$$

$$\sum_{n=1}^{M} y_n T_{\mathbf{\Phi}} + (R+1) T_{trans} \leq \tau \tag{5.11}$$

$$\sum_{k=1}^{K} \Big(x_k (1 - p_{ki}) + x_k \sum_{n=1}^{M} y_n (1 - p_{kn})(1 - p_{ni}) \Big) \geq 1 - \alpha^{\frac{1}{R}} \tag{5.12}$$

$$R \leq \Psi \tag{5.13}$$

$$R \in \{1, 2, \ldots, \Psi\} \tag{5.14}$$

$$x_k,\ y_n \in \{0, 1\}\ \forall\ k \in \{1, 2, \ldots, K\},\ n \in \{1, 2, \ldots, M\} \tag{5.15}$$

The objective function (5.7) wishes to maximise the datarate of the UE by choosing the optimal gNB-RIS pair among all available pairs. Constraint (5.8) shows that atleast one gNB has to be selected. If no new gNB is chosen then the UE must stick with its current one. Constraint (5.9) shows that at-most one RIS can be chosen along with a BS. The inequality allows for the case where no RIS is chosen. In constraint (5.10), we maintain that the SINR is never less than a threshold σ_{SINR} or else the call will be dropped. The constraint (5.11) specifies that the latency delay cannot be more than a threshold τ. Constraint (5.12) is the reliability constraint that dictates that the probability for successful communication should

be greater than the threshold $1-\alpha^{\frac{1}{R}}$. Let $p = \sum_{k=1}^{K}\Big(x_k(1-p_{ki}) + x_k\sum_{n=1}^{M} y_n(1-p_{kn})(1-p_{ni})\Big)$. Here, we assume that every retransmission is independent and thus the probability of failure is given by $(1-p)^R \leq \alpha$ [27]. After simplifying this expression we get the constraint (5.12). Constraint (5.13) shows that the number of retransmissions is below a threshold.

The optimization problem is a non-separable non-linear integer programming problem. The constraint (5.12) is a non-separable non-linear constraint. The objective function is also non linear and non-separable. Moreover, this optimization needs to be solved at every instant the UE i wishes to select a new gNB and RIS. To solve the optimization problem one needs the CSI of all candidate RISs which results in massive overhead and may violate the strict latency constraints. Furthermore, the precise number of retransmissions of data packets is also unknown beforehand thus leading one to only use an estimate of T_{trans}. The channel conditions and user location also changes over time which is difficult to precisely estimate beforehand.

Due to the aforementioned factors, a solution approach that is able to sequentially learn the best network choice and can make decisions instantly each time a UE needs to switch is essential. Furthermore, the trajectory of the UE is unknown in advance, and depending on its position, the choice of the gNB among the same subset of choices may change at a later time. Keeping the above factors in mind we propose a contextual adversarial bandit formulation for the network selection problem. The network environment acts as the adversary.

5.2.1 Contextual multi-arm bandit (CMAB)

A multi arm bandit framework [123] consists of an *agent* along with a set of actions it can choose from. These action are referred to as *arms*. At each instant of time the agent chooses an arm and receives a reward or suffers a loss. Thus, the agent has a reward function or a loss function which maps each arm to a real number. It may be observed that such a reward or loss is not revealed for any of the arms not chosen at that instant. The rewards or losses are unknown in advance. The objective is then to develop a strategy to discover the best arm over time and maximise the accumulated reward or minimize the suffered total loss over time. We call a multi-arm bandit framework an adversarial bandit [124] when the losses incurred have no underlying stochastic assumptions. The loss functions are assumed to be bounded by 1 and the values are generated by an adversary (in this case the network

environment). The strategy is to learn a near optimal probability distribution over the the arms according to which each arm will be selected at every time instant that minimizes the accumulated loss over time.

Now, we describe a contextual adversarial multi-arm bandit. A contextual bandit is a multi-arm bandit which is provided with an extra side information at each instant of time to help it make a better decision. This side information is called a context. The set of all contexts denoted by $\mathcal{C}$ is stored by the agent. Now, instead of calculating a near optimal probability distribution over the entire horizon, the agent calculates a separate near optimal distribution for each context.

We use the Exp3 algorithm [124] for solving the proposed contextual adverserial multi-arm bandit problem. In the Exp3 algorithm, a probability distribution is maintained for each context. At each round a context is observed and an arm is selected based on the distribution stored corresponding to that context. After the loss incurred for the choice is revealed and the losses for all other choices are estimated, the probability distribution is updated such that the probability of the arm having the least accumulated loss, becomes the highest over time.

5.3 Proposed network selection strategy

In this section, we formulate our network selection problem as a contextual adversarial bandit. An agent is maintained corresponding to each UE at the BSs. Each gNB stores the set of contexts that a UE can encounter in its cell. The UE in a given gNB cell can either choose a gNB-RIS pair or just a gNB among the neighbouring BSs whose coverage intersects with the current cell and the available RIS at the cell edge. All other BSs cannot become candidates for being chosen, as the UE does not fall in their coverage area.

In accordance with the above mentioned fact, we define the action space of an adversarial bandit agent corresponding to a UE as $\mathcal{A} = (\mathcal{K} \times \mathcal{M}) \cup (\mathcal{K} \times \{0\})$. We denote an action chosen from $\mathcal{A}$ by l. We say an action $l = (k_l, n_l)$ is chosen if the agent chooses gNB k_l and RIS n_l. If $n_l = 0$ it means that no RIS has been chosen. It may be noted that not all of the actions are available for the UEs residing in the coverage area of a particular BS. The available actions are determined by the context set stored at that BS.

Now, we define the finite set of contexts. The UE is mobile, and at each time slot, it falls within the intersection of the coverage area of a subset of BSs. It can determine the subset by the RSRP measurements and compare them with the A2 and A4 threshold values.

Moreover, RISs lying in that intersection are of interest only, as other RIS are beyond the reach of the candidate BSs.

For example, let us consider a gNB k that has P neighbouring BSs. Let us denote this set of neighbours as $\mathcal{P} = \{1, 2, \ldots, P\}$. This set includes the current BS. Let an UE be at the intersection of the coverage area of the set $\mathcal{P}' \subset \mathcal{P}$ of BSs. Similarly, let the set of available RISs for $\mathcal{P}'$ be $\mathcal{S}$. The actions available to such an UE are $((\mathcal{P}' \times \mathcal{S}) \cup (\mathcal{P}' \times \{0\})) \subset \mathcal{A}$.

Thus, at each time slot the UEs in a particular gNB cell have only a subset of actions from the set $\mathcal{A}$ to choose from. Each of these action subsets available to any UE at any time while in the coverage area of the gNB becomes a context to be stored at that BS. Given that the number of BSs and RISs are finite, the set of contexts is also finite. We denote $\mathcal{C}_k = \{\mathbf{C}_{1_k}, \mathbf{C}_{2_k}, \ldots, \mathbf{C}_{L_k}\}$ the set of contexts for gNB k with L contexts. We also denote $|\mathbf{C}_{j_k}|$ = number of available actions for context j in gNB k. Let $p_l^{j_k}$ be the probability to choose action $l = (k_l, n_l) \in \mathcal{A}$ for context j in gNB k. For each context j and each UE i we maintain a probability distribution vector $\mathbf{P}_{j_k}^i \in [0,1]^{(M+1)K}$. Now, for an arbitrary action l

$$P_{ij_k} = \begin{cases} 0, & \text{action } l \text{ not available} \\ p_l^{j_k}, & \text{otherwise} \end{cases}. \tag{5.16}$$

Here, $p_l^{j_k} = \frac{1}{|\mathbf{C}_{j_k}|}$ at the beginning when $t = 0$.

The following functions are defined for arbitrary UE i in gNB k. Hence, we omit the indices i and k from the notations for simplicity. The respective functions are defined similarly for other UE and gNB pairs.

Next, we define the loss function $loss_{lj}(t)$ of UE i and context j for an arbitrary action l as follows:

$$loss_{lj}(t) = \begin{cases} 1 - \overline{\Gamma}_i, & \text{successful transmission} \\ & \text{satisfying (5.11), (5.13)} \\ 1, & \text{otherwise} \end{cases}. \tag{5.17}$$

From (5.17), we calculate the estimated loss value for arbitrary action ℓ as:

$$\overline{loss}_{\ell j}(t) = \begin{cases} \frac{loss_{lj}(t)}{p_l^j} \mathbb{1}_{\ell=l}, & p_l^j \neq 0 \\ V, & \text{otherwise} \end{cases}, \tag{5.18}$$

Where $\mathbb{1}$ is the indicator random variable. Here, V is a large positive quantity. This strictly ensures that the action that has 0 a probability of being selected is never selected. The accumulated loss upto time T becomes:

$$\overline{L}_{lj}(T) = \sum_{t=1}^{T} \overline{loss}_{lj}(t). \tag{5.19}$$

The loss function is chosen such that the reliability and the delay constraints are satisfied after handover to the chosen gNB or gNB-RIS pair. Here we leverage the make before break handover policy of DAPS handover for URLLC services while the UE moves through the coverage intersection of multiple BSs. After choosing a network, the connection with the serving cell is not served immediately. The loss function is computed after acquiring CSI and observing whether the delay and reliability constraints are satisfied or not. If they are violated, the UE maintains connection with the serving cell, updates the probability vectors depending on the loss function and chooses the next gNB or gNB-RIS pair at the subsequent time slot. A neighbouring network choice is said to be successful if the UE can handover to the chosen network without violating the delay and reliability constraints.

Here, we make use the Exp3 algorithm [124] described earlier. At each point of time when an UE i needs to choose a new gNB or gNB-RIS pair, the Exp3 algorithm is called. Assume it is the t^{th} round of selection for UE i. At first the context is observed, and the appropriate probability distribution vector is chosen. Let it be $\mathbf{P}_j$. Using $\mathbf{P}_j$, an action l is selected. Estimated and cumulative losses are calculated using (5.18) and (5.19). Then the probabilities for this context are updated for $(t+1)^{th}$ as below:

$$p_l^j(t+1) = \begin{cases} 0, & p_l^j(t) = 0 \\ \dfrac{exp(-\eta_t \overline{L}_{lj})}{\sum_{a=1}^{|\mathcal{A}|} exp(-\eta_t \overline{L}_{aj})}, & \text{otherwise} \end{cases} \tag{5.20}$$

Here, $\eta_t = \sqrt{\frac{\ln|\mathcal{A}|}{t|\mathcal{A}|}}$ for a horizon independent adversarial bandit [124]. Furthermore, it is well known in literature that an adversarial bandit with K arms whose regret bound over time T is given by $O\sqrt{KT\ln K}$ which is sublinear in T [125]. Therefore, in our study the upper bound on the regret is $O\sqrt{K'T\ln K'}$, where K' is the largest number of available arms over all contexts. The sublinear regret bound guarantees the convergence of the contextual Multi-armed bandit-based algorithm.

5.4 Results and discussions

Table 5.2: 3GPP Urban Macro (UMa) Parameter Assumptions for Simulation (Based on TR 38.901)

Parameter	**Value**	**Unit/Note**
Minimum BS-UE 2D Distance	35	m
Reference Distance for Path Loss	Implicit (close-in ≈ 1)	m
Shadow Fading Std. Dev. (σ_{SF}) - LOS	4	dB
Shadow Fading Std. Dev. (σ_{SF}) - NLOS	6	dB
Mobility Model	Random Waypoint or Uniform	(UEs move at constant speed)
Delay Spread ($\mu_{\lg DS}$) - NLOS	-6.83	$\log_{10}$(s)

In this section, we present extensive system level simulations to compare the performance of our proposed scheme with the network choice mechanism guided by the traditional and widely implemented RSRP based A3 handover [83]. In this method the UE chooses the neighbouring gNB whose RSRP exceeds that of the current serving gNB by a threshold margin and is largest among all other neighbouring BSs. Here, an RIS closest to the selected gNB is always chosen. Most of the parameters considered in the simulation environment have been adopted from [36] and [27]. The radius of NR BSs have been set to 90 meters. The UEs move with a velocity ranging from 10 m/s to 20 m/s. We consider that there are 5 BSs and 5 RISs each having 10 elements. Pathloss exponents for gNB-UE, gNB-RIS and RIS-UE channels are -3.5, -2.2 and 2.8 respectively. All of these channels are assumed to be Rician fading channel (Rician factor is 10). Transmitting power of the NR gNB has been set to 33 dBm. The additive Gaussian noise is considered to be -97.5dBm. Other parameter details are as follows: time slot duration $= 0.5$ ms, $\tau = 0.5$ ms, $B = 17.28$ MHz and maximum allowed re-transmissions is 3. The values of A2 and A4 thresholds are -109 dBm and -105 dBm [122] respectively. In the simulation, user throughput is defined as the total data transmitted per unit time strictly satisfying the latency constraint (< 1) ms. The parameter values for the simulation are described in Tables 7.2 and 5.3.

Table 5.3: Simulation parameters and values for chapter 5

Parameter	**Value**
NR BS Radius	90 m
UE Velocity	10 to 20 m/s
Number of BSs	5
Number of RISs	5 (each with 10 elements)
Path Loss Exponent (gNB-UE)	-3.5
Path Loss Exponent (gNB-RIS)	-2.2
Path Loss Exponent (RIS-UE)	2.8
Rician factor	10
NR gNB Transmit Power	33 dBm
Additive Gaussian Noise	-97.5 dBm
Time Slot Duration	0.5 ms
τ	0.5 ms
Bandwidth (B)	17.28 MHz
Maximum Re-transmissions	3
A2 Threshold	-109 dBm
A4 Threshold	-105 dBm
Latency constraint	< 1 ms

5.4.1 Results

We first investigate the convergence of our proposed scheme. Figure 5.1 shows the normalized user throughput (log scale) with respect to time for 10 and 20 UEs. It can be observed that for the case of a network scenario with 10 UEs there is a sharp rise up-to 2100 milliseconds after which the rate of increase falls rapidly and the curve flattens out. This can be attributed to the fact that the bandit agent learns the optimum network selection strategy over time and converges. A similar pattern can be observed for the case of network scenario with 20 UEs. In this case, the rate of increase starts dropping at 3500 milliseconds time instant. Moreover, the throughput value is also less compared to the case of a network with 10 UEs. This is because, with increased number of UEs, the interference in the system increases. As a result, the agent takes more time to learn and the throughput value of the UE also drops.

In Figure 5.2, we investigate the effect of traffic load on normalized user throughput (log scale). Here the traffic load varies from 10 UEs to 25 UEs. It may be observed that throughput for our proposed scheme is greater compared to the traditional scheme when the traffic load is less than 20 UEs. Beyond that throughput for both the schemes are very

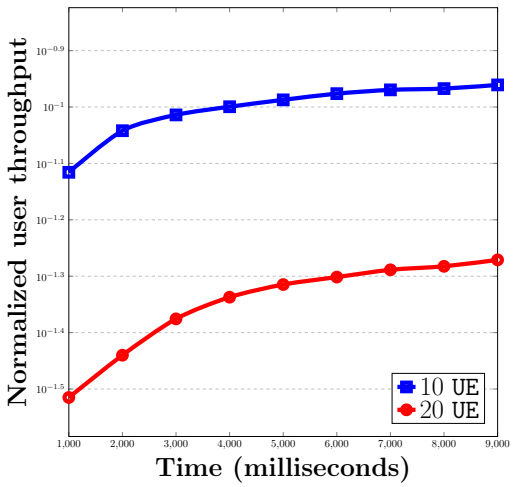

Figure 5.1: Normalized user throughput (log scale) vs. time.

close. The traditional A3 based scheme only considers the signal strength from the gNB and does not take the signal reflected by the RIS into account. The A3 event occurs when the difference between the received power from the serving cell and the neighbouring cell is greater than a predefined threshold. As a consequence, it is unable to make a proper choice on the RISs. This makes the UE unable to judge the channel conditions properly and causes multiple re-transmissions due to increased BLER which could have been avoided had it chosen the proper RIS. As a consequence, the latency constraint can not be satisfied whereas, in our proposed bandit scheme the loss function gives a low value only when the delay and the reliability constraints are satisfied. If either is violated it registers a loss of value 1 which is maximum. As a result, our scheme learns the best choice over time that satisfies these constraints and the loss is minimised. Thus in the traditional scheme, the UE looses more packets as compared to our proposed contextual bandit based scheme. We also observe a decline in the user throughput with increasing traffic load. This can be explained by the fact that the interference rises with increasing traffic load.

In Figure 5.3, we measure the handover reliability against increasing traffic load. We define handover reliability as the proportion of successful network choices out of the total number of times a new network is chosen. Here the traffic load varies from 5 to 25 UEs. It may be observed that our proposed scheme outperforms the traditional schemes. This is because our scheme learns the best gNB-RIS pair over time that maximises the throughput satisfying the latency and reliability constraints. The decline in reliability with increasing traffic load is due to the increase in interference which results in decreasing signal strength at

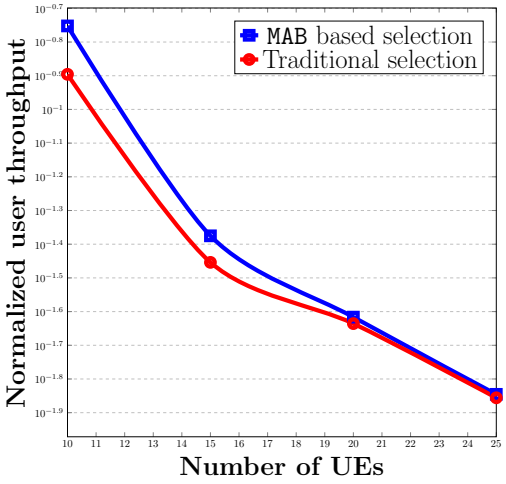

Figure 5.2: Normalized user throughput (log scale) vs. traffic load.

the UE causing more packet loss. Finally, we observe that the Contextual multi armed bandit (MAB) based RIS-BS pair selection algorithm achieves a maximum throughput gain of 58% relative to traditional A3 based base station selection [83] for 10 UEs, 5 RISs and a UE velocity of 20 m/s. The proposed algorithm also achieves a 35% gain in reliability relative to the traditional algorithm for 9 UEs, 5 RISs and a UE velocity of 20 m/s. Furthermore, the margin of error at 95% confidence for the measured normalised user throughputs are less than 0.049, demonstrating the high accuracy of the reported results.

Figure 5.4 shows the impact of UE velocity on packet-level failure probability for different handover latency values. The velocity values range from 10 m/s to 20 m/s. Handover blocking rate is defined by the number of handovers failed per unit time due to high handover latency, signal strength deterioration at the cell edge and resource scarcity at the target base station [126]. For a handover latency L_{ho} the handover blocking rate is computed as:

$$B = \frac{\mu \times L_{ho}}{1 + \mu \times L_{ho}}, \tag{5.21}$$

where $\mu = \frac{2v}{\pi R}$ is the border crossing ratio with v as the velocity of the UE and R as the radius of the NR gNB. For a packet-level failure to occur, a URLLC packet must arrive within the duration of handover latency namely L_{ho}. The URLLc UEs generate small bursts of data packets following the FTP3 model [127] with the mean arrival rate of 2.12 packets/10 ms. In the FTP3 traffic model, standardised by 3GPP for generating URLLC traffic, packet arrivals follow a Poisson process. Therefore, the probability of a packet arriving within a

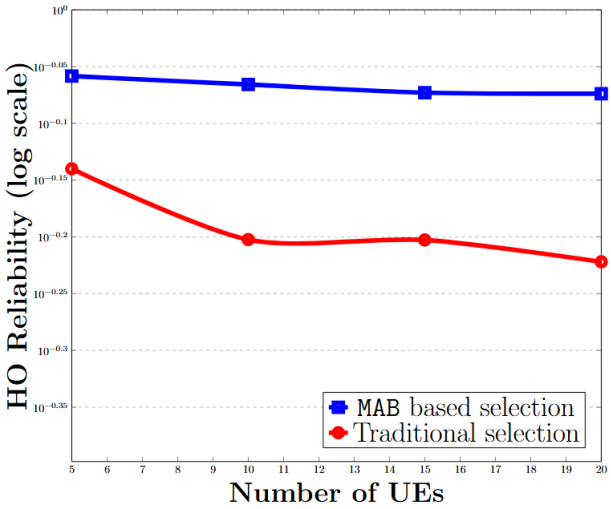

Figure 5.3: Hanover reliability vs. traffic load.

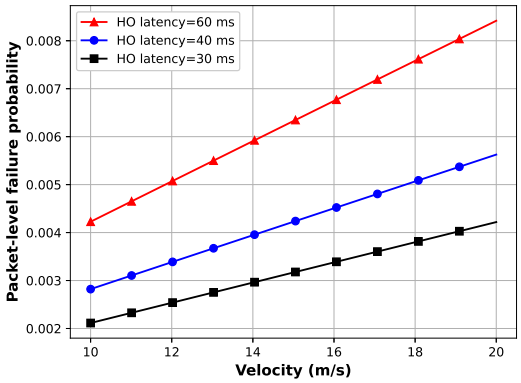

Figure 5.4: Packet-level failure probability vs velocity for different latencies

duration of L_{ho} is $P_{arr} = 1 - e^{-0.212 \times L_{ho}}$.

5.5 Conclusion

In this chapter, we formulate a non-linear integer programming problem to select either a gNB or gNB-RIS pair when a handover is initiated in a RIS assisted network for URLLC based UEs. Due to the non linear nature of the optimization problem and unknown parameters such as number of re-transmissions, we propose a contextual bandit based scheme to learn about the network environment and make the optimal choice. We have done extensive

simulations to show that our scheme outperforms the traditional A3 based approach in terms of user throughput and reliability.

Chapter 6

RB Allocation in RIS Assisted Wireless Network[1]

In the previous two chapters, efficient strategies for scheduling channel estimation and joint RIS-gNB selection have been proposed to mitigate the effect of massive pilot overhead on throughput and latency constraints respectively. In this chapter, we explore how RIS-assisted channels affect the RB allocation. The objective here is to establish that the CSI of only the direct channel is insufficient to optimally allocate RBs in an RIS assisted cellular network. To this end, we design a MAB based RB allocation algorithm that takes into account the presence of RIS, and compare its performance with traditional RB allocation methods that rely only on the direct channel between the gNB and the UE. The proposed MAB model explicitly considers the presence of an additional communication path through the RIS. For each UE, the gNB maintains an agent that selects appropriate RBs. In this formulation, each RB is treated as an arm of the bandit, and the reward for selecting an arm is determined based on the achievable throughput via the selected RB as well as the past average throughput obtained by the UE through both the direct channel and the RIS assisted channel. Building on this MAB model, we use an epsilon-greedy algorithm for RB selection in the RIS assisted setup. The algorithm operates in two phases: in the exploitation phase, it selects the RB that yields the highest reward with probability $1 - \epsilon$ and in the exploration phase, it selects any available RB at random with probability ϵ. Extensive simulations demonstrate that the

[1]This chapter is based on the following publication:
Souvik Deb, Shankar K. Ghosh and Sasthi C. Ghosh, "A Multi-arm-bandit based resource block allocation in RIS assisted wireless network," **The 20th IEEE International Symposium on Network Computing and Applications (IEEE NCA 2021)**, Boston, MA, USA, pp. 1-6, 23-26 November 2021.

proposed algorithm achieves better performance compared to a widely used proportional fairness-based RB allocation scheme, highlighting the benefits of leveraging RIS-assisted channels in RB allocation decisions.
The symbols used in this chapter and their respective meaning are given in Table 6.1.

6.1 System Model and assumptions

We consider a single gNB and N UEs. We also consider that in our environment there are multiple RISs installed on the walls of various buildings and houses. Let $\mathbb{M}$ be the set of all RISs installed. Each RIS is considered to have l reflecting elements. Hence, the total number of reflective elements from all RISs is $m = l \times |\mathbb{M}|$. The time is broken into discrete time slots of unit length. We assume time division multiple access (TDMA) where at each time slot the gNB having K antennas communicates with only one UE [128]. In our system model, we consider R as the set of r available RBs. Important notations have been summarized in table 6.1.

Table 6.1: Important notations for chapter 6

Symbols	Meaning
$\mathbf{h}_{j,n} \in \mathbb{C}^{K\times 1}$	Channel-coefficients from gNB to UE n for RB j
$\mathbf{g}_j \in \mathbb{C}^{m\times K}$	Channel-coefficients from gNB to RISs for RB j
$\mathbf{f}_{j,n} \in \mathbb{C}^{m\times 1}$	Channel-coefficients from RISs to UE n for RB j
s_n	Data symbol for UE n
$\mathbf{w}_n \in \mathbb{C}^{K\times 1}$	Beamforming vector at the BS
$\Gamma_{j,n}(t)$	SNR of UE n for RB j at time t
$\tau_{j,n}(t)$	Throughput of UE n for RB j at time t.
$\overline{R_n(t)}$	Past average throughput for UE n at time t.
$d_n(t)$	Data rate achieved by UE n at time t

6.1.1 Channel model

An UE communicating with the gNB at a time slot t may receive data from two different channels. One of them is the direct channel from the gNB to the UE and the other is the indirect one that comes to it after being reflected off from different RISs in the environment.

The channel coefficient vectors for these two channels can be estimated using standard channel estimation techniques such as [90] [119]. We also note that each RIS has a set of passive reflective elements that can change the phase and amplitude of the wave incident on it depending on the ways we configure them [11]. The configurations of an element is also called it's reflection levels. By doing so, they can direct the wave incident upon them towards the UE. The phase and amplitude of the reflected wave can be controlled so that it can be combined with the direct wave from gNB to UE to enhance the throughput. Hence, we need to properly configure the reflective elements of all the RISs.

According to our assumption, we have a total of m elements. The configuration of the elements is represented by the $m \times m$ reflection matrix $\mathbf{\Phi}$ as follows:

$$\mathbf{\Phi} = \sqrt{\eta} diag\{e^{i\theta_1}, e^{i\theta_2}, \ldots, e^{i\theta_m}\} \tag{6.1}$$

The reflection matrix $\mathbf{\Phi}$ includes reflection efficiency and phases resulting from the m elements. Here, $i = \sqrt{-1}$ and $diag$ is the diagonal matrix. We call $\eta \in [0,1]$ as the reflection efficiency. The θ_is are the phase shifts induced upon the incident wave by the reflecting element i.

Following the protocol as in [11] each transmission time interval (TTI) is divided into two parts. In the first part the gNB estimates the channel coefficients and calculates $\mathbf{\Phi}$. We consider the fact that the channel coefficients can vary with time as the UE moves in the environment. In the second part actual data transmission takes place. In reality a reflective element can have only finitely many reflection levels [15]. If τ is the finite number of reflection levels then θ_i's are given as:

$$\theta_i \in \left\{0, \frac{2\pi}{\tau}, \ldots, \frac{2\pi(\tau-1)}{\tau}\right\} \tag{6.2}$$

6.1.2 Throughput computation

If an UE n selects RB j to communicate with the gNB then the transmitted signal can be represented as $\mathbf{x} = s_n \mathbf{w}_n$, where s_n represents the data symbol for UE n and $\mathbf{w}_n \in \mathbb{C}^{K\times 1}$ represent the beamforming vector at the BS. Accordingly, the signal received at UE n on RB j can be expressed as:

$$\mathbf{y}_{j,n} = \mathbf{h}_{j,n}^H \mathbf{x} + \mathbf{f}_{j,n}^H \mathbf{\Phi} \mathbf{g}_j \mathbf{x} + u_{j,n} \tag{6.3}$$

Here, $u_{j,n} \in \mathcal{CN}(0, \sigma_j^2)$ is additive white Gaussian noise for UE n communicating in RB j and σ_j is the standard deviation. We assume $\mathbf{h}_{j,n} \in \mathbb{C}^{K\times 1}$ and $\mathbf{f}_{j,n} \in \mathbb{C}^{m\times 1}$ are the channel coefficients from gNB to UE n and from RISs to UE n for RB j respectively. Also, $\mathbf{g}_j \in \mathbb{C}^{m\times K}$ is the channel coefficients from gNB to all RISs for RB j.

Denoting by P_T, the transmission power, the received signal P_r can be computed as [82]:

$$P_r = |\mathbf{h}_{j,n}^H + \mathbf{f}_{j,n}^H \mathbf{\Phi} \mathbf{g}_j|^2 P_T \tag{6.4}$$

Accordingly, signal to noise ratio (SNR) at UE n communicating in RB j can be computed as:

$$\Gamma_{j,n} = \frac{|\mathbf{h}_{j,n}^H + \mathbf{f}_{j,n}^H \mathbf{\Phi} \mathbf{g}_j|^2 P_T}{\sigma_j^2} \tag{6.5}$$

After all such computations, the throughput $\tau_{j,n}$ of UE n communicating in RB j can be computed as:

$$\tau_{j,n} = B \log(1 + \Gamma_{j,n}) \tag{6.6}$$

where B is the bandwidth for RB j.

6.2 MAB based Resource allocation

In this section, we first briefly describe the basic MAB framework and then formulate the RB allocation problem in a RIS-assisted environment as a MAB problem. Finally, we present our the MAB based ϵ-greedy algorithm to allocate RBs for each UE to maximize the throughput.

6.2.1 Basic MAB framework

MAB [129] is a framework to model a sequential decision making problem. In this framework, we have an agent which repeatedly chooses one of multiple actions also called *arms*. Associated with each arm is an instantaneous *reward* which is unknown to the agent before actually selecting that arm. The objective is to maximize the expected total reward over some time period, for example, over 2000 action selections, or time steps. The average reward of an arm is called the *value* of that arm. At a given time step the agent can either *exploit* the current knowledge of the values of the arms and choose the arm with the greatest value or it can *explore* other arms to get better estimate of their values. To choose the best

arm in long run we need to strike a proper balance between *exploration* and *exploitation*. In the next subsection we give a formal MAB formulation of our problem.

6.2.2 MAB formulation of RB allocation problem

In every TTI, RBs are allocated to a particular UE based on the channel conditions, past average throughput and highest achievable throughput. In traditional RB allocation mechanism, the past average throughput and highest achievable throughput is computed only based on the direct channel from gNB to UE. However, in RIS assisted environment, the RIS-to-UE channel plays an important role.

In every TTI, a particular UE is scheduled by the gNB depending on the UE's channel conditions and past average throughput. We consider that for each UE the gNB contains one agent. For the agent corresponding to a particular UE, each arm of that agent corresponds to a RB that can be allocated to the UE. Hence, for r RBs we have r arms. After selecting a RB $j \in R$, i.e., the arm j, the gNB transmits in that RB.

The past average throughput for UE n at time t can be computed as [130]:

$$\overline{R_n(t)} = \beta \overline{R_n(t-1)} + (1-\beta) d_n(t) \tag{6.7}$$

where $\beta \in [0,1]$ and $d_n(t)$ is the data rate achieved by UE n at time t. At TTI t, the gNB schedules the UE with the minimum past average throughput.

Now we describe the average reward value of arm j of UE n up to time instant t. Let $R_{j,n}(t)$ be the instantaneous reward sampled for arm j of UE n at time t. Let at time instant t, UE n communicates with the gNB and chooses arm j. Once the gNB broadcasts the signal, the UE receives data from two channels. In the case of the direct gNB to UE channel, the gNB simply estimates coefficient vector $\mathbf{h}_{j,n}$ using standard estimation techniques such as [90] [119]. In the case of the reflected channel, apart from estimating the channel coefficients $\mathbf{g}_j$ and $\mathbf{f}_{j,n}$, the gNB computes the reflection matrix $\mathbf{\Phi}$ as well. Here $\mathbf{\Phi}$ is computed using the reflection phase selection algorithm (RPSA) reported in [11]. After all such computations, the throughput $\tau_{j,n}$ of the UE n communicating in RB j can be computed using (6.6). Now if, at time instant t, UE n communicates using RB j, then for an UE i and RB k, the instantaneous reward $R_{k,i}(t)$ can be computed as below:

$$R_{k,i}(t) = \begin{cases} \tau_{j,n}, & \text{if } k = j \text{ and } i = n \\ 0, & \text{otherwise.} \end{cases} \tag{6.8}$$

Accordingly, up to time instant t, the average reward value for the arm j of an UE n can be computed as:

$$Q_{j,n}(t) = (1 - \frac{1}{\gamma_{j,n}})Q_i(t-1) + \frac{1}{\gamma_{j,n}}R_{j,n}(t). \tag{6.9}$$

Here, $\gamma_{j,n}$ is the number of times arm j for UE n has been selected up to time instant t. Initially we assume that $\gamma_{k,i} = 0$ for all arms of all UEs. At time instant t, $\gamma_{k,i}$ is updated as below:

$$\gamma_{k,i} = \begin{cases} \gamma_{k,i} + 1, & \text{if } k = j \text{ and } i = n \\ \gamma_{k,i} + 0, & \text{otherwise.} \end{cases} \tag{6.10}$$

In the next subsection, using the above MAB formulation, we propose our ϵ-greedy algorithm to allocate RBs for each UE to maximize the throughput.

6.2.3 Proposed MAB based ϵ-greedy algorithm

We now describe our algorithm. At first, the past average throughput $\overline{R_n}(t)$ is initialised to 0 at time $t = 0$ for all UE n. We also initialise the average reward value $Q_{i,n}(t)$ with a large positive value for all arms i and all UE n at time $t = 0$. We define ϵ as the probability for exploration. In exploration phase, we choose a random arm. This notion is introduced to ensure that the agent visits different arms and is not restricted to choose among a particular subset of arm. Then, at time instant t, we either explore with probability ϵ or, with probability $1 - \epsilon$, we exploit the average reward values of the arms updated thus far and choose the arm with the maximum average reward value. When we assign large average reward values initially to all arms the agent is forced to visit different arms even when it is in the exploitation phase.

For each time instant t, the gNB schedules the UE with the minimum past average throughput. Then algorithm checks weather at current time t the UE n is scheduled to communicate with gNB or not. If so, then, either the agent corresponding to the UE explores with probability ϵ or exploits with probability $1 - \epsilon$. After choosing an arm i the UE communicates with the gNB using the RB corresponding to that arm. Then, for the UE n, $\gamma_{i,n}$, the number of times arm i is selected, instantaneous reward $R_{i,n}$, the average reward $Q_{i,n}$ and $\overline{R_n(t)}$ are all updated. If the UE n is not scheduled at time t then, the reward value of time $t-1$ is simply copied to that of time t and other variables are updated accordingly. Formally the algorithm is presented in Algorithm 10.

Algorithm 10: Proposed ϵ-greedy algorithm

Initialise:
For $t = 0$, $\overline{R_n(t)} = 0 \; \forall$ UE n;
For $t = 0$, $Q_{j,n}(t) =$ a large positive number $\forall$ arm j and $\forall$ UE n;
for $t = 1, 2, \ldots, T$ **do**
    $k = argmin_{1 \leq n \leq N}\{\overline{R_n(t-1)}\}$;
    Schedule UE k;
    for $n = 1, 2, \ldots, N$ **do**
        if $n = k$ **then**
            Set p as a random value in $[0, 1]$;
            if $p \leq \epsilon$ **then** `// exploration`
                Choose a random arm i;
            else `// exploitation`
                Choose arm $i = argmax_{j \in R}\{Q_{j,n}(t-1)\}$;
            BS transmits in RB i to UE n in time t and computes $\tau_{i,n}$;
            Update:
            $R_{i,n}(t) = \tau_{i,n}$;
            $\gamma_{i,n} = \gamma_{i,n} + 1$;
            $Q_{i,n}(t) = (1 - \frac{1}{\gamma_{i,n}})Q_{i,n}(t-1) + \frac{1}{\gamma_{i,n}}R_{i,n}(t)$;
            $\overline{R_n(t)} = \beta\overline{R_n(t-1)} + (1-\beta)\tau_{i,n}$;
        else
            Update for all arms i:
            $R_{i,n}(t) = 0$;
            $\gamma_{i,n} = \gamma_{i,n} + 0$;
            $Q_{i,n}(t) = Q_{i,n}(t-1)$;
            $\overline{R_n(t)} = \beta\overline{R_n(t-1)} + (1-\beta) \times 0$;

Our algorithm takes $O(Nr)$ time to initialise the reward values and $O(N)$ time to initialise the past average throughput for all UEs. In every TTI, it takes $O(N)$ time to select the UE with minimum past average throughput. Then for each UE n it takes $O(m)$ time complexity to compute $\tau_{i,n}$. After that, at every TTI, updating each of the $R_{i,n}(t)$, $Q_{i,n}(t)$, $\overline{R_n(t)}$ and $\gamma_{i,n}$ takes only constant time for each UE. Next, the algorithm chooses the arm with maximum average reward value with probability $1-\epsilon$ if the UE n is scheduled to communicate with the BS. This takes $O(r)$ time. Thus in the worst case scenario, at each TTI, our algorithm takes $O(N+Nm+Nr)$ time for RB allocation for all UEs. So, the overall complexity becomes $O(T(N+Nm+Nr))$, where T is the total number of considered time slots, N is number of UEs, m is the total number reflective elements and r is the total number of RBs.

6.3 simulation results

6.3.1 Simulation Parameters

Table 6.2: 3GPP Urban Macro (UMa) Parameter Assumptions for Simulation (Based on TR 38.901)

Parameter	**Value**	**Unit/Note**
Minimum BS-UE 2D Distance	35	m
Reference Distance for Path Loss	Implicit (close-in ≈ 1)	m
Shadow Fading Std. Dev. (σ_{SF}) - LOS	4	dB
Shadow Fading Std. Dev. (σ_{SF}) - NLOS	6	dB
Mobility Model	Random Waypoint or Uniform	(UEs move at constant speed)
Delay Spread ($\mu_{\lg DS}$) - NLOS	-6.83	$\log_{10}$(s)

Most of the network parameters are taken from [80]. The path loss exponent for gNB to UE channel is 4. Path loss exponent for gNB to RIS and from RIS to UE channels are 2 and 2.5 respectively. Noise is -114 dBm and transmission power is 27.5 dBm. The small scale fading for BS-UE channel is Rayleigh fading and the channel associated with RIS is Rician fading with Rician factor 10. Bandwidth for each subcarrier is 1 MHz. We also

Table 6.3: Simulation parameters and values for chapter 6

Parameter	**Value**
Path Loss Exponent (gNB-UE)	4
Path Loss Exponent (gNB-RIS)	2
Path Loss Exponent (RIS-UE)	2.5
Noise	-114 dBm
Transmission Power	27.5 dBm
BS-UE fading	Rayleigh fading
RIS associated channel	Rician fading
Rician factor	10
Bandwidth per Subcarrier	1 MHz
Call Drop Threshold	2 Mbps
Number of UEs	10
Number of RBs	5
Number of RISs	5

assume a call drop threshold of 2 Mbps which is the minimum threshold for multimedia applications. Here, we assume a total of 10 UEs and 5 RBs [80] and 5 RISs [11]. Based on the above setup, the numerical results are calculated by averaging over 10000 iterations. All simulation parameters are described in Tables 7.2 and 6.3.

6.3.2 Numerical results

In Figure 6.1, we can see how with different ϵ values the average reward value for the proposed MAB based approach varies with time. Initially there is some exploration after which the values of the arms are all learned and we choose the best possible arms for each UE. We also see that when ϵ decreases $(\epsilon = 0.001)$ there is less exploration because of which agent often chooses a less optimal arm. On the contrary, when the ϵ increases $(\epsilon = 0.1)$, there is less exploitation and this also hampers the system performance. The best result is obtained for $\epsilon = 0.01$ in this set up. This intuitively says that for a given set up, there is an optimal ϵ which gives the best average reward value.

In Figure 6.2, we see the average system throughput achieved for different values of ϵ. We can clearly see that there exists an optimal ϵ that gives the best average throughput. This is because, for ϵ larger than the optimal there is too much exploration whereas, for ϵ less that the optimal there is too much exploitation. Both cases hamper the average throughput. Thus, we need to strike a proper balance between exploration and exploitation.

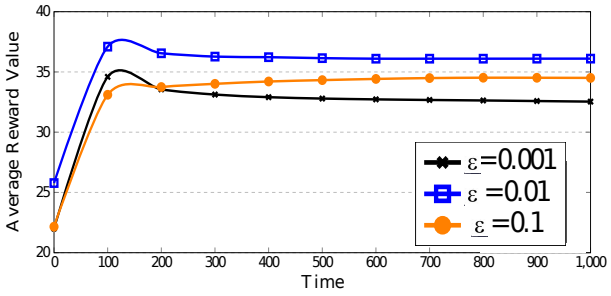

Figure 6.1: Average reward vs time

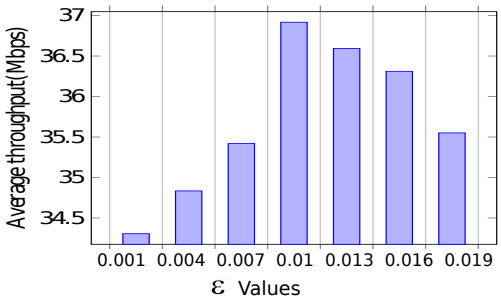

Figure 6.2: Average throughput vs ϵ

Now we compare our allocation strategy with an existing PF based resource allocation mechanism reported in [84]. In this mechanism, corresponding to every UE i and RB k pair, a metric $m_{i,k}$ is computed as follows [84]:

$$m_{i,k} = \frac{Expected\ data\ rate\ for\ UE\ i\ on\ RB\ k}{Past\ average\ throughput\ of\ UE\ i} \tag{6.11}$$

Then the RB k is allocated to UE j if it satisfies the following condition:

$$m_{j,k} = max_i\{m_{i,k}\}. \tag{6.12}$$

In Figure 6.3, we fix our ϵ value at 0.01 and compare the average system throughput up to time t with that of the PF based approach [84]. We can clearly see that our strategy gives a higher average system throughput. We note that our strategy considers both the direct gNB to UE channel as well as the channel reflected via the RISs for allocating RBs. In an RIS assisted environment, the direct channel condition of an UE may be poor, but it may still maintain a good quality link through a reflected channel. This significantly expands the coverage of the BS. The existing PF based strategy considers only the direct channel and

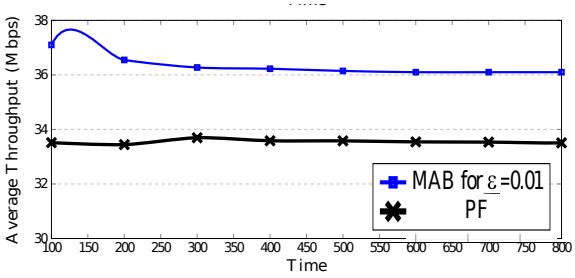

Figure 6.3: Average throughput vs time

hence, results relatively poorer throughput performance as compared to our proposed MAB based framework.

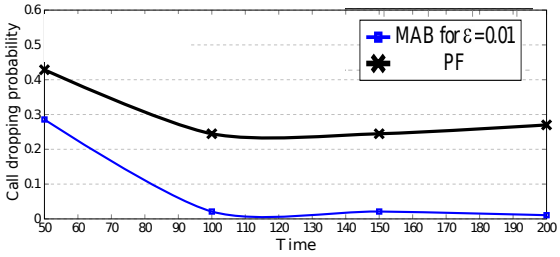

Figure 6.4: Call dropping probability vs Time

The effect of RISs in the environment can also be seen by computing the call dropping probability. We keep $\epsilon = 0.01$ and compare the call dropping probability of the two mechanisms. The call dropping probability is defined as the probability of a call being dropped due to resource scarcity and poor channel condition. Here, a call is considered to be dropped when it gets throughput less than a threshold value (2 Mbps). Figure 6.4 shows that the call drop probability for our MAB based proposed strategy is much smaller than that of the PF strategy. The low value and fast drop of call dropping probability for our MAB based strategy is because of the extended coverage of the gNB due to the indirect channel via RISs in the environment. Since, the existing PF based strategy only considers the direct channel, UEs with poor direct channel conditions that could have been connected via the reflected channel remain disconnected.

Finally, we observe that the MAB based resource block (RB) allocation algorithm achieves a maximum throughput gain of 12% relative to proportionally fair RB allocation algorithm [84] for 10 UEs, 5 RISs and 5 total RBs. Furthermore, the margin of error at 95% confidence for the measured average throughput and call drop probabilities are less than 0.043, showing high accuracy of the results.

6.4 Conclusion

In this chapter, we formulate the RB allocation problem in RIS assisted environment as a multi arm bandit (MAB) problem. Then based on the MAB formulation, we use an ϵ-greedy algorithm for RB allocation which explicitly considers the throughput achievable through the indirect (reflected) channel while selecting RBs. Finally, through extensive simulations, we have shown that our proposed algorithm significantly outperforms an existing proportional fair based RB allocation mechanism in terms of call dropping probability and system throughput. We observe that for achieving the highest throughput we need to strike a proper balance between exploration and exploitation. Furthermore, this study establishes that the CSI acquisition overhead for the RIS assisted channel cannot be avoided to optimally allocate the RBs. It may be observed that RBs are limited whereas the number of UEs can grow unbounded. As a result, to improve spectral efficiency for eMBB based UEs, non orthogonal multi access has emerges as a promising solution. In the next chapter, we develop an algorithm to select a RIS-RB pair for UEs in a mmWave small cell NOMA communication network.

Chapter 7

RIS-RB pair selection in millimeter wave NOMA systems[1]

In mmWave small cell non orthogonal multiple access communication, it is crucial to select an optimal RIS along with optimal RB allocation. This is because due to the effect of dynamic obstacles the signal received at the UE from the RIS may fall below a required threshold. However, obtaining CSI for all available RISs incurs massive pilot overhead thereby reducing system throughput. In this chapter, we first select the optimal RIS based on a multi-agent multi-arm bandit (MAMAB) based approach. Then we allocate RBs to a UE based on the CSI of only the selected RIS thereby avoiding unnecessary pilot overhead for all the RISs in the network. In our MAMAB formulation, the gNB maintains an agent corresponding for each UE. Role of the agents are to choose suitable RISs for corresponding UEs. Further, the UEs are grouped based on the RIS chosen. Building on this, we propose a novel iterative RB allocation algorithm that allocates the RBs to the UE groups. In each iteration, for every unallocated RB and UE group pair, we first compute the relative gain in data rate that the UE with the worst channel condition would have obtained if the considered RB had been allocated to that group. Then, the RBs are allocated to the groups in a way that maximizes the sum relative gain. The same has been achieved by solving the underlying maximum weight bipartite matching problem. Here the relative gain for each group is computed by optimizing both the active beamforming at the gNB and the passive

[1]This chapter is based on the following submitted manuscript:
Souvik Deb, Sasthi C. Ghosh and Shankar K. Ghosh, "An efficient RIS selection and resource block allocation algorithm for 5G millimeter wave NOMA systems", **The 27th International Conference on Modeling, Analysis and Simulation of Wireless and Mobile Systems (ACM MSWiM 2025)**, Barcelona, Spain, 27-31 October 2025 (Submitted).

beamforming at the RIS. The algorithm terminates when all RBs are allocated. Finally, we perform extensive simulations to evaluate and compare the performance of our proposed algorithm with that of an algorithm that utilizes full CSI information of all available RISs for jointly allocating a RIS-RB pairs to the UEs. Important notations used in this chapter are depicted in Table 7.1.

Table 7.1: Important Notations for chapter 7

Notation	**Meaning**	**Notation**	**Meaning**
R	Number of gNB antennas	N	Number of UEs
M	Number of RISs	K	Number of RBs
$\mathcal{N}$	Set of UEs	$\mathcal{M}$	Set of RISs
$\mathcal{K}$	Set of RBs	T	Consecutive TTIs in one communication block
$\mathcal{D}$	Radius of mobility region of UE	$\mathbf{x}_j^n$	Transmitted signal for UE n over RB j
s_j^n	Data symbol for UE n over RB j	$\mathbf{w}_j^n$	Beamforming vector at the gNB
$\mathbf{y}_{ji}^n$	Signal at UE n through RB j and RIS i	$\mathbf{h}_j^n$	BS-UE n channel coefficient for RB j
$\mathbf{g}_{ji}^n$	BS-RIS i channel matrix over RB j	$\mathbf{f}_{ji}^n$	RIS i-UE n channel coefficient over RB j
u_{ji}^n	Additive white Gaussian noise at UE n through RB j and RIS i	$\mathcal{I}_j^n$	Set of UEs on RB j with lower decoding order than UE n
P_T	Transmit power of the gNB	$\mathbf{\Phi}_i$	Reflection matrix for RIS i serving UE n
ψ	Reflection efficiency	$\Gamma_{ji}^n(t)$	SINR at UE n via RB j and RIS i
$\tau_{ji}^n(t)$	Instantaneous data rate for UE n on RB j-RIS i pair	$\bar{W}$	Bandwidth of an RB
T_o	CSI acquisition overhead	T_c	Channel coherence time
$a_i^n(b)$	Arm of MAB agent n corresponding to RIS i at block b	$r_i^n(b)$	Instantaneous reward for pulling arm a_i^n for UE n
$Q_i^n(b)$	Weight associated with arm a_i^n for UE n at step b	$\widetilde{r_i^n}(b)$	Estimate of the reward for action i of UE n up to step b
$\mathcal{G}$	Set of UE groups	$\mathcal{F}_g$	Set of UEs in group g
f_g	Number of UEs in group g	$(\Gamma_j^n)_{min}$	Minimum SINR threshold over RB j for UE n
$\mathcal{B}_{gi}$	Set of RBs already allocated to group g at iteration i	$\mathcal{R}$	Set of unallocated RBs
Γ^T	Minimum gain threshold for LoS	γ	parameter to mix probability distribution for selecting arms

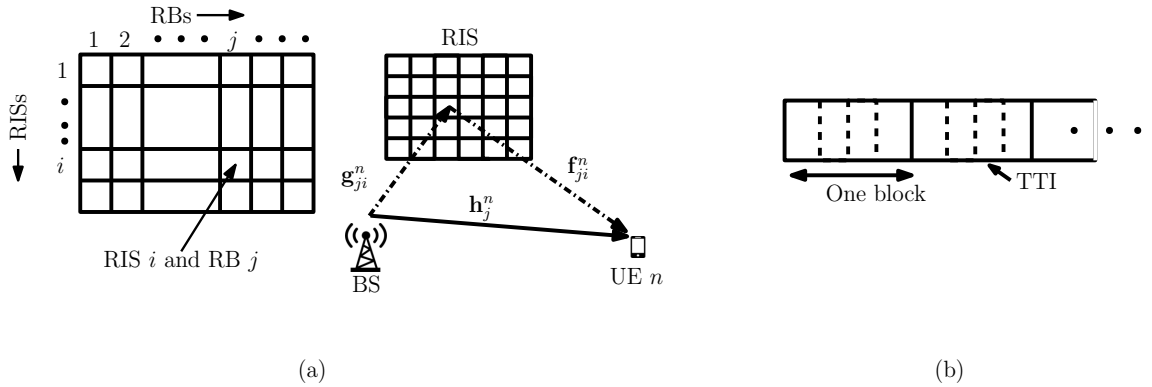

Figure 7.1: Considered system model: (a) UE n being served by RIS i and RB j pair. (b) Time frame

7.1 System model

We consider an RIS assisted NOMA system, where a new radio (NR) gNB with R antennas is providing ubiquitous coverage to N single antenna UEs assisted by M RISs mounted on the walls of buildings in the coverage area. The set of all UEs and RISs are denoted by $\mathcal{N}$ and $\mathcal{M}$ respectively. Each RIS is considered to have L reflecting elements. We denote $\mathcal{K}$ as the set of K RBs. We consider a resource limited scenario where the number of RISs and the number of RBs are less than the number of UEs: i.e. $N > K \geq M$ [42]. To avoid unnecessary CSI acquisition overhead, we assume that each RIS can serve multiple UEs, however, one UE can choose only a single RIS for communication. We considered that time is divided into discrete time slots of unit length called transmission time interval (TTI) with duration equal to channel coherence time [11]. We assume that a UE is served by a chosen RIS for a block of T consecutive TTIs before the UE decides to choose a new RIS. The value of T is set so that each communication block lasts 2000 ms. We consider that the low velocity pedestrian UEs move following random waypoint mobility model. The gNB is aware of the positions of the RISs, however, precise locations of the UEs are unknown, since UEs are changing positions over time. Moreover, UEs are unaware of the positions of the RISs. There are dynamic obstacles that are moving in the coverage area whose mobility pattern is also unknown. However, the positions of static obstacles are known by the BS.

7.1.1 Channel model

Data from two separate signal streams may be received by a UE communicating at time t: the direct signal from the gNB and the reflected signal via one of the M RISs. The

configuration of RIS i serving UE n at time t is represented by the $L \times L$ reflection matrix $\mathbf{\Phi}_i$ as: $\mathbf{\Phi}_i = \psi\ diag([e^{j\theta_1}, e^{j\theta_2}, \ldots, e^{j\theta_L}])$, where $\mathbf{\Phi}_i$ is a diagonal matrix, and $j = \sqrt{-1}$. Here $\psi \in [0,1]$ is the reflection efficiency and $\theta_l \in [0, 2\pi]$ is the phase shift caused by the reflecting element l. Let us consider that a set $\mathcal{S} \subseteq \mathcal{N}$ of UEs has selected RIS i and is being served on RB j. The signal transmitted to UE n through RB j can be represented as $\mathbf{x}_j^n = s_j^n \mathbf{w}_j^n$, where s_j^n denotes data symbol for UE n using RB j; $\mathbf{w}_j^n \in \mathbb{C}^{R\times 1}$ denotes the beamforming vector at the BS. Here $\mathbb{E}(s_j^n (s_j^n)^H) = 1$ where, $(.)^H$ denotes conjugate transpose. The transmitting power of the gNB is P_T. Subsequently, $\mathbf{y}_{ji}^n$, signal received at UE n through RB j and RIS i is represented as [29]:

$$\mathbf{y}_{ji}^n = \left(\mathbf{h}_j^n + \mathbf{f}_{ji}^n \mathbf{\Phi}_i \mathbf{g}_{ji}^n\right) \mathbf{x}_j^n + \left(\mathbf{h}_j^n + \mathbf{f}_{ji}^n \mathbf{\Phi}_i \mathbf{g}_{ji}^n\right) \sum_{m=1,\, m\neq n}^{|\mathcal{S}|} \mathbf{x}_j^m + u_{ji}^n. \tag{7.1}$$

where, $\mathbf{h}_j^n \in \mathbb{C}^{1\times R}$ denotes the channel vector of the direct channel from gNB to UE n through RB j; $\mathbf{g}_{ji}^n \in \mathbb{C}^{L\times R}$ denotes the channel matrix from the gNB to the RIS i serving UE n through RB j and $\mathbf{f}_{ji}^n \in \mathbb{C}^{1\times L}$ denotes the channel vector from the RIS i to UE n through RB j. Furthermore, u_{ji}^n is additive white Gaussian noise received by UE n through RB j and RIS i with power σ_{ji}^2. We assume that channels follow Rician fading. The channel vectors are estimated employing well known methods [67] [119]. The considered channel model has been demonstrated in Fig. 7.1. According to NOMA based successive interference cancellation (SIC), the UEs sharing the same RB are ordered in ascending sequence of their channel quality to facilitate decoding of signal [42], [131]. Let $\mathcal{I}_j^n$ is the set of UEs communicating using RB j which are lower in decoding order compared to UE n. The mechanism by which the UE performs SIC over different RBs is adopted from [43]. Accordingly, signal to interference plus noise ratio (SINR) at UE n communicating using RB j-RIS i pair is computed as [29]:

$$\Gamma_{ji}^n = \frac{|(\mathbf{h}_j^n + \mathbf{f}_{ji}^n \mathbf{\Phi}_i \mathbf{g}_{ji}^n)\mathbf{w}_j^n|^2}{|(\mathbf{h}_j^n + \mathbf{f}_{ji}^n \mathbf{\Phi}_i \mathbf{g}_{ji}^n) \sum_{m\in\mathcal{I}_j^n} \mathbf{w}_j^m|^2 + \sigma_{ji}^2}. \tag{7.2}$$

The achievable data rate for UE n communicating using RB j-RIS i pair is computed as:

$$\tau_{ji}^n = W \log_2(1 + \Gamma_{ji}^n), \tag{7.3}$$

where $W = \bar{W} \times \left(1 - \frac{T_o}{T_c}\right)$. Here, $\bar{W}$ is the bandwidth of each RB, $T_o = O(\sum_{\mathcal{S}_i:|\mathcal{S}_i|\neq 0}(L+1) + (\frac{L}{R}+1)(|\mathcal{S}_i|-1)$ is CSI acquisition overhead for N UEs [39]. and T_c is the channel coherence time. In the next section, we propose the the algorithm to allocate RIS-RB pair.

7.2 Proposed RIS selection and RB allocation algorithm

In this section, we propose the RIS-RB pair selection algorithm. Here, the RIS selection problem has been formulated as a adversarial MAMAB (one MAB agent corresponding to each UE) to deal with the stochastic behavior of the channel and the environment. At the beginning of each 2000 ms communication block, each agent selects an RIS to learn the choice of RIS with the best long-term channel gain. The UEs that have selected the same RIS are grouped together. In the second step, first we compute the maximum achievable sum data rate for each group by optimizing active and passive beamforming. Next, RBs are allocated to the groups in such a way that the relative gain in data rate obtained by the poorest UEs of each group is maximized. The details are provided in the following subsections.

7.2.1 MAMAB formulation for RIS selection

We consider that there is a adversarial MAB agent corresponding to each UE at the BS. Each arm of an agent corresponds to a RIS. Therefore, we have M arms for each agent. The set of actions for agent n is denoted by $\mathcal{A}^n$ where $M = |\mathcal{A}^n|$. A reward proportional to the channel gain at the UE n is generated only for the arm that is chosen at each block b. It may be observed that as a particular UE moves within the coverage of the BS, the relative distance between the UEs and the RIS changes continuously with the UE's motion, thereby resulting in a continuous change in the channel quality associated with the choice of each RIS. Such a scenario makes it impractical for the reward to be modeled a stationary distribution. Hence we treat the network environment as an adversary and model the RIS selection mechanism as an adversarial MAMAB. The adversarial MAMAB allows us to deal with the non stationary environment. The optimal policy for each agent is computed by employing the *Exp3* algorithm [132]. Corresponding to each arm there is a weight function which is used to determine the probability of selecting that arm. Upon choosing arm $a_i^n \in \mathcal{A}^n$ by agent n, channel estimation for RIS i is performed by UE n over all RBs $j \in \mathcal{K}$ using standard estimation techniques such as those described in [67] and [119]. We

denote by $Q_i^n(b)$, the weight associated with arm a_i^n computed upto communication block b. Now, we define the reward function for the choice of an arm. While UE n communicates with the gNB using RIS i at TTI t of communication block b, a dynamic obstacle may block the LoS between the RIS and the UE. The *RIS-UE* link blockage status are determined based on the estimated channel gain and a threshold [67]. The channel gain averaged over all available RBs at TTI t is computed as follows:

$$x(t) = \frac{1}{K} \sum_{k=1}^{K} |\mathbf{f}_{ki}^n \mathbf{\Phi}_i \mathbf{g}_{ki}^n|^2 \tag{7.4}$$

For the sake of generating the reward that captures the channel quality of the selected RIS-UE link, the phase shift matrix $\mathbf{\Phi}_i$ is computed following the *reflection phase selection* algorithm [11] that iterates over each RIS element and computes its phase shift value such that $|\mathbf{f}_{ki}^n \mathbf{\Phi}_i \mathbf{g}_{ki}^n|_t^2$ is maximized. The reward gained by UE n for communicating in block b after choosing arm a_i^n is given as follows:

$$r_i^n(b) = \begin{cases} \frac{1}{T} \sum_{t=1}^{T} \frac{1}{1 - \exp\{-x(t)\}}, & \text{If } x(t) > \Gamma^T \\ 0, & \text{otherwise} \end{cases} \tag{7.5}$$

Here, the link between the selected RIS and UE n is considered to have a suitable LoS condition if the average channel gain exceeds a predefined threshold denoted by Γ^T. Maximizing the reward implies choosing an RIS with the lowest likelihood of being blocked by dynamic obstacles and the highest expected gain achievable in the RIS-UE link. It may be observed that $r_i^n(b) \in [0,1]\ \forall\ 1 \leq i \leq M$ and $1 \leq n \leq N$, which ensures sublinear regret and thereby allowing each agent of the MAMAB to converge to the arm configuration with maximum expected reward values over time. The regret measures the gap between the solution presented by the algorithm and the optimal solution.

Let the probability of choosing arm a_i^n at the beginning of block b be denoted by $p_i^n(b)$. We define the estimate of the reward for all arms at block b as follows:

$$\widetilde{r_i^n}(b) = \begin{cases} r_i^n / p_i^n, & \text{If arm } i \text{ is chosen} \\ 0, & \text{otherwise} \end{cases} \tag{7.6}$$

The reward estimate defined in (7.6) is an unbiased estimate of the actual reward for the chosen arm at block b [132]. The probability distribution of choosing an arm is computed

as follows [132]:

$$p_i^n(b) = (1-\gamma)\frac{Q_i^n(b)}{\sum_{j=1}^{K} Q_j^n(b)} + \frac{\gamma}{M}. \tag{7.7}$$

Here, $Q_i^n(b)$ is the weight corresponding to arm i at block b which is updated as follows:

$$Q_i^n(b+1) = Q_i^n(b) \cdot \exp\left(\frac{\gamma \widetilde{r_i^n}(b)}{M}\right) \quad \forall \quad i. \tag{7.8}$$

The probability of selecting an arm i is a mixture of uniform distribution and a probability which is exponential in the estimated cumulative reward for that action [132]. The degree of mixture is controlled by the parameter $\gamma \in [0,1]$. The proposed MAB based RIS selection mechanism is depicted in Algorithm 11.

Algorithm 11: Adversarial MAB-based RIS Selection for UE n

Input: Learning rate $\gamma \in (0,1]$

Initialize $w_i(1) = 1$ for all $i = 1, \ldots, K$;

for $b = 1, 2, \ldots$ **do**

  for $i = 1$ **to** M **do**

    $p_i^n(b) = (1-\gamma)\frac{Q_i^n(b)}{\sum_{j=1}^{K} Q_j^n(b)} + \frac{\gamma}{M}$;

  Sample action i from the distribution $(p_1^n(t), \ldots, p_K^n(t))$;

  Receive reward $r_i^n(b) \in [0,1]$;

  for $j = 1$ **to** K **do**

    $\widetilde{r_i^n}(b) = \begin{cases} r_j^n / p_j^n, & \text{If arm } j \text{ is chosen} \\ 0, & \text{otherwise} \end{cases}$;

    $Q_j^n(b+1) = Q_j^n(b) \cdot \exp\left(\frac{\gamma \widetilde{r_j^n}(b)}{M}\right)$;

Since each agent run independently and the choice of action of one agent does not effect the other, the Algorithm 11 can run in parallel for each UE. Moreover, the *Exp3* algorithm is well suited for non stationary environments since it has a regret upper bound of $O(\sqrt{ZM \log M})$ where, Z is the total number of steps the *Exp3* algorithm has run [132]. This is sublinear in Z implying that the algorithm converges over time. The convergence behavior of the proposed MAMAB can be observed from Fig. 7.2 showing the expected cumulative regret over time. The result shows that the cumulative regret value asymptotically

converges over time, thus confirming that the regret per unit time tends to zero. Furthermore, the cumulative regret value is larger for a smaller number of RISs. This is because, with decreasing density of RIS deployment, the difference in rewards obtained between the optimal and non optimal choices of RIS increases.

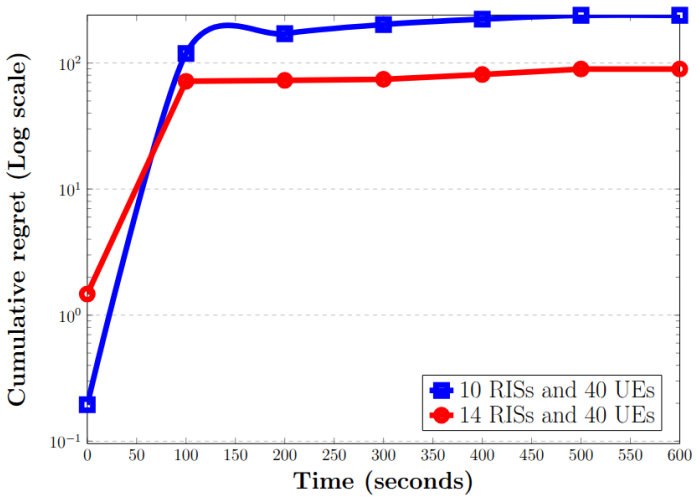

Figure 7.2: Cumulative regret over time

7.2.2 Beamforming and RB allocation

After executing the proposed MAMAB, each UE will select an RIS with the best expected reward value. The UEs being served by the same RIS are grouped together. Allocation of orthogonal RBs to such groups ensures that UEs served by different RISs do not share an RB thereby eliminating the need for each UE to acquire CSI for multiple RISs for interference mitigation. At each TTI t, the UEs perform channel estimation over all RBs. Now we compute the data rates of the UEs in each group for each available RB by optimizing the active and passive beamforming at the gNB and RIS respectively. We develop a novel iterative RB allocation algorithm that allocates each UE group with one RB from the unallocated RBs at each iteration such that the total relative gain in data rate obtained by the UEs with the least data rates of each group is maximized. The relative gain achieved by a UE after allocation of an RB r is defined as the ratio between the the increase in data rate resulting from the allocation of RB r and the data rate before the allocation. The details of the beamforming optimization and the corresponding RB allocation are presented in the following two subsections.

7.2.2.1 Passive and active beamforming

In this subsection, we compute the joint passive beamforming at the RIS and active beamforming at the gNB to maximize the sum data rate of every UE group. Let us denote the group corresponding to RIS i as $\mathcal{F}_i$, where $f_i = |\mathcal{F}_i|$. The set of RISs selected by at least one UE is represented as $\mathcal{G} = \{g| \quad f_g \neq 0\}$, leading to $F = |\mathcal{G}|$ many groups. Let $\mathcal{B}_g$ be the set of RBs that have already been allocated to group g and $\mathcal{R}$ be the set of RBs that are not yet allocated. Upon allocation of RB $r \in \mathcal{R}$ to group g, the maximum achievable sum rate needs to be recomputed by optimizing active and passive beamforming for all the RBs in $\mathcal{B}_g \cup \{r\}$. The passive beamforming at the RIS is denoted by the the phase optimization matrix $\mathbf{\Phi}_g$ and the active beamforming for UE n communicating using RB j is denoted by $\mathbf{w}_j^n$. The decoding order of UEs in each group g for each RB in $\mathcal{B}_g \cup \{r\}$ can be computed using the polynomial time optimization in [42]. Since the joint passive and active beamforming optimization is non-convex in both $\mathbf{w}_j^n$ and $\mathbf{\Phi}_g$, they are broken into two subproblems namely optimizing active beamforming for a fixed passive beamforming and optimizing passive beamforming for a fixed active beamforming. Finally, the joint problem is solved by alternatively optimizing them until the objective value converges. The first subproblem for each group g and the RBs in $\mathcal{B}_g \cup \{r\}$ is formulated as follows:

$$\text{Max } SumRate_{gr} = \sum_{n \in \mathcal{F}_g} W \log_2(1 + \zeta_{rg}^n) + \sum_{j \in \mathcal{B}_g} \sum_{n \in \mathcal{F}_g} W \log_2(1 + \zeta_{jg}^n) \tag{7.9}$$

Subject to :

$$\frac{|(\mathbf{h}_j^n + \mathbf{f}_{jg}^n \mathbf{\Phi}_g \mathbf{g}_{jg}^n)\mathbf{w}_j^n|^2}{|(\mathbf{h}_j^n + \mathbf{f}_{ji}^n \mathbf{\Phi}_g \mathbf{g}_{jg}^n) \sum_{m \in \mathcal{I}_j^n} \mathbf{w}_j^m|^2 + \sigma_{jg}^2} \geq \zeta_{jg}^n,$$

$$\forall n \in \mathcal{F}_g, \quad j \in \mathcal{B}_g \cup \{r\}, \tag{7.10}$$

$$\sum_{j \in \mathcal{B}_g \cup \{r\}} \sum_{n \in \mathcal{F}_g} |\mathbf{w}_j^n|^2 \leq \frac{f_g P_T}{N} \tag{7.11}$$

$$\zeta_{jg}^{n} \geq (\Gamma_{j}^{n})_{min} \quad \forall n \in \mathcal{F}_g, \quad j \in \mathcal{B}_g \cup \{r\}. \tag{7.12}$$

The objective (7.9) maximizes the sum data rate of group g when it is assigned the RBs in $\mathcal{B}_g \cup \{r\}$. The term computing the SINR in the objective function (7.9) is replaced by the auxiliary variable ζ_{jg}^{n} to make the objective function convex. The constraint (7.11) specifies that the power available to a group is proportional to the fraction of UEs in that group out of the total number of UEs. Constraint (7.12) specifies that the SINR for all UEs in the group must be atleast $(\Gamma_{j}^{n})_{min}$ which is the minimum SINR required over RB j such that the UE n is able to decode the signal. We define the positive semi-definite matrix $\mathbf{W}_{j}^{n} = \mathbf{w}_{j}^{n}(\mathbf{w}_{j}^{n})^{H}$ and the channel matrix $\mathbf{\Lambda}_{jg}^{n} = (\mathbf{h}_{j}^{n} + \mathbf{f}_{jg}^{n}\mathbf{\Phi}_{g}\mathbf{g}_{jg}^{n})(\mathbf{h}_{j}^{n} + \mathbf{f}_{jg}^{n}\mathbf{\Phi}_{g}\mathbf{g}_{jg}^{n})^{H}$. We can mitigate the non-convex constraint in (7.10) by defining a slack variable η_{jg}^{n} and rewrite the constraints (7.10) and (7.11) as follows:

$$Tr\left(\mathbf{\Lambda}_{jg}^{n}\mathbf{W}_{j}^{n}\right) \geq \eta_{jg}^{n}\zeta_{jg}^{n}, \tag{7.13}$$

$$\left(\sum_{m \in \mathcal{I}_{j}^{n}} Tr(\mathbf{\Lambda}_{jg}^{n}\mathbf{W}_{j}^{m})\right) + \sigma_{jg}^{2} \leq \eta_{jg}^{n} \tag{7.14}$$

$$\sum_{j \in \mathcal{B}_g \cup \{r\}} \sum_{n \in \mathcal{F}_g} Tr\left(\mathbf{W}_{j}^{n}\right) \leq \frac{f_g P_T}{N}, \tag{7.15}$$

$$\eta_{jg}^{n} \geq 0 \quad \forall j \in \mathcal{B} \cup \{r\}, \quad n \in \mathcal{F}_g. \tag{7.16}$$

To solve the non-convex optimzation problem (7.9) we adopt the well known successive convex approximation (SCA) method [30]. The non-convex constraint (7.13) is approximated as a convex constraint using the first order Taylor series expansion as follows:

$$\begin{aligned} Tr\left(\mathbf{\Lambda}_{jg}^{n}\mathbf{W}_{j}^{n}\right) \geq & (\eta_{jg}^{n})_{i-1}(\zeta_{jg}^{n})_{i-1} + (\eta_{jg}^{n})_{i-1}\left(\zeta_{jg}^{n} - (\zeta_{jg}^{n})_{i-1}\right) \\ & + (\zeta_{jg}^{n})_{i-1}\left(\eta_{jg}^{n} - (\eta_{jg}^{n})_{i-1}\right). \end{aligned} \tag{7.17}$$

Here, the subscript $i-1$ stands for the values of the variable at the $(i-1)^{th}$ iteration of the SCA. Therefore, at the i^{th} iteration we solve the following optimization problem:

$$\max \sum_{n \in \mathcal{F}_g} \log_2(1 + \zeta_{jg}^{n}) \tag{7.18}$$

Subject to: (7.17), (7.14), (7.15), (7.16), (7.12),

$$\mathbf{W}_j^n \succcurlyeq 0, \quad \forall n \in \mathcal{F}_g, \quad j \in \mathcal{B}_g \cup \{r\}, \tag{7.19}$$

$$rank(\mathbf{W}_j^n) = 1 \quad \forall n \in \mathcal{F}_g, \quad j \in \mathcal{B}_g \cup \{r\}. \tag{7.20}$$

The optimization problem (7.18) can be solved by well accepted method of semi definite reduction (SDR) [133], [30], by dropping the non convex rank constraint. Finally a rank 1 solution can be obtained after Gaussian randomization [134]. The process iterates until the objective value (7.9) converges. The SCA based method has been depicted in Algorithm 12.

Algorithm 12: SCA based beamforming for group g and RBs in $\mathcal{B}_g \cup \{r\}$

```
Initialize (η_jg^n)_0 = (ζ_jg^n)_0 = (Γ_j^n)_min,  ∀n ∈ F_g,  j ∈ B_g ∪ {r} and set i = 1;
while |(SumRate_gr)_i − (SumRate_gr)_{i−1}| ≥ ε do
    Compute constraint (7.17);
    Solve the optimization problem (7.18) by SDR and Gaussian randomization;
    i = i + 1;
```

For the second subproblem, we find the optimal passive beamforming for a fixed active beamforming using the optimal reflection coefficient computation algorithm (ORCC) proposed in [29]. Assuming that the decoding order for UE $n \in \mathcal{F}_g$ is higher than UE $\bar{n} \in \mathcal{F}_g$, the optimal passive beamforming must ensure the following constraints to guarantee successful SIC:

$$|(\mathbf{h}_j^n + \mathbf{f}_{jg}^n \mathbf{\Phi}_g \mathbf{g}_{jg}^n)|^2 \geq |(\mathbf{h}_j^n + \mathbf{f}_{jg}^{\bar{n}} \mathbf{\Phi}_g^{\bar{n}} \mathbf{g}_{jg}^{\bar{n}})|^2,$$
$$\forall n \geq \bar{n} \in \mathcal{F}_g, \ \forall j \in \mathcal{B}_g \cup \{r\} \tag{7.21}$$

$$|[\Phi_g]_{l,l}| = 1, \quad \forall 1 \leq l \leq L. \tag{7.22}$$

Therefore, we find Φ_g subject to constraints (7.10), (7.21) and (7.22). Finally the joint active and passive beamforming can be solved iteratively by alternatively solving the above mentioned two subproblems until the objective value converges as described in Algorithm 13.

7.2.2.2 RB allocation

The active and passive beamforming computed using Algorithm 13 aims to solely maximize the sum rate of the UEs of each group for each available RB. Such beamforming optimization may allocate more power to the UEs with stronger channel condition as opposed to the UEs

Algorithm 13: Alternatively optimizing active and passive beamforming

Set $i = 0$;
for $\forall j \in \mathcal{B}_g \cup \{r\}$ *and* $g \in \mathcal{G}$ **do**
  while $|\sum_{n \in \mathcal{F}_g} (\tau_{jg}^n)_i - \sum_{n \in \mathcal{F}_g} (\tau_{jg}^n)_{i+1}| \geq \epsilon$ **do**
    Solve for $(\mathbf{w}_j^n)_i \quad \forall n \in \mathcal{F}_g$ using Algorithm 12;
    Solve for $(\mathbf{\Phi}_g)_i$ subject to (7.10), (7.21) and (7.22) using ORCC ;
    $i = i + 1$;

with poorer channel conditions in order to increase the sum rate. Therefore, we propose an iterative RB allocation algorithm that aims to improve the data rate gain of the UE with the lowest data rate at each iteration. Note that for every combination of RBs assigned to a UE group, the optimal active and passive beamforming has to be computed using the Algorithm 13. Therefore, the search space for finding the optimal combination of RBs to be assigned to each UE group becomes exponential and therefore an iterative algorithm has been proposed to keep the RB allocation algorithm tractable. In this algorithm, initially a bipartite graph $\mathcal{T}^0$ is constructed where one set of vertices corresponds to the set of UE groups $\mathcal{G}$ and the other set of vertices corresponds to the set of RBs $\mathcal{K}$. An edge exists between each pair of vertices (g, j) where $g \in \mathcal{G}$ and $j \in \mathcal{K}$. At the first iteration, when no RBs are yet allocated, each edge (g, j) is assigned a weight $u_{gj}^0 = \sum_{n \in \mathcal{F}_g} \tau_{jg}^n$, which represents the sum rate obtained by group g if RB j is allocated to it. We start by finding the maximum sum rate, which can be obtained by finding the maximum weighted matching following the Hungarian algorithm [135]. Let at the i^{th} iteration the set of RBs allocated to group g is $\mathcal{B}_{gi}$. Let the data rate of the poorest performing UE in group g be U_g^i. Let $\mathcal{R} = \mathcal{K} \setminus \bigcup_{g \in \mathcal{G}} \mathcal{B}_{gi}$ be the set of unallocated RBs. Therefore, the residual bipartite graph $\mathcal{T}^i$ has edges only between the vertices corresponding to $\mathcal{G}$ and $\mathcal{R}$. For each edge (g, r) where $g \in \mathcal{G}$ and $r \in \mathcal{R}$, we first compute the achievable sum rate of group g after allocation of RB r to it using Algorithm 13. Let the data rate of the UE with the worst channel conditions in group g now becomes U_{rg}^{i+1}. Now we compute the weight of edge (g, r) as $u_{gr}^{i+1} = \frac{U_{rg}^{i+1} - U_g^i}{U_g^i}$. The edge weight signifies the relative gain in data rate by the worst performing UE in the group. Finally, maximum weighted matching is used at the $(i+1)^{th}$ iteration on the residual graph $\mathcal{T}^i$. This RB allocation procedure continues until all RBs are exhausted. The RB allocation is formally described in Algorithm 14.

Algorithm 14: Iterative RB allocation algorithm

Set $\mathcal{R} = \mathcal{K}$;
for *each edge* (g, j) *where* $g \in \mathcal{G}$ *and* $j \in \mathcal{R}$ **do**
    Compute active and passive beamforming using Algorithm 13;
    Compute edge weight $u^0_{gj} = \sum_{n \in \mathcal{F}_g} \tau^n_{jg}$;
Obtain maximum weighted matching on graph $\mathcal{T}^0$;
Set $i = 1$;
while $\mathcal{R} \neq \phi$ **do**
    Find $\mathcal{B}_{gi}$ and compute $\mathcal{R} = \mathcal{K} \setminus \bigcup_{g \in \mathcal{G}} \mathcal{B}_{gi}$;
    Form residual graph $\mathcal{T}^i$;
    for *each edge* (g, r) *where* $g \in \mathcal{G}$ *and* $r \in \mathcal{R}$ **do**
        Compute active and passive beamforming using Algorithm 13;
        Compute edge weight $u^{i+1}_{gr} = \frac{U^{i+1}_{rg} - U^i_g}{U^i_g}$;
    Obtain maximum weighted matching on $\mathcal{T}^i$;
    $i = i + 1$;

7.2.3 The proposed RIS selection and RB allocation algorithm

In this section, we propose the complete RIS selection and RB allocation algorithm. For each communication block b, the MAB agent corresponding to each UE selects an appropriate RIS according to (7.7) and subsequently groups the UEs that choose the same RIS together. Next, for each TTI within block b, each UE performs channel estimation, and accordingly RBs are allocated to each group based on Algorithm 14. Finally the reward value for each MAB agent obtained for the entire communication block b is computed and the corresponding arm values are updated. The process iterates over all blocks. The algorithm is formally presented in Algorithm 15.

7.3 Results and discussions

7.3.1 Simulation setup

The network parameters of the simulation results have been adopted from [42, 136, 79, 133] (shown in Tables 7.2 and 7.3). The considered simulation set-up consists of a single NR gNB

Algorithm 15: RIS selection and RB allocation algorithm

for *Communication block* b *in* $\{1,\ 2,\ \cdots\}$ **do**
  for *Agent* $n \in \mathcal{N}$ **do**
    Select the i-th arm $a_i^n(b)$ according to (7.7);
    Form the set of UE groups $\mathcal{G}$ according to the arm selected;
  for $1 \leq t \leq T$ **do**
    Perform channel estimation for all UEs;
    Allocate RBs to groups using Algorithm 14;
  for *Agent* $n \in \mathcal{N}$ **do**
    Compute reward estimate using (7.6);
    Compute probability distribution for choosing arms in block $b+1$ using Algorithm 11;

located at $(0,0)$. The locations of the RISs and the initial position of the UEs are generated uniformly randomly within the coverage area of the BSs. The UEs move following random waypoint mobility model within the coverage of the BS. The transmit power at the BSs is 27.5 dBm. All channels experience Rician fading with Rician factor 10. The pathloss exponent is considered to be 2.5 and the thermal noise is set at -114 dBm/Hz. The carrier frequency is set at 28 GHz and the total bandwidth is 100 MHz. We consider that a UE satisfies its QoS requirement if and only if its data rate crosses a given threshold value as considered in [137]. In our study, these threshold values are 100 Mbs and 200 Mbps. Let at time slot t, $Z(1,\ 2,\ 3\cdots N;\ 1,\ 2,\cdots K)$ be the matching obtained after executing the bipartite matching-based RB allocation algorithm, where N is the number of UEs and K is the number of RBs. After the RBs are allocated, UE i gets the data rate $R_i(t)$ at time slot t. Accordingly, we define a binary variable QS_i as follows:

$$QS_i = \begin{cases} 1 & R_i(t) > R_{th} \\ 0 & \text{Otherwise} \end{cases}. \tag{7.23}$$

Therefore, for a total of N UEs, the proportion of UEs achieving QoS is computed as follows:

$$\text{Proportion of UEs achieving QoS} = \frac{\sum_{i}^{N} QS_i}{N} \tag{7.24}$$

The results have been generated by averaging over 1000 independent runs of the simulation. The simulation time for generating an estimate of each data point is around 1 hours.

Table 7.2: 3GPP Urban Macro (UMa) Parameter Assumptions for Simulation (Based on TR 38.901)

Parameter	**Value**	**Unit/Note**
Minimum BS-UE 2D Distance	35	m
Reference Distance for Path Loss	Implicit (close-in ≈ 1)	m
Shadow Fading Std. Dev. (σ_{SF}) - LOS	4	dB
Shadow Fading Std. Dev. (σ_{SF}) - NLOS	6	dB
Mobility Model	Random Waypoint or Uniform	(UEs move at constant speed)
Delay Spread ($\mu_{\lg DS}$) - NLOS	-6.83	$\log_{10}$(s)

Table 7.3: Simulation parameters for chapter 7

Parameters	**Values**	**Parameters**	**Values**	**Parameters**	**Values**
BS coverage	100 m	Carrier frequency	28 Ghz	Bandwidth	100 Mhz
# of RIS elements	100	Pathloss exponent	2.5	Noise	-114 dBm/Hz
Transmission power	27.5 dBm	Rician factor	10	UE Velocity	0.5 mps
Obstacle velocity	1 mps	Blockage duration	0.5 s	Obstacle height	1.8 m
UE height	1.4 m	gNB height	5 m	RIS height	5 m
# of UEs	60-90	# of RISs	10-13	# of RBs	20
Number of iterations	1000	Γ^t	-5 dB	Simulation time	1 hour

We compare our proposed algorithm with the RIS selection and RB allocation algorithm proposed in [41]. The authors propose a joint UE clustering and RIS assignment algorithm utilizing perfect CSI to maximize the network sum rate. The algorithm iteratively pairs UEs with distinct RBs and assigns each UE cluster with an RIS that maximizes the channel gain of all UEs in that cluster. The algorithm stops when all UEs are assigned to an RB. Furthermore, to compute the sum rate, CSI is acquired for all UE-RIS channels. We term this algorithm as *RB based algorithm*. On the other hand, in our proposed algorithm, each UE selects an RIS based on a MAMAB framework which maximizes the expected gain of the UE-RIS channel. The UEs selecting the same RIS are grouped together. The RBs are then allocated to each group in such a way that the gain in data rate of the UE with the worst

channel condition in that group is maximized. Here CSI is acquired by an UE only for the chosen RIS thus avoiding overhead for unnecessary channel estimation.

7.3.2 Results

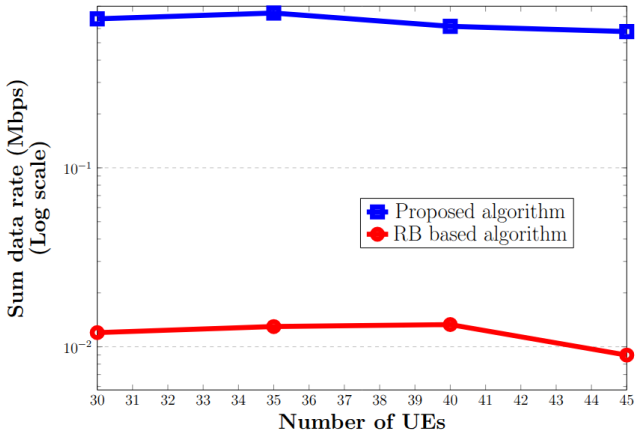

Figure 7.3: Sum rate (Mbps) vs. number of UEs

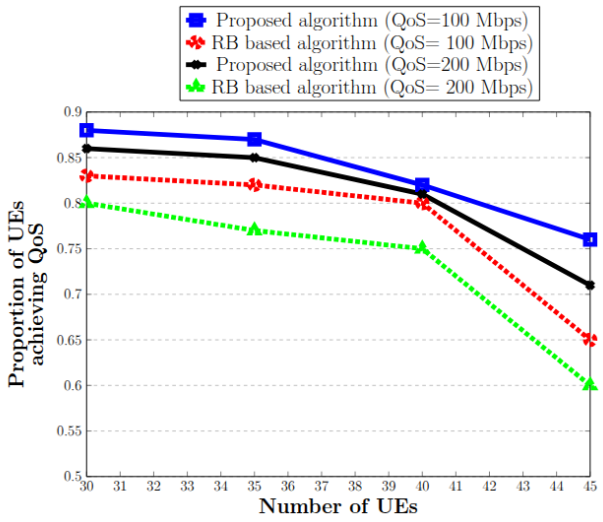

Figure 7.4: Proportion QoS achieving UEs vs. number of UEs

Figs 7.3 and 7.4 show the impact of traffic load (i.e., number of UEs in the system) on sum data rate, and the proportion of UEs that achieve desired QoS data rate threshold respectively. Here the number of UEs vary from 30 to 45 at a step of 5 UEs. The number of RBs is fixed at 15 and the number of RISs is fixed at 10. It may be observed that the sum

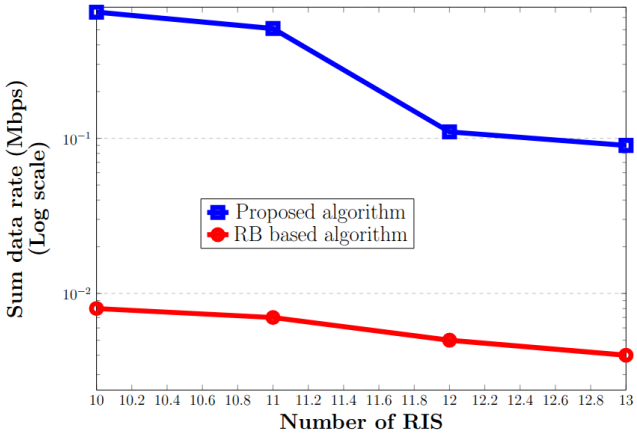

Figure 7.5: um rate (Mbps) vs. number of RISs

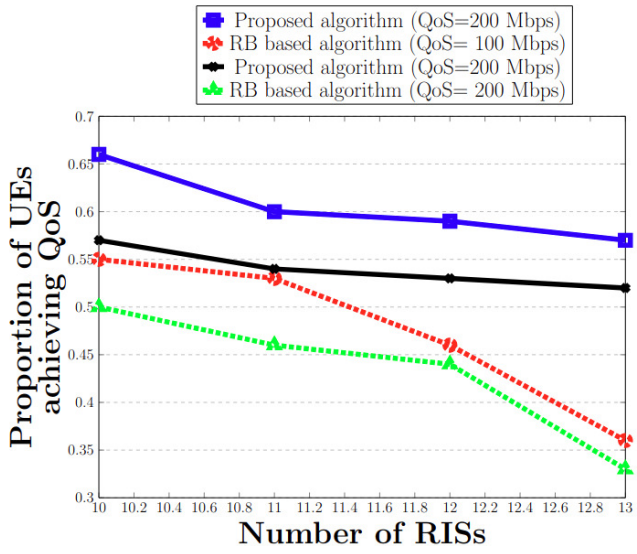

Figure 7.6: Proportion of QoS achieving UEs vs. number of RISs

rate of our proposed algorithm is greater than [41]. This is because our proposed algorithm learns and chooses an optimal RIS for each UE, thereby reducing the CSI overhead. This allows each UE to utilize a greater share of channel coherence time to be used for actual data communication as opposed to [41]. In can also be observed that the proportion of UEs achieving the desired QoS is higher for our proposed algorithm as compared to RB based algorithm. This is because the proposed RB allocation mechanism aims to improve the sum rate of the UE having the worst channel condition as much as possible, thereby pushing the data rates of more UEs above the desired QoS. Furthermore, both the sum rate and the proportion of QoS achieving UEs decreases monotonically with increasing number of UEs

because the time consumed for CSI increases. Margin of errors (MOEs) of the reported results are less than 0.061 showing high accuracy.

Figs 7.5 and 7.6 show the impact of the number of RISs on sum data rate and the proportion of UEs achieving the QoS. Here the number of RISs vary from 10 to 13 at a step of 1 RIS. The number of RBs is fixed at 15 and the number of UEs is fixed at 40. Results show that our proposed algorithm outperforms the RB based algorithm. The reason behind is similar to that stated for Figs 7.3 and 7.4. It may also be observed that the sum data rate and the proportion of UEs achieving QoS decrease with increasing number of RIS elements. For [41], decreasing trend is observed because the time consumed for CSI acquisition increases with increasing number of RISs. For the proposed algorithm, the decreasing trend is observed because the number of UE groups increases with number of RISs, which results in fewer RBs in each group. MOEs in the reported results are less than 0.055 showing high accuracy.

Finally, we observe that the adverserial bandit and bipartite matching based RIS-RB pair selection algorithm achieves a maximum throughput gain of more than 300% relative to the RB based algorithm that utilizes full channel state information for RIS selection and RB allocation [41]. This has been achieved for 40 UEs, 10 RISs and 15 RBs.

7.4 Conclusion

In this chapter, an algorithm based on MAMAB framework has been proposed to select RISs for each UE. Then, UEs choosing the same RIS are grouped together and finally RBs are allocated to each group using CSI for the RIS corresponding to that particular group only. The RBs are allocated such that the relative gain in data rate obtained by the UEs with the worst channel condition of each group is maximized. The simulation results confirm the superiority of the proposed algorithm over an existing RIS selection and RB allocation algorithm that uses full CSI for all the available RISs.

Chapter 8

Conclusion and future research direction

8.1 Conclusive remarks

This thesis has explored several methods to overcome some of the challenges faced when using RISs for 5G cellular and mmWave D2D communication. RIS is a promising new technology which can be utilised to enhance the performance of eMBB and URLLC based services by improving connectivity, throughput, spectral efficiency and reliability of the wireless network. However, effective utilisation of RISs brings forth several operational challenges. These challenges, when left unaddressed, deteriorate the performance of eMBB and URLLC services.

In chapters 2 and 3, we study the challenges faced in RIS assisted mmWave D2D networks. RISs provide a reflected path when the direct LoS between transmitter and receiver UEs is blocked. This ensures link reliability and improves the system throughput compared to D2D networks without RIS. However, RISs are two dimensional boards that are deployed on the walls of building or atop poles and hence remain stationary once placed. An RIS serving a D2D pair at some point of time may no longer be available as the UEs move to a different location. Furthermore, the number of RISs deployed must be limited for the system to be cost and energy efficient. In chapter 2, we address this challenge, by proposing a set cover based strategy for placing RISs at a minimal number of locations such that D2D pairs lacking direct LoS can still establish reliable communication by leveraging nearby RISs that provide reflected paths. Simulations show that our RIS placement strategy outperforms both wall-mounted and random deployment approaches. In real-world scenarios however, optimal RIS locations may not always be accessible due to factors like third-party ownership. In such cases, UEs must select the best available RIS from suboptimal placements. It is

critical to account for RIS-UE LoS status and avoid CSI overhead and phase shift complexity when selecting optimal RISs in D2D communication. To this end, in chapter 3, we propose a visibility polygon based algorithm that selects either the best RIS for D2D links or opts for gNB-assisted communication when no such RIS is available. Simulation results show its superiority over CSI based and location based approaches.

In chapters 4, 5, 6 and 7 we deal with some of the key challenges of RIS in 5G cellular network. RIS is instrumental in enhancing spectral efficiency for sub-6 GHz macro cellular and mmWave small cell communication. When optimally configured, the RIS can increase throughput for eMBB based UEs and reduce BER for URLLC based UEs. However, dense urban areas with urban canyons and multiple dynamic obstacles result in multipath propagation channel. This results in massive pilot overhead for acquiring CSI which scales linearly with the number of RIS elements. In chapter 4, we study the impact of CSI overhead on system throughput by taking into account the fact the CSI becomes outdated due to UE mobility. To mitigate CSI overhead, we propose an algorithm that dynamically determines the duration between consecutive CE periods by explicitly considering the velocities and outdated channel conditions of different UEs in the network. Simulations show that our proposed time varying CE achieves higher throughput in comparison to coherence time based fixed CE interval and a POMDP based adaptive channel estimation algorithm designed for a single UE network. In chapter 5, we observe that while optimally configuring the RIS by using precise CSI reduces BER and enhances reliability but the pilot overhead may lead to violation of strict latency constraints for URLLC based UEs. To overcome this limitation, we propose a contextual bandit based scheme to learn about the network environment and make the optimal choice of either selecting a gNB or a gNB-RIS pair during handover. Simulations show that that our scheme outperforms the traditional A3 based approach in terms of user throughput and reliability. It is to be noted that optimal resource allocation is crucial for eMBB and URLLC based communication. In chapter 6, we establish that CSI overhead impacts RB allocation as well. In this chapter, we model the RB allocation problem in a RIS assisted environment as a MAB problem and apply an ϵ-greedy algorithm that accounts for throughput via reflected channels. Simulations show our method significantly outperforms proportional fair RB allocation in terms of call drop rate and system throughput. We find that balancing exploration and exploitation is key to maximizing throughput, and that CSI acquisition overhead is essential for optimal RB allocation. After establishing this fact, in chapter 7, we address the limitation of CSI overhead for RIS assisted channels in resource limited scenario by proposing a RIS-RB pair selection algorithm in mmWave

NOMA small cell. RISs are selected for each UE based on a MAMAB framework. UEs selecting the same RIS are grouped, and RBs are allocated to the UE group using only the CSI for the particular RIS chosen for that group. This eliminates the need to estimate channels for all available RISs, reducing overhead and enhancing overall system throughput. Simulations show our approach outperforms an existing full-CSI-based RIS selection and RB allocation method. This studies in this thesis may be helpful for the mobile operators towards serving stringent data rate of eMBB services and strict latency for URLLC services in RIS assisted 5G networks.

8.2 Future research direction

Our future research scope includes the following:

- **Studying the impact of dynamic obstacles in RIS assisted D2D:** Apart from static obstacles like buildings and trees, the LoS between the transmitter and receiver in a D2D pair may also be blocked by dynamic obstacles such as cars and other users. The motion and positions of dynamic obstacles are unpredictable. Incorporating the impact of dynamic obstacles while placing and selecting RISs in mmWave D2D networks is a challenging avenue that needs to be explored. This can be done by integrating the deterministic algorithms with reinforcement learning based algorithms that can learn the mobility patterns of the dynamic obstacles.

- **Managing imperfect CSI:** Imperfect CSI refers to the mismatch or uncertainty between the true wireless channel and the estimated channel used for beamforming and RIS phase control. When CSI is imperfect, the RIS's phase shifts cannot be perfectly aligned to coherently reflect and enhance the desired signal. Future research work includes the extension of the algorithms proposed in the thesis to incorporate the effect of imperfect CSI.

- **Balancing UE load on the RISs:** With proper configuration of the RIS elements, an RIS is able to serve multiple UEs simultaneously. However, studies on the performance deterioration of RIS caused by increasing number of UEs are limited in recent literature. The impact of the number of UEs being served by an RIS needs to be studied and incorporated in RIS selection strategies to evenly balance the workload among different RISs.

- **RIS selection and RB allocation in multicell NOMA:** In this thesis, an RIS-RB pair selection algorithm is proposed for a single-cell NOMA. Extending this to a multi-cell environment introduces significant challenges. Each UE's MAB agent can no longer operate independently within one BS. Moreover, RB assignment must be coordinated among neighbouring cells. This cooperative task dramatically increases complexity due to inter-cell interference, the need for inter gNB signalling, and joint optimisation of RB assignments across cells. Therefore, our future research scope includes overcoming these challenges and extending our proposed algorithm for multi cell NOMA via distributed learning and designing inter gNB interference aware RB allocation mechanism.

- **Dynamic RIS elements grouping:** Grouping RIS elements can significantly reduce CSI overhead. However, there is a trade-off where fewer groups reduce estimation overhead but increase CSI error due to assuming a uniform channel within each group. In recent literature, studies on dynamic groupings based on changing channel conditions are limited. Optimal groupings need to be recalculated every time the channel conditions change. The studies in thesis may be extended by incorporating dynamic element groupings. Such an adaptive grouping can strike a balance by tailoring group sizes to channel conditions to maintain performance while controlling overhead.

Bibliography

[1] Mahmoud Aldababsa, Anas M. Salhab, Ali Arshad Nasir, Monjed H. Samuh, and Daniel Benevides da Costa. Multiple RISs-Aided Networks: Performance Analysis and Optimization. *IEEE Transactions on Vehicular Technology*, 2023.

[2] GSMA. The Mobile Economy, 2025. https://www.gsma.com/solutions-and-impact/connectivity-for-good/mobile-economy/wp-content/uploads/2025/04/030325-The-Mobile-Economy-2025.pdf, 2025.

[3] Abdelhamied A. Ateya, Ammar Muthanna, Maria Makolkina, and Andrey Koucheryavy. Study of 5G Services Standardization: Specifications and Requirements. In Proc. 10th Int. Congr. Ultra Modern Telecommun. Control Syst. Workshops, (ICUMT), pages 1–6, 2018.

[4] Hyunho Lee and Young-Chai Ko. Physical layer enhancements for ultra-reliable low-latency communications in 5G new radio systems. *IEEE Commun. Stand. Mag.*, 5(4):112–122, Dec. 2021.

[5] 3GPP TR 38.913 version 17.0.0 Release 17. 5G; Study on scenarios and requirements for next generation access technologies , 2022. https://www.etsi.org/deliver/etsi_tr/138900_138999/138913/17.00.00_60/tr_138913v170000p.pdf.

[6] Anutusha Dogra, Rakesh Kumar Jha, and Shubha Jain. A survey on beyond 5g network with the advent of 6g: Architecture and emerging technologies. *IEEE access*, 9:67512–67547, 2020.

[7] Jun Zhang, Xianghao Yu, and Khaled B Letaief. Hybrid beamforming for 5G and beyond millimeter-wave systems: A holistic view. *IEEE Open Journal of the Communications Society*, 1:77–91, 2019.

[8] RIS Tech Alliance. Reconfigurable intelligent surface technology white paper. *Mar*, 2023.

[9] ETSI GR RIS 004 V1.1.1. Reconfigurable intelligent surfaces (ris); implementation and practical considerations. https://www.etsi.org/deliver/etsi_gr/RIS/001_099/004/01.01.01_60/gr_ris004v010101p.pdf, 2025.

[10] Fabian Bette and Heinz Mellein. RECONFIGURABLE INTELLIGENT SURFACES Test andmeasurement aspects. https://8928696.fs1.hubspotusercontent-na1.net/hubfs/8928696/Reconfigurable-intelligent-surfaces_wp_en_3683-4178-52_v0200_fg.pdf, 2023.

[11] Minchae Jung, Walid Saad, Mérouane Debbah, and Choong Seon Hong. On the Optimality of Reconfigurable Intelligent Surfaces (RISs): Passive Beamforming, Modulation, and Resource Allocation. *IEEE Transactions on Wireless Communications*, 20(7):4347–4363, 2021.

[12] Theodore S Rappaport. *Wireless communications: principles and practice*. Cambridge University Press, 2024.

[13] Rafael P Torres and Jesús R Pérez. A lower bound for the coherence block length in mobile radio channels. *Electronics*, 10(4):398, 2021.

[14] Eduard E Bahingayi, Nemanja Stefan Perović, and Le-Nam Tran. Weighted sum-rate maximization for large-scale ris-assisted multi-user miso systems. In *2025 IEEE Wireless Communications and Networking Conference (WCNC)*, pages 1–6. IEEE, 2025.

[15] Huayan Guo, Ying-Chang Liang, Jie Chen, and Erik G Larsson. Weighted sum-rate maximization for intelligent reflecting surface enhanced wireless networks. In *2019 IEEE Global Communications Conference (GLOBECOM)*, pages 1–6. IEEE, 2019.

[16] Yang Lu, Ke Xiong, Pingyi Fan, Bo Ai, and Zhangdui Zhong. Outage-constrained sum transmission rate maximization in ris-assisted miso systems. *IEEE Transactions on Wireless Communications*, 23(4):2505–2518, 2024.

[17] Ekansh Panwar, Shankar K. Ghosh, Rajeev Kumar Singh, and Souvik Deb. Analysing Blackout Probability for RIS Assisted Cellular Network. In *2023 IEEE Future Networks World Forum (FNWF)*, pages 1–6, 2023.

[18] 3GPP TS 38.101-1 version 17.5.0 Release 17. 5G; NR; User Equipment (UE) radio transmission and reception; Part 1: Range 1 Standalone , 2022. https://www.etsi.org/deliver/etsi_ts/138100_138199/13810101/17.05.00_60/ts_13810101v170500p.pdf.

[19] 3GPP TS 38.101-2 version 17.5.0 Release 17. 5G; NR; User Equipment (UE) radio transmission and reception; Part 2: Range 2 Standalone , 2022. https://www.etsi.org/deliver/etsi_ts/138100_138199/13810102/17.05.00_60/ts_13810102v170500p.pdf.

[20] Aamina Akbar, Sobia Jangsher, and Farrukh A. Bhatti. Noma and 5g emerging technologies: A survey on issues and solution techniques. *Computer Networks*, 190:107950, 2021.

[21] Debbarni Sarkar, Satyendra Singh Yadav, Vipin Pal, Neeraj Kumar, Sarat Kumar Patra, et al. A comprehensive survey on IRS-assisted NOMA-based 6G wireless network: Design perspectives, challenges and future directions. *IEEE Transactions on Network and Service Management*, 21(2):2539–2562, 2024.

[22] Jia Ye, Abla Kammoun, and Mohamed-Slim Alouini. Reconfigurable Intelligent Surface Enabled Interference Nulling and Signal Power Maximization in mmWave Bands. *IEEE Transactions on Wireless Communications*, 21(11):9096–9113, 2022.

[23] Mohammed Almekhlafi, Mohamed Amine Arfaoui, Chadi Assi, and Ali Ghrayeb. Enabling urllc applications through reconfigurable intelligent surfaces: Challenges and potential. *IEEE Internet of Things Magazine*, 5(1):130–135, 2022.

[24] Ramin Hashemi, Samad Ali, Nurul Huda Mahmood, and Matti Latva-aho. Average rate and error probability analysis in short packet communications over ris-aided urllc systems. *IEEE Transactions on Vehicular Technology*, 70(10):10320–10334, 2021.

[25] Fabio Saggese, Federico Chiariotti, Kimmo Kansanen, and Petar Popovski. Efficient urllc with a reconfigurable intelligent surface and imperfect device tracking. In *ICC 2023 - IEEE International Conference on Communications*, pages 2722–2728, 2023.

[26] Qimei Chen, Jing Wu, Jiajia Wang, and Hao Jiang. Coexistence of urllc and embb services in mimo-noma systems. *IEEE Transactions on Vehicular Technology*, 72(1):839–851, 2023.

[27] Hao Yin, Lyutianyang Zhang, and Sumit Roy. Multiplexing urllc traffic within embb services in 5g nr: Fair scheduling. *IEEE Transactions on Communications*, 69(2):1080–1093, 2021.

[28] Jinyeop Na, Jinkyu Kang, and Joonhyuk Kang. Intelligent reflecting surface-assisted uplink noma for embb and urllc coexistence. *IEEE Transactions on Vehicular Technology*, 73(5):7406–7411, 2024.

[29] Hosein Zarini, Narges Gholipoor, Mohammad Robat Mili, Mehdi Rasti, Hina Tabassum, and Ekram Hossain. Resource Management for Multiplexing eMBB and URLLC Services Over RIS-Aided THz Communication. *IEEE Transactions on Communications*, 71(2):1207–1225, 2023.

[30] Zhaohui Yang, Mingzhe Chen, Walid Saad, Wei Xu, Mohammad Shikh-Bahaei, H. Vincent Poor, and Shuguang Cui. Energy-Efficient Wireless Communications With Distributed Reconfigurable Intelligent Surfaces. *IEEE Transactions on Wireless Communications*, 21(1):665–679, 2022.

[31] Abdolrasoul Sakhaei Gharagezlou, Mehdi Rasti, Samad Ali, Shiva Kazemi Taskooh, and Matti Latva-aho. XL-RIS Placement Strategies for Beam Focusing in Coexisting Near-Field and Far-Field mmWave Communications. In *2025 IEEE Wireless Communications and Networking Conference (WCNC)*, pages 1–6, 2025.

[32] Gui Zhou, Zhendong Peng, Cunhua Pan, and Robert Schober. Individual Channel Estimation for RIS-Aided Communication Systems—A General Framework. *IEEE Transactions on Wireless Communications*, 23(9):12038–12053, 2024.

[33] Ruonan Zhang, Yang Wang, Changyou Li, Yi Jiang, and Bin Li. Spatial Propagation Measurement and Analysis of Millimeter-Wave Channels at 28 GHz. In *Simulation*

Tools and Techniques: 11th International Conference, SIMUtools 2019, Chengdu, China, July 8–10, 2019, Proceedings 11, pages 549–558. Springer, 2019.

[34] Yali Chen, Bo Ai, Hongliang Zhang, Yong Niu, Lingyang Song, Zhu Han, and H Vincent Poor. Reconfigurable intelligent surface assisted Device-to-Device communications. *IEEE Transactions on Wireless Communications*, 20(5):2792–2804, 2020.

[35] Yan Zhang, Jiayi Zhang, Marco Di Renzo, Huahua Xiao, and Bo Ai. Reconfigurable Intelligent Surfaces With Outdated Channel State Information: Centralized vs. Distributed Deployments. *IEEE Transactions on Communications*, 70(4):2742–2756, 2022.

[36] Mohammed Almekhlafi, Mohamed Amine Arfaoui, Mohamed Elhattab, Chadi Assi, and Ali Ghrayeb. Joint Scheduling of eMBB and URLLC Services in RIS-Aided Downlink Cellular Networks. In *2021 International Conference on Computer Communications and Networks (ICCCN)*, pages 1–9, 2021.

[37] Hui Zhou, Shiwen Mao, and Prathima Agrawal. Approximation algorithms for cell association and scheduling in femtocell networks. *IEEE Transactions on Emerging Topics in Computing*, 3(3):432–443, Jan. 2015.

[38] Gui Zhou, Cunhua Pan, Hong Ren, Kezhi Wang, and Marco Di Renzo. Fairness-Oriented Multiple RIS-Aided mmWave Transmission: Stochastic Optimization Methods. *IEEE Transactions on Signal Processing*, 70:1402–1417, 2022.

[39] A. Lee Swindlehurst, Gui Zhou, Rang Liu, Cunhua Pan, and Ming Li. Channel Estimation With Reconfigurable Intelligent Surfaces—A General Framework. *Proceedings of the IEEE*, 110(9):1312–1338, 2022.

[40] Phuc Quang Truong, Tan Do-Duy, Van-Ca Phan, and Antonino Masaracchia. Jointly power allocation and phase shift optimization for RIS empowered downlink cellular networks. *EAI Endorsed Transactions on Industrial Networks and Intelligent Systems*, 10(4):e4–e4, 2023.

[41] Fatih Kilinc, Recep A Tasci, Abdulkadir Celik, Asmaa Abdallah, Ahmed M Eltawil, and Ertugrul Basar. RIS-assisted grant-free NOMA: User pairing, RIS assignment,

and phase shift alignment. *IEEE Transactions on Cognitive Communications and Networking*, 9(5):1257–1270, 2023.

[42] Jiakuo Zuo, Yuanwei Liu, Zhijin Qin, and Naofal Al-Dhahir. Resource Allocation in Intelligent Reflecting Surface Assisted NOMA Systems. *IEEE Transactions on Communications*, 68(11):7170–7183, 2020.

[43] Lou Salaün, Marceau Coupechoux, and Chung Shue Chen. Joint subcarrier and power allocation in NOMA: Optimal and approximate algorithms. *IEEE Transactions on Signal Processing*, 68:2215–2230, 2020.

[44] Maliheh Forouzanmehr and Soroush Akhlaghi. Sum-Rate Maximization for RIS-Aided Full-Duplex Non-Orthogonal Multiple Access Networks: Joint Passive Beamforming and Resource Allocation. *IEEE Transactions on Green Communications and Networking*, 2023.

[45] Xin Tan, Zhi Sun, Dimitrios Koutsonikolas, and Josep M. Jornet. Enabling Indoor Mobile Millimeter-wave Networks Based on Smart Reflect-arrays. In *IEEE INFOCOM 2018 - IEEE Conference on Computer Communications*, pages 270–278, 2018.

[46] Hongyang Du, Jiayi Zhang, Julian Cheng, and Bo Ai. Millimeter Wave Communications With Reconfigurable Intelligent Surfaces: Performance Analysis and Optimization. *IEEE Transactions on Communications*, 69(4):2752–2768, 2021.

[47] Shuhao Zeng, Hongliang Zhang, Boya Di, Zhu Han, and Lingyang Song. Reconfigurable Intelligent Surface (RIS) Assisted Wireless Coverage Extension: RIS Orientation and Location Optimization. *IEEE Communications Letters*, 25(1):269–273, 2021.

[48] Shuaiqi Jia, Xiaojun Yuan, and Ying-Chang Liang. Reconfigurable Intelligent Surfaces for Energy Efficiency in D2D Communication Network. *IEEE Wireless Communications Letters*, 10(3):683–687, 2021.

[49] Sarbani Ghose, Deepak Mishra, Santi P. Maity, and George C. Alexandropoulos. Jointly Optimal RIS Placement and Power Allocation for Underlay D2D Communications: An Outage Probability Minimization Approach. *IEEE Transactions on Cognitive Communications and Networking*, 10(2):622–633, 2024.

[50] Chang Cai, Huiyuan Yang, Xiaojun Yuan, Ying-Jun Angela Zhang, and Yi Liu. Reconfigurable Intelligent Surface Assisted D2D Underlay Communications: A Two-Timescale Optimization Design. *Journal of Communications and Information Networks*, 5(4):369–380, 2020.

[51] Yashuai Cao and Tiejun Lv. Sum rate maximization for reconfigurable intelligent surface assisted device-to-device communications. *arXiv preprint arXiv:2001.03344*, 2020.

[52] Zhangjie Peng, Tianshu Li, Cunhua Pan, Hong Ren, Wei Xu, and Marco Di Renzo. Analysis and optimization for ris-aided multi-pair communications relying on statistical csi. *IEEE Transactions on Vehicular Technology*, 70(4):3897–3901, 2021.

[53] Anirban Bhowal and Sonia Aïssa. Device-to-Device Communications With Selection-Based Cooperative RIS. *IEEE Transactions on Communications*, 73(3):2002–2015, 2025.

[54] Mostafa M Elsherbini, Osama A Omer, and Mostafa Salah. Low-complexity cooperative active and passive beamforming multi-RIS-assisted communication networks. *EURASIP Journal on Wireless Communications and Networking*, 2024.

[55] Yuting Fang, Saman Atapattu, Hazer Inaltekin, and Jamie Evans. Optimum Reconfigurable Intelligent Surface Selection for Wireless Networks. *IEEE Transactions on Communications*, 70(9):6241–6258, 2022.

[56] Jiawei Hu, Ying Ju, Haoyu Wang, Lei Liu, Qingqi Pei, Yinbo Guo, and Celimuge Wu. Multi-RIS Intelligent Collaboration Empowered Secure MmWave D2D Communication. In *GLOBECOM 2024 - 2024 IEEE Global Communications Conference*, pages 3243–3248, 2024.

[57] Hao Guo, Behrooz Makki, Magnus Åström, Mohamed-Slim Alouini, and Tommy Svensson. Dynamic blockage pre-avoidance using reconfigurable intelligent surfaces. *arXiv preprint arXiv:2201.06659*, 2022.

[58] Neel Kanth Kundu, Zan Li, Junhui Rao, Shanpu Shen, Matthew R. McKay, and Ross Murch. Optimal Grouping Strategy for Reconfigurable Intelligent Surface Assisted Wireless Communications. *IEEE Wireless Communications Letters*, 11(5):1082–1086, 2022.

[59] Shraddha Tripathi, Om Jee Pandey, and Rajesh M. Hegde. An Optimal Reflective Elements Grouping Model for RIS-Assisted IoT Networks Using Q-Learning. *IEEE Transactions on Circuits and Systems II: Express Briefs*, 70(8):3214–3218, 2023.

[60] Zan Li, Neel Kanth Kundu, Junhui Rao, Shanpu Shen, Matthew R. McKay, and Ross Murch. Performance Analysis of RIS-Assisted Communications With Element Grouping and Spatial Correlation. *IEEE Wireless Communications Letters*, 12(4):630–634, 2023.

[61] Neel Kanth Kundu and Matthew R. Mckay. Large Intelligent Surfaces With Channel Estimation Overhead: Achievable Rate and Optimal Configuration. *IEEE Wireless Communications Letters*, 10(5):986–990, 2021.

[62] Changsheng You, Beixiong Zheng, and Rui Zhang. Channel Estimation and Passive Beamforming for Intelligent Reflecting Surface: Discrete Phase Shift and Progressive Refinement. *IEEE Journal on Selected Areas in Communications*, 38(11):2604–2620, 2020.

[63] Syed Waqas Haider Shah, Marwa Qaraqe, Saud Althunibat, and Joerg Widmer. On the Impact of Age of Channel Information on Secure RIS-Assisted mmWave Networks. In *2024 IEEE 99th Vehicular Technology Conference (VTC2024-Spring)*, pages 1–7, 2024.

[64] Shuying Lin, Yulong Zou, and Derrick Wing Kwan Ng. Ergodic Throughput Maximization for RIS-Equipped-UAV-Enabled Wireless Powered Communications With Outdated CSI. *IEEE Transactions on Communications*, 72(6):3634–3650, 2024.

[65] Tasneem Alshamaseen, Elmehdi Illi, Syed Waqas Haider Shah, Saud Althunibat, and Marwa Qaraqe. Secrecy Performance of a RIS-Assisted Wireless Network: A Comprehensive Analysis Under Outdated CSI. *IEEE Open Journal of the Communications Society*, 6:1914–1930, 2025.

[66] Syed Waqas Haider Shah, Sai Pavan Deram, and Joerg Widmer. On the Effective Capacity of RIS-enabled mmWave Networks with Outdated CSI. In *IEEE INFOCOM 2023 - IEEE Conference on Computer Communications*, pages 1–10, 2023.

[67] Ankur Bansal, Neelima Agrawal, Keshav Singh, Chih-Peng Li, and Shahid Mumtaz. RIS Selection Scheme for UAV-Based Multi-RIS-Aided Multiuser Downlink Network With Imperfect and Outdated CSI. *IEEE Transactions on Communications*, 71(8):4650–4664, 2023.

[68] Helin Yang, Zehui Xiong, Jun Zhao, Dusit Niyato, Liang Xiao, and Qingqing Wu. Deep Reinforcement Learning-Based Intelligent Reflecting Surface for Secure Wireless Communications. *IEEE Transactions on Wireless Communications*, 20(1):375–388, 2021.

[69] Meng Xu, Shun Zhang, Jianpeng Ma, and Octavia A. Dobre. Deep Learning-Based Time-Varying Channel Estimation for RIS Assisted Communication. *IEEE Communications Letters*, 26(1):94–98, 2022.

[70] Jie Zhang, Zhe Wang, Jun Li, Qingqing Wu, Wen Chen, Feng Shu, and Shi Jin. How Often Channel Estimation is Required for Adaptive IRS Beamforming: A Bilevel Deep Reinforcement Learning Approach. *IEEE Transactions on Wireless Communications*, 23(8):8744–8759, 2024.

[71] Kotaru Kiran and D Rajeswara Rao. Analytical Review and Study on Various Vertical Handover Management Technologies in 5G Heterogeneous Network. *INFOCOMMUNICATIONS JOURNAL: A PUBLICATION OF THE SCIENTIFIC ASSOCIATION FOR INFOCOMMUNICATIONS (HTE)*, 14(2):28–38, 2022.

[72] Mahmoud M Elsayed, Khalid M Hosny, Mostafa M Fouda, and Marwa M Khashaba. Vehicles communications handover in 5G: A Survey. *ICT Express*, Jan. 2022.

[73] Mingfang Ma, Anqi Zhu, Songtao Guo, and Yuanyuan Yang. Intelligent Network Selection Algorithm for Multiservice Users in 5G Heterogeneous Network System: Nash Q-Learning Method. *IEEE Internet Things Journal*, 8(15):11877–11890, Apr. 2021.

[74] Hyun-Seo Park, Yuro Lee, Tae-Joong Kim, Byung-Chul Kim, and Jae-Yong Lee. Handover mechanism in NR for ultra-reliable low-latency communications. *IEEE Network*, 32(2):41–47, Apr. 2018.

[75] Nguyen Cong Luong, Nguyen Thi Thanh Van, Shaohan Feng, Huy T. Nguyen, Dusit Niyato, and Dong In Kim. Dynamic Network Service Selection in IRS-Assisted Wireless Networks: A Game Theory Approach. *IEEE Transactions on Vehicular Technology*, 70(5):5160–5165, 2021.

[76] Mrinal Das, Arpita Singh, Pydimarri Naga Sreenivas, Goutham Ponnamreddy, and Satya Ganesh. Optimizing NR Handover by using Doppler Shift along with Legacy Power Level Algorithm. In *2022 IEEE International Conference on Electronics, Computing and Communication Technologies (CONECCT)*, pages 1–5, 2022.

[77] Ahmed Masri, Teemu Veijalainen, Henrik Martikainen, Stephen Mwanje, Janne Ali-Tolppa, and Márton Kajó. Machine-Learning-Based Predictive Handover. In *2021 IFIP/IEEE International Symposium on Integrated Network Management (IM)*, pages 648–652, 2021.

[78] Mengbing Liu, Chongwen Huang, Marco Di Renzo, Mérouane Debbah, and Chau Yuen. Cooperative beamforming and RISs association for multi-RISs aided multi-users mmWave MIMO systems through graph neural networks. In *ICC 2023-IEEE International Conference on Communications*, pages 4286–4291. IEEE, 2023.

[79] Shizhao Yang, Jun Zhang, Yongxu Zhu, Shi Jin, and Chau Yuen. The application of distributed RIS to massive access MISO systems: NOMA or OMA? *IEEE Transactions on Wireless Communications*, 2023.

[80] Minghui Zhang, Ming Chen, Zhaohui Yang, Hamid Asgari, and Mohammad Shikh-Bahaei. Joint User Clustering and Passive Beamforming for Downlink NOMA System with Reconfigurable Intelligent Surface. In *2020 IEEE 31st Annual International Symposium on Personal, Indoor and Mobile Radio Communications*, pages 1–6, 2020.

[81] Mahyar Nemati, Jihong Park, and Jinho Choi. RIS-Assisted Coverage Enhancement in Millimeter-Wave Cellular Networks. *IEEE Access*, 8:188171–188185, 2020.

[82] Yuanbin Chen, Ying Wang, Jiayi Zhang, and Zhendong Li. Resource Allocation for Intelligent Reflecting Surface Aided Vehicular Communications. *IEEE Transactions on Vehicular Technology*, 69(10):12321–12326, 2020.

[83] Qianyu Liu, Chiew Foong Kwong, Sun Wei, Lincan Li, and Sibo Zhang. Intelligent handover triggering mechanism in 5G ultra-dense networks via clustering-based reinforcement learning. *Mob. Netw. Appl.*, 26(1):27–39, Nov. 2021.

[84] Lanlan Li, Wentao Shao, and Xin Zhou. A flexible scheduling algorithm for the 5th-generation networks. *Intelligent and Converged Networks*, 2(2):101–107, 2021.

[85] Durgesh Singh and Sasthi C. Ghosh. Mobility-Aware Relay Selection in 5G D2D Communication Using Stochastic Model. *IEEE Transactions on Vehicular Technology*, 68(3):2837–2849, 2019.

[86] Rathindra Nath Dutta and Sasthi C. Ghosh. Resource Allocation for Millimeter Wave D2D Communications in Presence of Static Obstacles. In Leonard Barolli, Isaac Woungang, and Tomoya Enokido, editors, *Advanced Information Networking and Applications - Proceedings of the 35th International Conference on Advanced Information Networking and Applications (AINA-2021), Toronto, ON, Canada, 12-14 May, 2021, Volume 1*, volume 225 of *Lecture Notes in Networks and Systems*, pages 667–680. Springer, 2021.

[87] Durgesh Singh, Arpan Chattopadhyay, and Sasthi C. Ghosh. Distributed Relay Selection in Presence of Dynamic Obstacles in Millimeter Wave D2D Communication. In *2020 IEEE International Conference on Communications, ICC 2020, Dublin, Ireland, June 7-11, 2020*, pages 1–6. IEEE, 2020.

[88] Subhojit Sarkar and Sasthi C. Ghosh. Relay selection in millimeter wave D2D communications through obstacle learning. *Ad Hoc Networks*, 114:102419, 2021.

[89] Marina L de SC Vieira, Marina De Lara, Marcelo Eduardo Pellenz, Mauricio Biczkowski, Marcos Alberto Mochinski, Fabricio Enembreck, Edgard Jamhour, and Voldi Costa Zambenedetti. Satellite imagery-assisted link-budget analysis algorithm for smart grid wireless backhaul network planning. In *Proceedings of the 39th ACM/SIGAPP Symposium on Applied Computing*, pages 151–158, 2024.

[90] Zhen-Qing He and Xiaojun Yuan. Cascaded channel estimation for large intelligent metasurface assisted massive MIMO. *IEEE Wireless Communications Letters*, 9(2):210–214, 2019.

[91] Dan E Willard. New data structures for orthogonal range queries. *SIAM Journal on Computing*, 14(1):232–253, 1985.

[92] Herbert Edelsbrunner. *Dynamic data structures for orthogonal intersection queries*. Technische Universität Graz/Forschungszentrum Graz. Institut für ..., 1980.

[93] Edward M McCreight. Priority search trees. *SIAM Journal on Computing*, 14(2):257–276, 1985.

[94] Mark De Berg, Marc Van Kreveld, Mark Overmars, and Otfried Schwarzkopf. Computational geometry. In *Computational geometry*, pages 1–17. Springer, 1997.

[95] Uriel Feige. A threshold of ln n for approximating set cover. *Journal of the ACM (JACM)*, 45(4):634–652, 1998.

[96] Akram Al-Hourani, Sathyanarayanan Chandrasekharan, and Sithamparanathan Kandeepan. Path loss study for millimeter wave device-to-device communications in urban environment. In *2014 IEEE International Conference on Communications Workshops (ICC)*, pages 102–107, 2014.

[97] Lakshmikanta Sau, Priyadarshi Mukherjee, and Sasthi C. Ghosh. Priority-Aware Grouping-Based Multihop Routing Scheme for RIS-Assisted Wireless Networks. *IEEE Transactions on Network Science and Engineering*, 2025.

[98] Durgesh Singh and Sasthi C. Ghosh. Network-Assisted D2D Relay Selection Under the Presence of Dynamic Obstacles. In *2019 IEEE 44th Conference on Local Computer Networks (LCN)*, pages 129–132, 2019.

[99] Ravi Shukla and Sasthi C Ghosh. Distributed relay switching in the presence of dynamic obstacles in millimeter wave D2D communication. *Computer Communincations*, 2022.

[100] Syed Waqas Haider Shah, Adnan Noor Mian, Shahid Mumtaz, Anwer Al-Dulaimi, Chih-Lin I, and Jon Crowcroft. Statistical QoS Analysis of Reconfigurable Intelligent Surface-Assisted D2D Communication. *IEEE Transactions on Vehicular Technology*, 71(7):7343–7358, 2022.

[101] Mohammed Almekhlafi, Mohamed Amine Arfaoui, Mohamed Elhattab, Chadi Assi, and Ali Ghrayeb. Joint resource allocation and phase shift optimization for RIS-aided eMBB/URLLC traffic multiplexing. *IEEE Trans. Commun.*, 2021.

[102] Subir Kumar Ghosh. *Visibility Algorithms in the Plane*. Cambridge University Press, 2009.

[103] Rathindra Nath Dutta and Sasthi C. Ghosh. Mobility aware resource allocation for millimeter-wave D2D communications in presence of obstacles. *Computer Communications*, 200:54–65, 2023.

[104] Long Jiao, Pu Wang, Amir Alipour-Fanid, Huacheng Zeng, and Kai Zeng. Enabling Efficient Blockage-Aware Handover in RIS-Assisted mmWave Cellular Networks. *IEEE Transactions on Wireless Communications*, 2022.

[105] Qin Tao, Junwei Wang, and Caijun Zhong. Performance Analysis of Intelligent Reflecting Surface Aided Communication Systems. *IEEE Communications Letters*, 2020.

[106] Zheng Chu, Zhengyu Zhu, Xingwang Li, Fuhui Zhou, Li Zhen, and Naofal Al-Dhahir. Resource allocation for IRS-assisted wireless-powered FDMA IoT networks. *IEEE Internet of Things Journal*, 9(11):8774–8785, 2021.

[107] Alessio Zappone, Marco Di Renzo, Farshad Shams, Xuewen Qian, and Mérouane Debbah. Overhead-aware design of reconfigurable intelligent surfaces in smart radio environments. *IEEE Transactions on Wireless Communications*, 20(1):126–141, 2020.

[108] Donghong Cai, Yanqing Xu, Fang Fang, Zhiguo Ding, and Pingzhi Fan. On the impact of time-correlated fading for downlink NOMA. *IEEE Transactions on Communications*, 67(6):4491–4504, 2019.

[109] Jingwen Tong, Hongliang Zhang, Liqun Fu, Amir Leshem, and Zhu Han. Two-stage resource allocation in reconfigurable intelligent surface assisted hybrid networks via multi-player bandits. *IEEE Transactions on Communications*, 70(5):3526–3541, 2022.

[110] Jingwen Tong, Ming Jin, Qinghua Guo, and Long Qu. Energy detection under interference power uncertainty. *IEEE Communications Letters*, 21(8):1887–1890, 2017.

[111] Cunhua Pan, Hong Ren, Kezhi Wang, Jonas Florentin Kolb, Maged Elkashlan, Ming Chen, Marco Di Renzo, Yang Hao, Jiangzhou Wang, A. Lee Swindlehurst, Xiaohu You, and Lajos Hanzo. Reconfigurable Intelligent Surfaces for 6G Systems: Principles, Applications, and Research Directions. *IEEE Communications Magazine*, 59(6):14–20, 2021.

[112] Tobias Lindstrøm Jensen and Elisabeth De Carvalho. An Optimal Channel Estimation Scheme for Intelligent Reflecting Surfaces Based on a Minimum Variance Unbiased Estimator. In *ICASSP 2020 - 2020 IEEE International Conference on Acoustics, Speech and Signal Processing (ICASSP)*, pages 5000–5004, 2020.

[113] M. Grant and S. Boyd. CVX: Matlab software for disciplined convex programming, version 2.1, March 2014. http://cvxr.com/cvx.

[114] Mohamed Elhattab, Mohamed Amine Arfaoui, Chadi Assi, and Ali Ghrayeb. Reconfigurable intelligent surface enabled full-duplex/half-duplex cooperative non-orthogonal multiple access. IEEE Trans. Wireless Commun., 21(5):3349–3364, 2021.

[115] Wei Yu and Raymond Lui. Dual methods for nonconvex spectrum optimization of multicarrier systems. *IEEE Transactions on communications*, 54(7):1310–1322, 2006.

[116] Naum Zuselevich Shor. *Minimization methods for non-differentiable functions*, volume 3. Springer Science & Business Media, 2012.

[117] Dimitri P Bertsekas. Nonlinear programming. *Journal of the Operational Research Society*, 48(3):334–334, 1997.

[118] Andrea Goldsmith. *Wireless communications*. Cambridge University Press, 2005.

[119] Qurrat-Ul-Ain Nadeem, Abla Kammoun, Anas Chaaban, Mérouane Debbah, and Mohamed-Slim Alouini. Intelligent Reflecting Surface Assisted Wireless Communication: Modeling and Channel Estimation. *ArXiv*, abs/1906.02360, 2019.

[120] 3GPP TS 38.300 version 16.4.0 Release 16. 5G; NR; NR and NG-RAN Overall description; Stage-2 , 2021. https://www.etsi.org/deliver/etsi_ts/138300_138399/138300/16.04.00_60/ts_138300v160400p.pdf.

[121] 3GPP TS 38.300 version 18.1.0 Release 18. 5G; NR; NR and NG-RAN Overall description; Stage-2 , 2024. https://www.etsi.org/deliver/etsi_ts/138300_138399/138300/18.01.00_60/ts_138300v180100p.pdf.

[122] 3GPP TS 38.331 version 17.1.0 Release 17. 5G; NR; Radio Resource Control (RRC); Protocol specification , 2022. https://www.etsi.org/deliver/etsi_ts/138300_138399/138331/17.01.00_60/ts_138331v170100p.pdf.

[123] Setareh Maghsudi and Ekram Hossain. Multi-armed bandits with application to 5G small cells. *IEEE Wireless Commun.*, 23(3):64–73, Jun. 2016.

[124] Sébastien Bubeck, Nicolo Cesa-Bianchi, et al. Regret analysis of stochastic and nonstochastic multi-armed bandit problems. *Foundations and Trends® in Machine Learning*, 5(1):1–122, Dec. 2012.

[125] Peter Auer, Nicolo Cesa-Bianchi, Yoav Freund, and Robert E Schapire. The non-stochastic multiarmed bandit problem. *SIAM journal on computing*, 32(1):48–77, 2002.

[126] Shankar K Ghosh and Sasthi C Ghosh. Analyzing handover performances of mobility management protocols in ultra-dense networks. *Journal of Network and Systems Management*, 28(4):1427–1452, 2020.

[127] Praveenkumar Korrai, Eva Lagunas, Shree Krishna Sharma, Symeon Chatzinotas, Ashok Bandi, and Björn Ottersten. A ran resource slicing mechanism for multiplexing of embb and urllc services in ofdma based 5g wireless networks. *IEEE Access*, 8:45674–45688, 2020.

[128] C. Santivanez and I. Stavrakakis. Study of various TDMA schemes for wireless networks in the presence of deadlines and overhead. *IEEE Journal on Selected Areas in Communications*, 17(7):1284–1304, 1999.

[129] Richard S Sutton and Andrew G Barto. *Reinforcement learning: An introduction*. MIT press, 2018.

[130] F. Capozzi, G. Piro, L.A. Grieco, G. Boggia, and P. Camarda. Downlink Packet Scheduling in LTE Cellular Networks: Key Design Issues and a Survey. *IEEE Communications Surveys Tutorials*, 15(2):678–700, 2013.

[131] Min Fu, Yong Zhou, and Yuanming Shi. Intelligent Reflecting Surface for Downlink Non-Orthogonal Multiple Access Networks. In Proc. IEEE Glob. Commun. Conf. Workshops, pages 1–6, 2019.

[132] Peter Auer, Nicolo Cesa-Bianchi, Yoav Freund, and Robert E Schapire. The non-stochastic multiarmed bandit problem. *SIAM journal on computing*, 32(1):48–77, 2002.

[133] Penglu Liu, Yong Li, Wei Cheng, Xiang Gao, and Xiaojing Huang. Intelligent reflecting surface aided NOMA for millimeter-wave massive MIMO with lens antenna array. *IEEE Transactions on Vehicular Technology*, 70(5):4419–4434, 2021.

[134] Zhi-Quan Luo, Wing-Kin Ma, Anthony Man-Cho So, Yinyu Ye, and Shuzhong Zhang. Semidefinite relaxation of quadratic optimization problems. *IEEE Signal Processing Magazine*, 27(3):20–34, 2010.

[135] Mike B Wright. Speeding up the hungarian algorithm. *Computers & Operations Research*, 17(1):95–96, 1990.

[136] Ish Kumar Jain, Rajeev Kumar, and Shivendra S Panwar. The impact of mobile blockers on millimeter wave cellular systems. *IEEE Journal on Selected Areas in Communications*, 37(4):854–868, 2019.

[137] Abdelhamied A Ateya, Ammar Muthanna, Maria Makolkina, and Andrey Koucheryavy. Study of 5G services standardization: Specifications and requirements. In *2018 10th international congress on ultra modern telecommunications and control systems and workshops (ICUMT)*, pages 1–6. IEEE, 2018.